REPORT 297

ADVISORY GROUP FOR AERONAUTICAL RESEARCH AND DEVELOPMENT

64 RUE DE VARENNE, PARIS VII

(1)

REPORT 297

AN INVESTIGATION OF INTERFERENCE EFFECTS ON SIMILAR MODELS OF DIFFERENT SIZE IN VARIOUS TRANSONIC TUNNELS IN THE UNITED KINGDOM

by

F. O'HARA, L. C. SQUIRE and A. B. HAINES

MARCH 1959

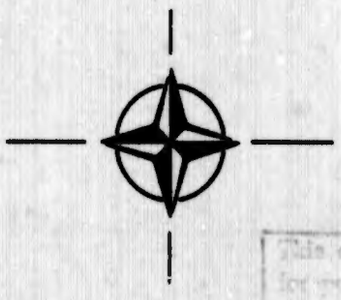

NORTH ATLANTIC TREATY ORGANISATION

REPORT 297

NORTH ATLANTIC TREATY ORGANIZATION

ADVISORY GROUP FOR AERONAUTICAL RESEARCH AND DEVELOPMENT

AN INVESTIGATION OF INTERFERENCE EFFECTS ON SIMILAR MODELS OF DIFFERENT SIZE IN VARIOUS TRANSONIC TUNNELS IN THE U.K.

by

F. O'Hara, L.C. Squire and A.B. Haines

This Report is one in the Series 292-305, inclusive, of papers presented at the Interference Effects Meeting of the AGARD Fluid Dynamics Panel (formerly Wind Tunnel and Model Testing Panel) held 2-5th March 1959, at the Training Center for Experimental Aerodynamics, Rhode, St. Genèse, Belgium

SUMMARY

Details are given of a programme of tests being made on similar swept-wing models in transonic tunnels of different types. Force measurement results at subsonic speeds in the RAE 3ft × 3ft slotted tunnel show only small interference effects for models of moderate blockage at low incidence; at higher incidences, the interference effect on lift becomes appreciably greater than estimated by theory, and significant pitching moment differences occur, apparently due to wall interference on the wing flow field. Comparable but smaller effects are evident in the results from the ARA 9ft × 8ft perforated tunnel. At speeds just above M = 1, the force fluctuations as speed is increased, because of wave reflection interference. The magnitude of the fluctuations diminishes as speed is further increased and this reduction is more marked in the perforated tunnel. Pressure measurements along the top of the body at zero incidence show delay in shock movements at high subsonic speeds indicating a blockage effect on speed; the effect is larger in the perforated tunnel though smaller than predicted by theory. Above M = 1, both expansion and shock waves are strongly reflected in the slotted tunnel but considerable alleviation, particularly of shock waves, is achieved in the perforated tunnel, for which an analysis of the effects is given, showing for example, the effect of the open-area distribution of the walls.

533.6.071.4

3b8b7c

SOMMAIRE

Ce rapport décrit le programme d'essais en cours sur des maquettes identiques à aile en flèche, dans des souffleries transsoniques de type différent. Les résultats de mesures de moments à des vitesses subsoniques effectuées dans la soufflerie RAE de 3 pieds sur 3 pieds à veine d'essai à fentes ne montrent que de petits effets d'interaction pour les maquettes à blocage moyen à faible incidence; aux incidences plus élevées l'effet d'interaction sur la portance accuse une valeur sensiblement plus importante que la valeur calculée et il intervient des différences signifiantes du moment de tangage, dues, à ce qu'il paraît, à l'interaction pariétale sur le champ d'écoulement alaire. Des effets comparables, mais plus faibles, se manifestent dans les résultats obtenus dans la soufflerie ARA de 9 pieds sur 8 pieds. A des vitesses légèrement supérieures à $M = 1$, il y a une variation de la force avec augmentation des réflections d'onde. L'importance de ces variations diminue avec augmentation à nouveau de la vitesse, diminution qui s'avère plus prononcée dans le cas de la soufflerie à fentes. Des mesures aux pressions effectuées le long du dessus du corps à incidence nulle montrent un retard apporté aux mouvements de chcc à des vitesses élevées en subsonique, ce qui indique l'influence du blocage sur la vitesse; pour être plus grande dans la soufflerie à trous, cette influence a, toutefois, une valeur inférieure à celle calculée. Au-dessus de $M = 1$ tant les ondes de dilatation que de choc sont fortement réfléchies dans la soufflerie à fentes, alors que la soufflerie à trous permet de réaliser une atténuation importante, notamment, des ondes de choc; l'analyse des effets obtenus montre par exemple l'influence de la répartition de la région ouverte des parois.

533.6.071.4

3b8b7c

CONTENTS

LIST OF TABLES

LIST OF FIGURES

NOTATION

$\bar{c}$	aerodynamic mean chord
C_D	drag coefficient (= drag/qS)
C_L	lift coefficient (= lift/qS)
C_m	pitching moment coefficient about 40% of aerodynamic mean chord (= moment/qS$\bar{c}$)
H	total pressure
M	Mach number
p	static pressure
q	kinetic pressure
R	Reynolds number based on aerodynamic mean chord
S	wing area
α	incidence

AN INVESTIGATION OF INTERFERENCE EFFECTS ON SIMILAR MODELS OF DIFFERENT SIZE IN VARIOUS TRANSONIC TUNNELS IN THE U.K.

F. O'Hara, L.C. Squire and A.B. Haines*

1. INTRODUCTION

The use of ventilated tunnel walls has made it possible to operate without choking at the model, throughout the transonic speed range. There are still various interference effects, however, which can affect test accuracy and possibly restrict the way in which such tunnels can reliably be used. At subsonic speeds, for example, the opposing interference effects of the closed and open sections of the boundary wall make it possible to reduce model blockage effects to a low level, but not in general to eliminate upwash effects at the same time. At low supersonic speeds shock or expansion wave reflections from the tunnel walls may intersect the model and so result in a small speed range in which the test conditions are definitely not representative of free air conditions. Some of these effects may be reduced or eliminated by specially designed ventilated walls, possibly of variable geometry, or alternatively, accepting the reduction in scale involved, by simply using smaller models.

At an early stage, however, in the use in this country of transonic tunnels, other unexpected interference effects were observed, in the first instance in tests by Roe in the English Electric Company's tunnel of a Mark IX pitot static head[1]. The main feature in these results, of interest from the point of view of interference, was a delay in movement with Mach number, along the cylindrical portion of the body, of the shock terminating the supersonic region associated with expansion round the nose; the speed at which the shock reached the rear of the model increased with model size, varying from below $M = 1.0$ for a very small model of only 0.002% blockage to over $M = 1.1$ for 0.21% blockage.

These characteristics were investigated further by Sutton[2]† in the RAE 3ft × 3ft tunnel, on a series of ogive-cylinder bodies and one wing-body combination.

The nature of the results of this investigation suggested that this wall interference for the ogive-cylinder arose when the supersonic region following the shoulder expansion is large enough to be significantly influenced by the wall; some results on a body with a converging afterbody[4] showing a more rapid shock movement, are consistent with this suggestion.

For the wing-body combination similar shock delays were observed, although the delay was much smaller than on the body of revolution. However, as Sutton points out[2] these shock movements will cause distortion in the pressure distributions and delays in the drag rise, aerodynamic centre shift, and also changes in the flow over the tailplane.

---

* *United Kingdom*

† Briefly reported in Reference 3

The impression formed from these early tests was that interferences of this kind were unlikely to be altogether avoidable in ventilated working sections with fixed open-area ratio. It was considered of the greatest importance in consequence to find out what size of model could be tested without invalidation of the results by excessive wall interference effects. No reliable theoretical basis of assessment being available it was decided to seek empirical rules from tests of similar models of different sizes, of the same model in tunnels with working sections of different dimensions. A meeting was held with representatives of firms and establishment in late 1954 to discuss the matter, and an outline of the programme of work agreed on, together with an account of some results already available, is given in the following sections.

2. TRANSONIC TUNNEL INTERFERENCE PROGRAMME

The programme of interference tests planned involves the measurement of forces and some pressures on a particular wing-body combination and is being undertaken in various transonic tunnels in Great Britain. Reasons for the choice of this wing-body model, together with details of the test programme, are given below and an outline of some of the initial results is given in Sections 3, 4 and 5.

2.1 Choice of Model

In planning the programme it was considered that the following features were desirable for a model to investigate transonic interference.

The model shape should be reasonably simple, to ease the problem of reproducing a series of models of different sizes accurately to scale, and to make them cheaper to manufacture. A shape symmetrical about the wing chord plane was preferred, to allow asymmetry of the flow to be detected easily and to reduce the uncertainties due to flow and model imperfections.

The model configuration should include at least a wing, and a fuselage big enough to hold a strain-gauge balance for the measurement of lift, drag, and pitching moment. The addition of a tailplane would make it possible to measure the effect of tunnel interference on the downwash behind the wing, but would add considerably to the cost and difficulty of accurate manufacture and it was not included in the first stage of the test programme.

While the model need not resemble an aircraft realistically (for example, the afterbody could be cylindrical), it should be representative, in the more important respects, of aircraft shapes which would be tested in transonic tunnels. Thus a swept wing would be more typical than a straight wing and the ratios of wing span to body diameter, and wing area to cross-sectional area, should be realistic.

In the absence of a tailplane a swept wing would show up streamwise variations of interference effects better than a straight wing.

The changes in aerodynamic characteristics of the model with Mach number at transonic speeds should not be so small and gradual that it would be difficult to find features suitable for showing up small blockage effects in the form of apparent

Mach number displacement. A very slender, highly swept shape would be unsatisfactory, and an unswept wing would be preferred, in this respect. The aerodynamic characteristics should, on the other hand, be as insensitive as possible to changes in Reynolds number.

Very useful information could be obtained from a small number of pressure holes, for example measuring wing trailing edge pressure and pressures along the body.

Consideration of these various factors suggested that no models in existence were completely suitable and accordingly a new wing-body combination was suggested. This model (Fig.1) has an ogive-cylinder body of fineness ratio 10 and a 6% thick RAE 102 section wing 45° mid-chord sweep, aspect ratio 2.83 and taper ratio 1/3. This model fitted into an existing research programme in the RAE Bedford 3ft × 3ft tunnel, and tests on a half model of the same wing have been made by the NPL, ARA and the RAE 3ft tunnel. Four complete models of this shape have been manufactured with body diameters of 1¾in., 2½in., 5in. and 7in.; principal dimensions of the models are given in Table I. All four models are equipped with strain-gauge balances for the measurement of lift, drag and pitching moment and in addition a row of pressure holes is provided along the top of the body, in the vertical plane of symmetry, and also two on the wing trailing edge (Fig.1).

At the moment there is no provision for testing these models with tailplanes; however, yawmeters will be attached to the models in some tests to find the effects of tunnel interference on the downwash at the tailplane position.

2.2 Scope of Comparisons

Particulars of the tunnels included in the programme are shown in Table II. The cross-sectional areas of their working sections vary between 430 and 10,350 square inches, while the maximum cross-sectional areas of the models vary between 3.2 and 51 square inches. Table III shows the range of cross-sectional area ratio and Reynolds number of the proposed test range. Tests on the 2½in. diameter model in the ARA tunnel, at a cross-sectional area ratio of only 0.06%, should provide a satisfactory standard, almost interference free and at a reasonable Reynolds number of about 2 million, by which results of the other tests can be judged. The reflection of the bow wave will be clear of the base of the model by a Mach number of 1.06 to 1.07 in this test.

In addition to the tunnel programme some models are being tested in free flight by the ground-launched rocket technique. Details of these models, and the quantities measured, are given in Table IV.

To help in the analysis of results the programme of model tunnel tests has been standardised. This programme was based on early tests and other experiments in wind tunnel interference. Forces are measured through an incidence range of up to 15° (where possible) at steps of 0.02 in Mach number between $M = 0.9$ and the supersonic Mach number at which the reflected bow wave clears the model. Mach number steps much smaller than 0.02 have in fact been found necessary to enable accurate analysis to be made of zero-lift drag and body pressures.

Table III also shows the tests which have already been made: it will be noted that so far results are only available from three tunnels, the Aircraft Research

Association 8ft x 9ft perforated tunnel, the Royal Aircraft Establishment (Farnborough) 8ft x 6ft slotted tunnel and the Royal Aircraft Establishment (Bedford) 3ft x 3ft slotted tunnel. In the analysis which follows, these three tunnels will be referred to as the perforated tunnel, the large slotted tunnel and the small slotted tunnel respectively.

The free-flight programme is now complete, but analysis of the results for lift curve slope and aerodynamic centre, from the oscillating model, are not yet complete.

3. RELIABILITY OF RESULTS

The results from the interference tests carried out so far can be conveniently considered in two sections, the first part dealing with the overall forces and moments, and the second presenting a study of the wall interference on the model flow field as shown by the body pressures. The overall forces are considered in Section 4 and the pressures in Section 5. Before discussing the detailed results it may be advantageous to consider three points, which, although not strictly concerned with tunnel interference as such, are of prime importance in assessing the interference effects. These points are the measurement of tunnel speed, or Mach number, the accuracy of results, and the effect of boundary-layer transition on the overall results.

Tunnel Mach number, in all three tunnels, is based on a static pressure measured in the plenum chamber. The Mach number obtained from this plenum pressure is related to tunnel Mach number by a relationship derived in the empty tunnel calibration. To find the effect of the presence of a model on this relationship, some tests have been made in the 3ft slotted tunnel[11]. A sample set of results is shown in Figure 2, where the plenum chamber Mach number (M_p) is compared with a Mach number (M_w) based on a wall pressure measured sufficiently far upstream to be unaffected by the presence of the models. It will be seen that the difference, $M_w - M_p$, for all the models lies within a scatter band of approximately 0.0015, which is about the accuracy of Mach number measurement. Similar results were obtained for Mach numbers based on pressures measured in other parts of the plenum chamber. Thus it may be assumed that the relationship between plenum and tunnel Mach number is unaffected by the presence of models (of up to 0.5% blockage); a similar result has been obtained in the 9ft x 8ft perforated tunnel. It is hoped that more information on this point will be obtained during the current tunnel-interference programme.

The accuracy of the assessment of interference effects depends on the accuracy of measurement and also on the accuracy and consistency observed in the manufacture of the models. The first of these can be assessed fairly definitely: for example 95% of the 2½in. model results are estimated to be within the following limits:-

$C_L \pm 0.005$

$C_m \pm 0.0015$

$C_D \pm 0.0005$

$\alpha \pm 0.03^\circ$ (together with a possible constant setting error)

Estimated errors for the other models are of the same order. In free-flight tests there are more uncertainties and the errors in C_D are probably larger than 0.0005; in addition there is some inaccuracy in Mach number measurement.

The inaccuracies introduced by differences in models are more difficult to assess; all that can be done at this stage is to state the accuracy of the model manufacture. The two smallest models, of 1⅝in. and 2½in. diameter, were made by the same manufacturer, and all dimensions are within the tolerances which are 0.001 diameter (up to a maximum of 0.005in.) on linear dimensions. In both cases wing profile is smooth, and the surface lies just inside the upper tolerance limit, that is the wings are slightly thick. The accuracy of the wings of the 7in. model, however, is not quite as good with one of the wings about 0.007in. under size on total thickness. The effects introduced by this error should be small, except possibly on pitching moment at high lift.

The problem of boundary-layer transition is of importance in that unless transition takes place at the same position in all tests, it is difficult to separate out differences due to transition movements from those due to interference effects. To try to eliminate this source of uncertainty all tests have been made with bands of carborundum powder on the first 10% chord of the wing on both surfaces, and also on the body on the band 0.6 to 0.8 diameter from the model nose. Early tests suggested that the sizes of carborundum powder in use were not always sufficient to fix transition at the same point in corresponding tests. However, some tests made in the small slotted tunnel at Reynolds number of one million with various grades of carborundum from 0.0025in. to 0.007in. have shown that within these grades there were only very small changes in lift and pitching moment (see Figs. 3 and 4); the trends shown are in general consistent with increasing roughness size except at the lowest subsonic speeds where there is a reversal of effect at the highest C_L. Significant changes are evident in the overall level of drag (Fig.5); however, in this case the effect of a change of grade of carborundum was to add a drag increment which was almost independent of Mach number (Fig.5). Thus the addition of a fixed increment to give agreement at one Mach number allows the results to be compared at all Mach numbers.

4. OVERALL FORCE MEASUREMENTS

4.1 Presentation of Results

The variation of C_L with incidence, C_m with C_L, and C_D with C_L are shown in Figures 6, 7, 8 for Mach numbers of 0.7, 0.8, 0.9, 0.98, 1.06, 1.14, 1.24; these results, obtained with a model of 0.06% blockage (the 2½in. model in the perforated tunnel) are probably effectively interference free except possibly near and just above $M = 1.0$. The curves show that very few of the results are linear except at very small incidences, and some of the C_M-C_L curves are not linear anywhere. This non-linearity has made comparisons of zero lift slopes difficult and so in general results have been compared on a slightly different basis. This consists, in the case of lift, for example, of comparing the variation with Mach number of the lift at incidences of 5° and 10°. Similarly the moments are compared at C_L's of 0.2, 0.4 and 0.6. The effects of angularity and curvature of the basic tunnel flow, and of model asymmetry are assumed to have been removed by subtracting C_L at $\alpha = 0$ and C_M at $C_L = 0$ from the results. The drag has only been compared at $C_L = 0$. The comparisons which have been made and presented are:-

(a) Tests on the 2½in. diameter model in the small slotted tunnel at Reynolds numbers of 1 and 2 million (Figs. 9 - 11);

(b) The 2½in. diameter model in the small slotted tunnel (0.5% blockage) and in the perforated tunnel (0.06% blockage) - Figures 12, 13, 14;

(c) Tests in the perforated tunnel on the 2½in. diameter model (0.06% blockage; $R = 2 \times 10^6$) and the 7in. diameter model (0.5% blockage; $R = 5 \times 10^6$) - Figures 16 - 19;

(d) Comparison of the 1¾in. model in the large slotted tunnel (0.05% blockage; $R = 1 \times 10^6$) and the 2½in. diameter model in the perforated tunnel (0.06% blockage, $R = 2 \times 10^6$) - Figures 20 - 22;

(e) Comparison of zero-lift drag in free flight and in the tunnel (Fig. 23).

4.2 Effects of Reynolds Number

The effects of Reynolds number for one model are shown in Figures 9 to 11, where results for Reynolds numbers of 1 and 2 million are plotted. These results were obtained from the 2½in. model in the small slotted tunnel using different grades of carborundum to ensure fixed transition at the two Reynolds numbers.

In the case of lift it will be seen that increasing the Reynolds number from 1×10^6 to 2×10^6 causes a decrease in lift of about 1% for Mach numbers below $M = 1.04$, and an increase of similar magnitude above this speed. The difference in this case is just outside the measuring accuracy, but appears significant as the results at the higher Reynolds number are consistently low below $M = 1.04$, and high above.

At speeds below $M = 0.9$ the effect of increasing Reynolds numbers appears to be to move the aerodynamic centre forward by about 0.5% $\bar{c}$; above $M = 0.9$ the results are in very good agreement, except for slight differences in the range from $M = 1.0$ to 1.3 when apparently reflected waves strike the model. The drag curves plotted in Figure 11 show the increment in drag at zero incidence above the value of C_D at $M = 0.8$. This method of plotting eliminates the shift in C_D due to increases in skin friction, and shows that the shapes of the C_D-M curves are very similar at the two Reynolds numbers, although there are again small differences when the reflected waves strike the model.

It is interesting to note that the estimate of the variation of subsonic drag with Reynolds number, based on the Royal Aeronautical Society's Data Sheets[12], is in good agreement with the experimental variation. For example, the experimental drag changes from 0.0125 to 0.0180 with decrease of Reynolds number from 5 to one million, the estimated change being from 0.012 to 0.0185.

4.3 Effect of Blockage

In discussing the effects of blockage it must be remembered that we are only concerned with a small part of the total results and so the conclusions reached are only tentative and may be modified when more data are available. The results of the comparisons listed in Section 4.1 will now be considered.

4.3.1 *Comparison of Test Results Obtained from the 2½in. Model in the Small Slotted and the Perforated Tunnels*

Figures 12 to 14 show a comparison of the lift, drag and pitching moment obtained on the 2½in. diameter model at a Reynolds number of 2 million in the small slotted tunnel (0.5% blockage) and in the perforated tunnel (0.06% blockage). The latter set of results, plotted with a full line, should be almost interference free, except near $M = 1.0$ and just above.

In studying these results it is convenient to divide the Mach number range into three parts; the first part is the speed range in which the flow is essentially subsonic in character, the second the speed range of the change from subsonic to supersonic flow and finally the range of supersonic flow. The speed ranges cannot be rigidly fixed, but the following ranges will serve as a framework for the subsequent analysis:

$$M < 0.95; \quad 0.95 \leqslant M \leqslant 1.05; \quad M > 1.05$$

In the subsonic range the main tunnel interference is essentially similar to the well known subsonic interference, that is an apparent change in speed, and an apparent change in incidence. In the next speed range these effects are still to some extent present, but in addition there is an interference effect caused by the presence of the tunnel walls modifying the shape of the sonic boundaries of the local supersonic regions and so changing the supersonic flow within this region; for example there may be changes in the position and strength of the shock waves terminating these regions. Finally, when the flow is supersonic all the interference effects can be thought of as coming from the reflection* of the model field by the walls.

A study of Figures 12 to 14 shows that the greatest interference is on lift, the lift at a given incidence in the small slotted tunnel being much lower than the interference-free results from the perforated tunnel. The loss of lift, at 10° incidence for example, is about 2.5% up to $M = 0.9$, and then increases to almost 5% at $M = 0.98$. At 5° incidence, the percentage loss is smaller. These lift results are considered in more detail in Figure 15. Here, plotted on a larger scale, are shown the variation with Mach number of C_L at 5° and 10° and also $(\partial C_L/\partial \alpha)_{\alpha=0}$, up to $M = 0.95$. Also shown in this figure are the results from the slotted tunnel corrected**: (a) by the full open-jet corrections and (b) by the slotted tunnel corrections as given by Maeder[13]. At zero incidence the open-jet correction applied to $\partial C_L/\partial \alpha$ gives a result which is much higher than the interference-free result whereas $\partial C_L/\partial \alpha$ with the slotted tunnel correction is only just too low. On the other hand at 10° incidence C_L corrected by the open-jet value is in excellent agreement with the interference-free C_L, but C_L with the slotted tunnel correction applied is now too small. This trend is evident at 5° incidence where the interference-free value is about half way between the two corrected curves. The possible reasons for this apparently non-linear interference will be discussed after the interference effects on C_m have been considered.

---

* Reflected in the sense of thrown back, possibly with some change in character and strength.

** The corrections have been applied to the faired curves through the slotted tunnel experimental points, and not to the actual experimental points.

Up to $M = 0.90$ the curves of C_m against Mach number are similar and although there are some differences in value, these variations are probably of minor importance since the C_m against C_L curves in this region are non-linear (see Fig. 7) and so small differences in tunnel conditions can cause large changes in C_m. Above $M = 0.9$ there is a rapid decrease in C_m with Mach number and differences in the position of this decrease on the Mach number scale should be an indication of tunnel interference. At $C_L = 0.2$ and 0.4 this lateral displacement is small whereas at $C_L = 0.6$ there are signs of a blockage effect of 0.01 in Mach number at $M = 0.96$, the error being similar in sign to that in an open jet. Taken with the previous results on lift it appears that the small slotted tunnel behaves more like an open jet tunnel as the model incidence increases. There appear to be at least two possible reasons for this behavior; either the pressure field of the lifting model causes changes in the flow through the slots, or the separation from the models at higher incidence (see Figs. 6 - 8) causes an increase in the effective blockage ratio of the model. It is hoped that future tests in the programme will shed more light on this point.

In the curve of C_D against Mach number (Fig. 14) there is a difference in the shape of the drag rise. In the small slotted tunnel the start of the drag rise appears to be delayed by about 0.01 in Mach number and the drag rises less steeply before becoming equal to the non-interference drag at about $M = 0.99$. Since the curves of C_m against M gave no indication of a blockage effect at low lift it must be assumed that this change in the drag rise is caused by the interference of the wall on the local supersonic regions, with changes in the local shock pattern on the wing. At low incidence such changes could have a large influence on the drag without a noticeable effect on lift and pitching moment.

At supersonic speeds a main feature of the force results is the presence of waves or fluctuations in the variation of all three components with Mach number, the largest fluctuations occurring in drag. These fluctuations are due to the reflection of the model field, but they will not be discussed fully here since the speed range in which this type of interference occurs is normally omitted in testing in slotted tunnels. They are of interest, however, as a point of comparison of slotted and perforated tunnels, and as such will be considered below.

4.3.2 Comparison of Test Results for the 2½in. and 7in. Models in the Perforated Tunnel

Figures 16 to 19 show a comparison of the test results obtained in the perforated tunnel on the 2½in. model (0.06% blockage) and the 7in. model (0.50% blockage). Because this tunnel has only a limited total pressure range, however, the Reynolds numbers of the two models are also different, being 2×10^6 and 5×10^6 respectively. For this reason it is difficult at this stage to make a full analysis of the results. However, it should be noted that the trends of the results are, in general, consistent with those of previous results. For example, at subsonic speeds the lift of the 7in. model is less than that of the 2½in. model, as in the earlier comparison (Fig. 12) where there was a difference of blockage; at 10° incidence the lift of the larger model is about 2.5% less up to $M = 0.9$, over 5% less at $M = 1.0$, and about 3% less at supersonic speeds. Part of the difference at subsonic speeds may be due to Reynolds number effects (if the conclusions from Figure 9 apply) but conversely at supersonic speeds, Reynolds number effects may have reduced the lift differences.

The force results for the larger model at supersonic speeds fluctuate more with Mach number than the results for the smaller model. It is notable, however, that the fluctuations at supersonic speeds in the perforated tunnel are smaller than those for the same blockage in the small slotted tunnel; this is in accord with the conclusions in Section 5 from analysis of pressure records that more alleviation of incident disturbances is achieved at the perforated walls than at the slotted walls.

Some differences exist between the zero-lift drag results from the models of 0.5% blockage in the slotted and perforated tunnels (Figs. 14 and 19). In the slotted tunnel, as just noted, there is a delay in the speed at which the drag rise starts but at $M = 0.99$ the drag is in good agreement with the interference-free drag. In the perforated tunnel, on the other hand, there is a delay in the start of the drag rise of just over 0.01, which continues in the drag curve to beyond $M = 1.0$. At supersonic speeds the similarity of the modulations in the drag curves suggests that the interference on $(C_D)_0$ is similar in type in the slotted and perforated tunnels, but that the magnitude of the interference is much less in the perforated tunnel.

One point of difference in the results which has not so far been explained is the discrepancy in the level of the pitching moment results for the 7in. and 2½in. models (Fig. 17). This is equivalent to a difference of 1% $\bar{c}$ in the position of the pitching moment centre but the origin of the difference has not yet been traced. Some light may be cast on the matter by tests to be made in other models.

Some other possible interference effects are shown in Figure 18, where C_m vs C_L curves are compared at Mach numbers near unity. It will be seen that in addition to the aerodynamic centre shift with Mach number there is also a change of character in the curves at high C_L with increase in Mach number; in particular the C_L at which the moment curve becomes unstable increases from about 0.5 at $M = 0.94$ to 0.9 at $M = 1.04$.

These changes are associated with the development of shock waves on the wing, and the change over from leading-edge to shock-induced separation.

For the 2½in. model the main changes take place between $M = 0.94$ and $M = 0.98$, the shape of the curves above this Mach number being essentially similar; for the 7in. model on the other hand the curves between $M = 0.94$ and $M = 1.0$ are similar and the change takes place between $M = 1.0$ and $M = 1.04$. Some of this difference could be due to the different test Reynolds number, and also possibly to the inaccuracy of the 7in. model mentioned in Section 3. However, it would appear that at high C_L there is a marked interference on the development of the flow at Mach numbers close to unity.

4.3.3 Comparison of Test Results of Small Blockage on Slotted and Perforated Tunnels

The comparison between these two sets of results is shown in Figures 20 - 22. It should be noted that in the large slotted tunnel the results were obtained at a Reynolds number of 1×10^6 on the 1¾in. diameter model (0.046% blockage) while the results in the perforated tunnel are from the 2½in. diameter model (0.06% blockage) at a Reynolds number of 2×10^6. Thus the results include differences in tunnel,

model and Reynolds number and are included mainly to show the extent of the differences which can occur even when blockage effects should be negligible; further tests are intended with both models to separate out the different effects.

The curves of Figure 20 show that the lift tends to be less at subsonic speeds on the 1¾in. model for which the Reynolds number was lower, and slightly higher at supersonic speeds; these trends are opposite to those found on the 2½in. model in the small slotted tunnel, but the differences in question here are small and generally below the level of accuracy attainable on the two models. There is again, as in the results considered in the previous section, a discrepancy between the pitching moments for the two models shown in Figure 21; some of the difference in this case, however, would appear (on the basis of the results of Figure 10) to be due to Reynolds number effects, and the general shapes of the pitching moment curves are very similar.

The zero-lift drag results of Figure 22 are in good agreement; a satisfactory comparison of the interference effects just above $M = 1$ is not possible, however, because scatter due to instrument vibration resulted in only a mean drag curve being available for the 1¾in. model in the large slotted tunnel.

4.3.4 Comparison of Tunnel and Free-Flight Zero-Lift Drag

Figure 23 shows very good agreement between the tunnel and free-flight results. There are small differences between the shapes of the drag rise between $M = 0.96$ and $M = 0.99$ but this may be due to the inaccuracy of the free-flight data. The only real difference in the results is between Mach numbers of 1.0 and 1.05, where the absence of modulations in the free-flight curves confirms that the fluctuations in the tunnel results in this region are due to the interference effects of the reflection of the model flow field from the tunnel walls.

4.4 Discussion of Force Results

The overall impression from analysis of the force results is that the interference effects are small except near $M = 1$ and at low supersonic speeds, where wave reflections intersect the model. The smallness of the effects may raise doubts as to the reliability of the conclusions drawn; however, although in some cases the differences border on the probable level of accuracy of determination of individual points, curves based on the points can be expected (in regions of regular variation at least) to provide higher accuracy, and from these, well-defined systematic trends have been observed. The general consistency of the results is considered to be well illustrated by the relatively small differences occurring in the results for the small models in the perforated and large slotted tunnels.

It appears that adequate accuracy of overall force measurements could be obtained, accepting some restrictions on test conditions, with models of larger blockage than so far considered, and tests with larger blockages are to be made. However, increased model size will result in a wider speed range in which wave reflection interference is of consequence, and note has to be taken of the fact that significant differences have been found in the results even at the low blockages tested, particularly at higher incidences.

Little uncertainty has arisen with reference to Reynolds number effects in the limited range covered, and in general roughness bands have been effectively used to

fix transition. The one irregularity in this connection was at high C_L at subsonic speed where apparently excessive roughness caused a reversal of effect on pitching moment; this might have been due to an effect on wing leading-edge separation characteristics. The other instance of a marked discrepancy in pitching moment variation (comparing results for the large and small models), which might be partly attributed to Reynolds number effect, occurred for high C_L at speeds near $M = 1.0$; the effect in this case would more likely be on the extent of shock-induced separation on the wings.

The interference effect on lift at subsonic speeds in the small slotted tunnel is in reasonable agreement with estimates from theory at low incidence but in excess of those at high incidence; tests may be possible to indicate whether this is due to an increased blockage effect or to some change in wall characteristics with pressure difference. The corresponding effects in the perforated tunnel are smaller than in the slotted tunnel, although still showing appreciable change with C_L; the need for a suitable theoretical basis for analysing the performance of perforated walls is underlined.

The zero-lift drag results show a blockage effect on speed near $M = 1.0$, the delay in the drag rise speed increasing with blockage.

The interference effects at low supersonic speeds appear as fluctuations in the forces as speed is increased due to wave reflections from the tunnel walls. These fluctuations are of comparable magnitude in both tunnels at speeds just above $M = 1.0$, but die away more quickly in the perforated tunnel at higher speeds; there is a suggestion of lift reduction and pitching-moment change with blockage at supersonic speeds, particularly in the perforated tunnel. It is possible that alleviation of reflected waves at supersonic speeds in the small slotted tunnel would be improved with perforated screens along the slots; the very limited number of slots however make it unlikely to approach the standard in this respect of the perforated wall tunnel.

Further understanding of the nature of the interference effects discussed here may follow from the tests at higher blockage, in which the effects should appear in a more marked form. The analysis of the pressure results in the following section provides an explanation of the nature and variation of the wave reflection interference for the model at zero incidence; pressure measurements would also be of assistance in connection with the changes of interference with incidence.

5. ANALYSIS OF PRESSURES ON THE TOP OF THE BODY

An analysis has been made of the pressures measured at zero incidence at various points along the top of the bodies of the different models in order to gain some idea of how the tunnel walls interfere with the flow field around the models.

5.1 Sources of Test Data

Data have been obtained from the same tests as those already considered when discussing the overall force results but for convenience the tests are listed again here, noting particularly any features that are specially relevant to the analysis of the pressure results.

(a) *Free flight tests*

Tests have been made on three models. Two of these were to a scale giving a body diameter of 5in.; a third had a body diameter of 1.75in. The third model was intended to reproduce as closely as possible the wind tunnel models and so no fins were mounted on the body and a tapered sting coming out of the base of the body was included as in the wind tunnel. The 5in. models are less representative because they did not include a sting and because a cruciform fin arrangement was mounted at the rear of the bodies. On the other hand, the data from the 5in. models should be basically more reliable because the deceleration of these models in flight near $M = 1.0$ was not as great as for the 1.75in. model. The results of various free flight tests have tended to suggest that the apparent Mach number at which a shock wave passes any position on the model may be influenced by the deceleration of the model. Accordingly, for the further forward pressure-plotting holes away from the influence of the stabilising fins, it seemed best to rely on the data from the large models.

The two 5in. models were geometrically the same but in the tests on one of these models transition was fixed near the model nose and wing leading-edge by roughness bands, while in the second case the body nose and wing leading-edge were left smooth. The data used in the present analysis have been taken from the tests on the model with fixed transition. Data are available for pressure holes at 4, 5.2, 6.0, 6.8 and 7.6 body diameters from the nose (the body length is 10 body diameters). Data for a hole at 8.4D at Mach numbers near 1.0 were thought to be possibly invalidated by the fact that the leading-edge apex of the fins was only a little way behind this hole and so the data for this position and also for 9.2D have been taken from the tests on the 1.75in. model. Combining the data from the different models in this way should have given the most reliable set of results, but where relevant, comment is made about the scatter between the results from the different models.

(b) *Wind tunnel models at small blockage*

Test data are available for the 2½in. model in the 9ft × 8ft ARA tunnel and for the 1¾in. model in the 8ft × 6ft tunnel at the RAE, Farnborough. This means that there are data for a model of 0.06% blockage in a perforated wall tunnel and for a model at 0.05% blockage in a slotted wall tunnel.

The pressure holes for the 2½in. model are at the same positions as on the third free-flight model (4, 5.2, 6.0, 6.8, 7.6, 8.4 and 9.2D). The same holes are present on the 1¾in. model with additional holes at 3.2, 3.6, 4.4 and 4.8D.

(c) *Wind tunnel models at 0.5% blockage*

Data are available for the 2½in. model in the 3ft tunnel at the RAE, Bedford and for the 7in. model in the ARA tunnel. This affords a comparison between a perforated and a slotted wall tunnel for models at 0.5% blockage.

Various tests have been made on the 7in. model in the 9ft × 8ft perforated tunnel. In particular, tests have been made with the model at two alternative longitudinal positions in the tunnel. The significance of this is that as regards bow wave reflections etc., the model is effectively being tested in the presence of tunnel walls

of different open-area ratio. This is possible because the working section of the ARA tunnel is relatively short, and as a result the forward part of typical models lies opposite the region in which the open-area ratio of the walls is still increasing up to its final value. In the present case, with the 7in. model in its forward position, the open-area ratio of the walls opposite the nose of the model is only 5% on the top and bottom walls and 7.5% on the side walls as compared with the final open-area ratio of 22.5% which applies aft of a station 38in. downstream of this. The model was then moved back 8in. and in this second position, the corresponding open-area ratio values opposite the model nose were 8.5% and 7.5% respectively. For both model positions, the open-area ratio of the walls at the point where they are struck by the model bow wave increases with increasing Mach number and this fact plays a major part in the subsequent analysis of the results - see Section 5.8 and Figure 32, for example.

Also, tests on the 7in. model in the perforated tunnel were made with the side walls both converged and diverged in addition to the main series of tests which were made with the walls parallel. Except where stated, all the results included here are for the case with walls parallel but some indication is given of the effect of converging the walls or, in effect, of varying the outflow through the walls.

All the wind tunnel tests were made over a range of model incidence but so far only the results at zero incidence have been analysed and it is therefore only these results that are discussed here.

5.2 General Nature of Flow Field Above the Body and of Possible Wall Interference Effects

No theoretical calculations have been made of the pressure distribution over the top of the body at transonic speeds. This would be difficult for the present arbitrary wing-body combination but it is intended later to calculate at least the pressure distribution over the forebody. In the meantime, an attempt has been made to derive from the available experimental data the pressure distributions that would apply in the absence of any tunnel interference effects. The free-flight and small-blockage results have been used for this purpose together with data from the 7in. model in the perforated tunnel since there were not sufficient pressure-plotting holes on the other models. Some typical results are plotted in Figure 24 for free-stream Mach numbers of 0.98, 1.00, 1.04 and 1.10.

Ahead of the body nose, at supersonic speeds, there will be a bow shock. Theoretical calculations suggest that at $M = 1.05$ this is situated about 0.3D ahead of the nose and that it should probably attach near $M = 1.12$. No schlieren pictures have been taken in any tunnel test to verify these results but the tunnel wall pressure distributions obtained in the perforated tunnel suggest that the bow shock may be somewhat further forward than predicted. It is difficult however to be definite about this because the curvature of the bow shock is not known. Away from the body, further compression will occur in the almost conical flow field immediately aft of the bow shock. This has been discussed in detail with reference to a purely conical nose in Reference 14, and similar effects should be present to some extent in the present case very close behind the bow shock - further aft, the compressions in this conical flow field will be neutralised by the expansions from the ogival forebody. In the subsequent discussion, this region of gradual compression behind the

bow shock will be referred to briefly as the 'nose compression'. It is followed by the expansion over the forebody which on the surface of the model continues up to near the shoulder of the ogive-cylinder. The maximum of this expansion and the succeeding shock tend to move downstream with increasing Mach number towards the wing root leading edge, where the latter combines with the wing leading-edge shock; this combined shock is referred to, for convenience, as the wing leading-edge shock. Behind this, the body pressures decrease again owing to the carry-over of the wing flow field. It is noteworthy that the peak of this wing-induced expansion is less than the peak in the forebody expansion. This point is worth noting because it indicates that the forebody expansion can have a significant influence on transonic tunnel interference even if the body has a rounded nose shape. The subsequent discussion will show that it is very important even for the present models for which the nose has a slightly blunted circular arc ogival shape fairing tangentially into the cylinder.

The rear wing shock for these Mach numbers occurs near or slightly downstream of the wing root trailing edge (at somewhat lower Mach numbers, such as $M = 0.96$, it would be somewhat further forward). The main deceleration of the flow occurs through this wing trailing-edge shock but at Mach numbers close to unity there is a further shock behind it. This 'terminal shock' travels down to the base of the body very rapidly in both the free-flight and small-blockage test results: it has reached the base by about $M = 1.01$ to 1.015.

The types of possible tunnel interference can be broadly classified under three headings. First, at high subsonic speeds, there are possible blockage effects of the type experienced in either closed or open tunnels. Secondly, at or near $M = 1.0$, there can be more serious interference effects of the type shown in various tests on bodies[2,15] or pitot static heads[1,16]. This usually takes the form of a retarded movement with increasing Mach number and a strengthening of the terminal shock. Finally, at low supersonic speeds, incident shock or expansion waves can be reflected from the tunnel walls and these reflected waves can intersect the models.

To some extent, this classification is somewhat artificial because one type of interference progressively merges into the next. For example, it will be found that the appropriate blockage corrections for these partly open tunnels are of the same sign as for an open tunnel and thus would in themselves imply a retarded rearward movement of the terminal shock. Crudely, the distinction between the first and second types of interference lies possibly in the fact that the first type carries the implication that the observed results can be converted to free flight by applying a blockage correction on speed, whereas with the second type no simple correction can be devised to convert the measured pressure distributions to interference-free conditions. Similarly, there is a link between the second and third types of interference. All the tests on bodies have tended to suggest that the retarded movement of the terminal shock bears some relation to where the walls intersect the forebody expansion field, while at higher Mach numbers this forebody expansion will be reflected from the walls as either a shock or a fan of expansion waves. Once again, therefore, it is difficult to draw a precise dividing line between the second and third types of interference.

Despite these reservations, however, it is still convenient to think in terms of these three types of interference and this point is borne in mind in the succeeding analysis.

One further point can be made by reference to Figure 24. Even in the absence of tunnel interference effects, the pressure distribution along the top of the body is clearly difficult to draw precisely unless there are a very large number of pressure-plotting holes and this difficulty is magnified considerably when tunnel-interference effects are present. As a result, a much more accurate assessment of the interference effects can be obtained by plotting the pressures at a given hole position against Mach number. By obtaining results at very small increments in Mach number (not more than 0.003 in many cases) it is possible to define these curves in close detail. By plotting this to a large scale and comparing the results for different stations, it is possible to identify the different reflected waves, etc., as they travel down the body with increasing Mach number and only then, after completing this quantitative analysis, can one hope to plot the pressure distributions along the top of the body with any accuracy. Even then, it is only really possible to do this for the large model which has pressure plotting holes at every 0.4D: for the 2½in. model, the gap between 4.0D and 5.2D is particularly difficult to plot reliably. Much of the succeeding discussion is therefore based on plots of $\Delta p/H$ vs Mach number for different hole positions. $\Delta p/H$ is the difference between the value of p/H measured at the hole and the free-stream value. Negative values of $\Delta p/H$ imply therefore a suction relative to the free stream.

5.3 Comparison of Results for Tunnel Models at Small Blockage with Free-Flight Results

The variation of $\Delta p/H$ with Mach number for the model at zero incidence at x = 4D, 6D, 7.6D and 9.2D for the two tunnel tests at small blockage and for free flight are plotted in Figures 25(a,b,c,d). The point x = 4D is just ahead of the wing root leading edge and so the large decrease in $\Delta p/H$ between about M = 0.98 and M = 1.01 corresponds to the wing leading-edge shock crossing the hole. The wing trailing-edge shock does not affect any of the pressures at these particular holes; the terminal shock can be seen crossing the holes at 7.6D and 9.2D.

The first and most striking result shown by Figure 25 is that almost irrespective of Mach number and hole position there is a consistent difference of about 0.01 in $\Delta p/H$ between either tunnel test and the free-flight results. The tunnel results give a more negative value of $\Delta p/H$, i.e. indicate a higher suction.

It has been noted that, qualitatively at least, this discrepancy is not peculiar to only this series of tests. It also existed in the comparison between the results in free flight and in the 3ft slotted tunnel at the RAE, Bedford on an ogive-cylinder body reported in References 2 and 3 and it has also been noted in tests on a pitot-static head. Such a difference has therefore been found between results in free flight and results in three different wind tunnels and this in itself would tend to suggest that it is the free-flight result that is open to question. The discrepancy cannot be dismissed as mere experimental scatter because it is so consistent. The scale of the graphs for Figure 25 is such that for the tunnel results, 0.01 in $\Delta p/H$ or 1in. on the graph corresponds to about 3in. on the manometer on which the pressures were recorded*; the probable errors in $\Delta p/H$ should not be more than ±0.002. The

---

* The pressures were recorded on an alcohol manometer as differences of pressures from tunnel plenum pressure, i.e. Δp was recorded directly in inches of alcohol.

possible scatter in the free-flight results is greater than this but is still not thought to be more than ±0.005 in $\Delta p/H$ at the most and comparison of the results for upper and lower surface pressure tappings on the body and between different models suggests that it is usually better than this except for Mach numbers close to $M = 1.00$. It appears therefore that the discrepancy can be treated as genuine. The fact that it is so little dependent upon hole position suggests that the value of the free-stream static pressure used in the reduction of either wind tunnel or flight results is in error. If it is the wind tunnel results that are at fault, this would imply that the presence of even a 0.05% blockage model in the tunnel is sufficient to alter the difference between free-stream static pressure by the equivalent of 0.02 in Mach number and this appears quite inconceivable. The tunnel wall pressures confirm this. A comparison of the tunnel wall pressures in the perforated tunnel has shown that the pressures ahead of where the model bow wave strikes the wall are not more than 0.003 different from the empty-tunnel case even when the larger 7in. model (0.5% blockage) is present. This has been checked over a range of Mach numbers and seems to be fairly convincing proof that the use of plenum pressure as a measure of static pressure in the tunnel is quite satisfactory even with a model present in the perforated tunnel, as already indicated (Sec. 3) to be the case for the slotted tunnel. On the other hand, a close investigation into the way in which a free-stream static pressure has been derived for the free-flight results has also failed to reveal any error of the magnitude being discussed here.

One other suggestion that might be made is that, certainly near $M = 1.00$, blockage effects on the pressures on the tunnel models might be significant even for the small models. Even if this were true, however, this would not be expected to apply over the full Mach number range.

It seems therefore that for the present, this discrepancy can only be noted and that it is not possible to give any convincing explanation for it.

The next point that might in theory be studied with reference to Figure 25 would be whether the comparisons suggest that any blockage corrections are present near $M = 1.00$ for the small models. There is some difficulty in practice here, however, because, as already mentioned, it is possible that the decelerations of the free-flight model through $M = 1.0$ may have some effect on the apparent Mach number at which a shock wave crosses any particular hole. Figure 25(c) shows an example of this. The arrow indicates the difference in Mach number for the passage of the terminal shock as between the 5in. model for which the curve has been plotted, and the 1½in. model for which the results were thought to be possibly less reliable because of this deceleration effect. This uncertainty in this case is clearly of the same order as any difference between the free-flight and tunnel results. Also, it appears that any conclusions that might be drawn from the passage of the leading-edge shock over the hole at $x = 4D$ would be at variance with the conclusions based on the behaviour of the terminal shock. It seems, however, that any blockage effects for the tunnel models near $M = 1.00$ are unlikely to exceed 0.01 in Mach number. Incidentally, it is worth pointing out that, theoretically, the effect would not have been expected to have been negligible even though the blockage ratio is as low as 0.05%. Reference 18 has explained that the blockage area ratio is not a good criterion on which to judge possible interference effects near $M = 1.00$. The corrections are much more likely to be a function of the linear distance of the walls in terms of model size and of the actual shape and fineness ratio of the model. It

is shown that the corrections are likely to be larger for a body of high fineness ratio and the formula suggested for a circular slotted tunnel is that the Mach number correction ΔM_0 at sonic speed should be given by

$$\Delta M_0 = - 0.9g \left(\frac{r^*}{h}\right)^{6/7} \left(\frac{r^*}{x^*}\right)^{2/7}$$

where g depends on the open-area ratio and for the slotted tunnels being considered here would be about 0.35 and $M_0 = M_{\text{free stream}} - M_{\text{tunnel}}$

r^*, x^* are the coordinates of the sonic point

and h is the tunnel semi-height.

An extension of the theory to cover a perforated tunnel is referred to in Reference 15 which quotes a corresponding formula for a perforated tunnel which is the same as above except for a change in the numerical constant, the values being appreciably larger for a perforated tunnel, and of opposite sign. Using the experimentally determined position of a sonic point (from the 7in. model results), the above formulae would suggest values of ΔM_0 of 0.007 and 0.020 for the present small-blockage models in the large slotted and perforated tunnels respectively. These values are about 40% of the values that would be predicted for the larger 0.5% blockage models and cannot therefore be classed as negligible in comparison. The experimental results suggest that these theories overestimate the corrections since the differences in Mach number between the results from the two tunnels are much less than 0.027 inch.

With regard to wave reflections from the walls, the only serious effects with the small models would be expected to be reflections of the bow wave. This is clearly evident as a reflected shock in the results for the slotted tunnel: the reflection passes the holes at 6.0D, 7.6D and 9.2D at $M = 1.03$, 1.04 and 1.047 respectively. In the perforated tunnel, the bow shock appears to be reflecting as a fan of expansion waves. In both tunnels the reflections should be clear of the base of the model by about $M = 1.06$. The strength of the reflected waves in terms of $\Delta p/H$ at a Mach number of about 1.04 is about 0.01 in the slotted tunnel and -0.007 in the perforated wall tunnel. The small model was mounted sufficiently far back in the working section of the perforated tunnel for the bow wave shock always to be striking the wall with an open-wave ratio of the full value of 22.5%. The fact that a perforated wall as open as this reflects shock waves at low supersonic Mach numbers as expansion waves is consistent with evidence obtained elsewhere (Ref. 17) and in particular with the evidence from the tests on the large models discussed later in Section 5.8. The latter evidence suggests that to eliminate these reflections it would have been necessary to reduce the open-area ratio to less than 5%.

5.4 General Comparison of Results for Tunnel Models at 0.5% Blockage

The variation of $\Delta p/H$ with Mach number for eight of the holes along the top of the body of the 7in. model in the perforated tunnel is plotted in Figure 26(a to h). For seven of the holes a comparison is made with the results for the 2½in. model in both the slotted and the perforated tunnels. This gives a comparison therefore between results at 0.5% blockage in both a perforated and a slotted tunnel, using the results

at the small blockage in the perforated tunnel as a datum. These have been used in preference to the free-flight results because of the uncertainty near $M = 1.00$ (model deceleration) and because of the unexplained difference in the general level of the pressures; it was also decided to choose the results in the perforated tunnel rather than those in the slotted tunnel because, as shown by Figure 25, the results in the perforated tunnel were less affected by reflections of the bow wave.

It will be seen that the results, particularly for the 0.5% blockage model in the perforated tunnel, contain a large number of maxima and minima. These are considered to be real variations and not to be due solely to experimental scatter. On the other hand, it is possible that some of them may be influenced partly by irregularities in the axial static pressure distribution in the empty tunnel but it is not thought that this affects the subsequent analysis to any great extent. This view is supported by the close correlation obtained between the disturbances evident at different holes.

Before considering the detailed analysis of these results, it should be noted that any feature of the flow field around the model that is reflected by the walls of the perforated tunnel can lead to three systems of reflected waves because the tunnel is not square and because the model is not mounted on the centre line of the tunnel. It is actually mounted 6in. above the centre line (this is standard practice in this tunnel and was not done specially for this test) and as a result, the model centre line is 42in. from the top wall and 54in. from both the side walls and the bottom wall. For the 7in. model, the top of the body at which the pressures are being measured is therefore 38.5in. from the top wall, 54in. from the side walls and 57.5in. from the bottom wall. These differences become more significant as the Mach number is increased and ultimately three separate reflections of the bow shock and nose compression can be distinguished.

It is useful first to note the most outstanding effects evident in Figure 26. These will then be analysed in detail in succeeding sections:

(1) All three sets of data agreed closely at $M = 0.96$ - both in their actual values of $\Delta p/H$ and in the trend of the variation of $\Delta p/H$ with Mach number. The only exception to this is the hole at 9.2D for which, although the same trends are evident, the actual values disagree (Fig. 26g). Since this is the nearest hole to the model base for which any direct comparison can be made, it is possible that the discrepancy in this case is due to the fact that the tests were not all made at the same Reynolds number. It is also possible that the difference is due to some fault in the model near this particular hole. Whatever the cause, it seems fairest to judge the interference effects at 9.2D by assuming that the values of $\Delta p/H$ for the 0.5% blockage model in the perforated tunnel should be increased by about 0.008; if this is done, reasonable agreement between the results at $M = 0.96$ exists as at other stations and also the results at the high Mach number end of the graph become more intelligible.

(2) There are various examples of the need for a blockage correction at high subsonic speeds close to $M = 1.0$ of the same sign as for an open tunnel - the correction being evidently larger for the perforated tunnel than for the slotted tunnel - see Section 5.5.

(3) The rearward movement of the terminal shock which for the small models reached the base by about $M = 1.015$ is delayed for the larger models particularly in the perforated tunnel where it does not clear the base until just beyond $M = 1.05$. This is analysed in Section 5.6 with reference to Figure 27.

(4) The subsequent interference effects are appreciably larger in magnitude in the slotted tunnel than in the perforated tunnel. The various reflected waves which travel down the models with increasing Mach number are shown in Figure 28.

(5) In the slotted tunnel, two strong reflected shock systems are evident and in between the passage of these the pressure does not recover to the zero interference value but to a value appreciably less than this, indicating a succession of reflected expansion waves of significant strength. Analysis has shown that the two shock systems are reflections of the wing leading-edge shock and of the bow shock (and nose compression) while the reflected expansions consist partly of reflections of the forebody expansion field and partly are a consequence of the strong bow shock reflection. The usual strength of these reflections varies between $\Delta p/H = |0.02|$ and $\Delta p/H = |0.04|$ and any given point on the body is subject to either expansion or compression reflections approaching this magnitude over a wide range of Mach number, e.g., from Figure 28, $x = 8D$ is subject to appreciable interference from $M = 1.04$ to $M = 1.20$.

(6) In the perforated tunnel, two reflected shock systems pass down the model and on analysis these appear to be reflections of the forebody expansion field in the top and side walls respectively. The strength of these shock reflections tends to be between $\Delta p/H = 0.01$ and $\Delta p/H = 0.015$ while all the other reflections which pass down the model tend to be weaker than this. In between the passage of these reflected waves, the body pressures in the perforated tunnel tend to revert fairly closely to the zero-interference values.

Summing up it would appear that the two main difference between the behaviour in the slotted and perforated tunnels as regards reflected waves are:

(a) The reflection of the bow shock (and nose compression) is much less severe in the perforated than in the slotted tunnel;

(b) In between the major shock reflections there is a long region of serious reflected expansion waves in the slotted tunnel and these do not exist to any comparable extent in the perforated tunnel.

General conclusions as to the relative merits of perforated and slotted walls cannot immediately be drawn however from these results; in particular it should be noted that the slotted tunnel has a very limited number of slots (one main slot in each wall and half slots at the corners - see Table II) and is unlikely in consequence to have any wave cancellation properties.

5.5 Blockage Effects

Blockage effects at high subsonic speeds near $M = 1.0$ can be deduced from considering the appearance and movement with increasing Mach number of the wing leading-edge

and trailing-edge shocks and of the terminal shock. Comparing results for the 0.5% blockage models with those at 0.06% blockage, the movement of the wing leading-edge shock across the hole at $x = 4.0D$, which occurs near $M = 0.98$, appears to be delayed by about 0.01 in Mach number in the slotted tunnel or 0.020 in Mach number in the perforated tunnel. The wing trailing-edge shock crosses the hole at $x = 6.8D$ near $M = 0.95$ and the delay in this is negligible in the slotted tunnel and about 0.01 in the perforated tunnel. The terminal shock crosses the holes at $x = 8.4D$ near $M = 1.00$ and the delay is about 0.01 in the slotted tunnel and about 0.02 in the perforated tunnel.

These results and others tend to suggest that blockage corrections of the same sign as for an open tunnel should be applied to both the slotted and the perforated tunnel results and that for these models the corrections should amount to about

ΔM = -0.01 at $M = 1.0$ in the slotted tunnel

and ΔM = -0.01 at $M = 0.95$ rising to about
-0.02 at $M = 1.00$ in the perforated tunnel.

If these corrections were applied, it seems that the results for the three cases for corrected Mach numbers* up to $M = 0.99$ would be in good agreement and that application of a simple correction to the indicated free stream speed would have been sufficient to correct the whole pressure distribution and not merely one feature in it. Thus, up to this Mach number, it is fair to interpret the interference as a simple blockage effect. It should be noted that the application of a blockage correction to the curves of Figure 26 results in a change both in Mach number and in $\Delta p/H$. In fact, near $M = 1.0$ a ΔM of -0.01 gives a change of -0.0062 in $\Delta p/H$. An example of the resultant shift is shown in Figure 26(a).

The theoretical corrections according to the formulae quoted earlier are as follows:

For M_0 = *1.00 in free flight*

M_0	for 0.5% blockage in perforated tunnel:	1.049
M_0	for 0.5% blockage in small slotted tunnel:	0.984
M_0	for 0.06% blockage in perforated tunnel:	1.020

These corrections are certainly not valid as they stand because the results for the 0.5% blockage model in the perforated tunnel at $M = 1.049$ contain various interference effects that cannot be eliminated by any simple Mach number correction. Broadly speaking, the results appear to confirm rather more clearly the conclusion drawn from the results at smaller blockage, viz., that the actual blockage corrections near $M = 1.0$ are smaller than those predicted according to these theories. They also show that the actual correction required in the slotted tunnel is of opposite sign to that predicted by the theory. The different distances of the tunnel walls away from the model in perforated and slotted tunnels helps to contribute to this latter

---

* It is possible that for larger, or for other shapes of model, the application of blockage corrections in this way will only be satisfactory up to lower Mach numbers.

result but it seems that this can only be part of the answer, and that the conclusion would remain valid if the comparison could be made for a given value of h/r^*.

5.6 Terminal Shock Movement

Figure 26(e-h) shows that in both the perforated and the slotted tunnels the rearward movement relative to the body of the terminal shock with increasing Mach number is retarded for the models at 0.5% blockage as compared with the smaller models. The actual movement is plotted in Figure 27(a). This shows that whereas the terminal shock has reached the base of the model by about $M = 1.01$ for the 0.06% blockage model, Mach numbers of about 1.035 and 1.055 are needed for the 0.5% blockage models in the slotted and perforated tunnels respectively.

Figure 27(b) shows that the strength of the terminal shock increases with Mach number up to about $M = 1.03$ and so the wall interference leads not only to a retarded shock movement but also to a stronger shock.

It appears that, up to at least $M = 1.03$, the terminal shock is a near-normal shock across the stream. In the perforated tunnel, the shock is evident in the tunnel wall pressure distributions at about the same longitudinal station as on the model body. The tunnel wall pressures also show that the position of this shock corresponds roughly to where the tunnel wall intersects the maximum expansion in the wing expansion field. This is confirmed by tracing back from the wall to the model along Mach lines based on the observed local Mach numbers at the wall and at the model. These conclusions are analogous to what has been observed in experiments on bodies of revolution in which it appeared that the position of the terminal shock was determined by where the tunnel walls inersect the expansion flow fluid originating from, say, the shoulder of an ogive-cylinder or cone-cylinder body. The present wing-combination can be thought of in terms of the equivalent body of revolution with a bulge taking the place of the wing. It would then be a simple extrapolation of the body results to say that the position of the terminal shock would be dictated by where the tunnel walls intersect the flow field associated with this bulge and this is precisely what the present results suggest. It follows that there will be less retarded movement of the terminal shock for a wing-body combination than for a simple body of revolution. It depends to a large extent on how far the last expansion region is ahead of the base.

The next question is whether this phenomenon is affected by whether the walls are perforated or slotted. A direct comparison of the present results is not possible because of the different distances of the tunnel walls away from the model (in terms of model diameters). A very crude attempt has been made to allow for this difference - the result is shown in Figure 27(a). This crude attempt has almost certainly overestimated the possible correction because effectively it has been assumed that the incident expansion waves from the model to the wall are swept at a constant angle whereas in fact, this angle will decrease with distance away from the model. In other words, the effect of moving the tunnel walls away from the model would be less than indicated by this correction. It follows from Figure 27 that the slowing down

of the terminal shock movement would appear to be rather more serious in the perforated tunnel than in the slotted tunnel*.

It may be wrong to generalise this last conclusion as it could well be a function of the actual open-area ratio of the open and slotted walls. Reduction of the open-area ratio to a very small value might be a means of eliminating the effect.

Tests were made in the perforated tunnel with the walls alternatively diverged up to 48 minutes or converged up to 24 minutes. These changes would affect the outflow from the walls and the boundary layer thickness on the walls but they did not appear to have any significant effect on either the terminal shock position or its strength.

There is one other peculiarity to be noted in the results for the perforated tunnel. Up to about $M = 1.03$, the terminal shock appears in the measured pressure distributions as a single shock (see, e.g., the results for $x = 9.2D$ in Figure 26g). At higher Mach numbers when the shock is further downstream, it seems as if the single shock has been replaced by a double shock system (see, e.g., the results for $x = 9.83D$ in Figure 26h for which there are two pressure maxima marked E and G). There seems to be no doubt that this change is a genuine experimental result and not experimental scatter because it has been confirmed in tests with the model in both longitudinal positions in the tunnel and also in the various supplementary tests with walls diverged or converged. It was thought at first that the appearance of this double shock system might be related to the different distances of the top and bottom walls from the model but a quantitative analysis showed that it was not possible to correlate the results on this basis. It seems therefore that instead of there being a single near-normal terminal shock, this is replaced beyond about $M = 1.03$ by a double shock system originating from about the same point on the tunnel wall but with one limb sloping forward and the other limb sloping rearward. An effect such as this has been observed in the schlieren photographs obtained during tests on a body of revolution in the Ames 2ft transonic tunnel - this can be seen by comparing the pictures for $M = 1.02$, 1.04 and 1.06 for the 0.25% blockage model in Figure 12 of Reference 15. Further evidence in support of this suggestion is that, as shown in Figure 27(b), beyond the Mach number at which this change is thought to occur, the strength of these shocks appears to decrease with Mach number whereas up to this point it has been steadily increasing.

One can be fairly confident therefore that a change of this nature has occurred. It is more difficult however to explain why. A tentative suggestion might be that the rearward limb is due to the wing expansion field reflecting from the perforated wall

---

* This might have been expected on grounds of continuity of effects through the Mach number range: on the one hand, it has already been seen that the blockage corrections appear to be greater in the perforated tunnel and later it will be seen also that the reflection characteristics are dominated by reflections of shocks in a slotted tunnel and of expansion fields in a perforated tunnel. Henc it could be argued that in the perforated tunnel it is the inability of the wall to cope with the wing expansion field that leads to the terminal shock effect, whereas in the slotted tunnel it is the additional inability of the wall to cope with the wing trailing-edge shock. If this is a valid comparison, then it would also suggest that the retarded shock movement should be greater in the perforated tunnel since the wing expansion field is of course ahead of the wing-trailing-edge shock.

as a shock in the same way as it will be seen later the forebody expansion reflects. It is not possible however to think of the forward limb as a reflection because, as looked at from the wall, it is sloping forward. It must therefore be regarded as an incident disturbance which would not be in this position if the tunnel walls were absent, i.e. it seems that the terminal shock is tending to become an oblique shock as the Mach number increases. It would be of interest to carry out a further test with the body of the model extended rearward so that the further development of this effect with increasing Mach number beyond $M = 1.05$ can be studied. The effect is important because it accentuates the slowing up of the terminal shock movement.

5.7 Reflections of the Wing Leading-Edge Shock and Forebody Expansion Field

After the passage of the terminal shock down the body, the next serious disturbance in both the slotted and the perforated tunnels is a further shock system. This can be seen in Figure 28, where it is labelled D in the slotted-tunnel results and C in the perforated-tunnel results. Beyond about $M = 1.03$, in the perforated tunnel, there are two shock disturbances labelled C, viz., C_T and C_S; analysis indicates that these are related to the same feature in the incident flow field, C_T being the reflection in the top wall and C_S being the reflection in the side walls and bottom wall. In addition the curves of $\Delta p/H$ against Mach number (Fig. 26) for the 0.5% blockage model in the perforated tunnel suggest that between the terminal shock and the reflection C_S and again between the reflection C_S and C_T some reflected expansion waves may be present. These are labelled D_S and D_T in Figure 26. In the slotted tunnel the shock is followed by an extensive expansion labelled C.

At first sight it might be thought that the reflected shocks C and D in the perforated and slotted tunnels were both due to the same cause, but the following simple analysis suggests that this is not so. Approximate sources of the disturbances can be found if one traces back from the disturbance on the model to the wall and then back to the model, assuming that both the incident and reflected waves are propagated at the Mach angle for the free-stream Mach number. The indicated sources of reflected shocks, together with the sources of the neighbouring reflected expansions, are shown in Figure 29. It will be seen that disturbances D in the slotted tunnel and D_S and D_T in the perforated tunnel appear to originate from the region on the body which corresponds to the position of the leading-edge shock (Fig. 24), whereas the disturbance C_S and C_T in the perforated tunnel and C in the slotted tunnel originate from further forward on the body, in the region of the nose body expansion. Although the analysis based on Mach angles considerably oversimplifies the tracking of the disturbances, the separation on Figure 29 of the sources of the disturbances labelled D from the disturbances labelled C can be taken as evidence that these disturbances originate from the wing leading-edge shock and the forebody expansion respectively. This being so, it is interesting to note that in the perforated tunnel the reflections of the wing leading-edge shock D_S and D_T appear as expansions whereas the reflection in the slotted tunnel D appears as a shock; also, in the perforated tunnel the disturbances originating from the forebody expansion C_S and C_T appear as discrete shocks, while in the slotted tunnel they are a wave of expansions.

The relative strength of these reflected waves is plotted in Figure 30. Various factors affect the variation of wave strength with Mach number, e.g., the variation

in strength of the incident disturbance, the variation in the alleviating properties of the walls, the gradual disappearance of a focussing effect, particularly in the nearly square slotted tunnel and so on. Hence there is not much point in saying more than that the leading-edge shock reflects as a shock with a strength of about $\Delta p/H = 0.03$ in the slotted tunnel and as expansions with a strength of about -0.005 in the perforated tunnel while the forebody expansion leads to expansion reflections in the slotted tunnel with a strength of about 0.02 and a shock of strength of about 0.013 - 0.018 in the perforated tunnel.

This radical difference in behaviour between the slotted and perforated tunnels is in qualitative agreement with what has generally been observed elsewhere. Since no corresponding results are available for a closed wall tunnel, it is not possible to say whether the slotted walls are affording any great alleviation of the reflection of the leading-edge shock. All that can be said is that the perforated walls are much better in this respect than these particular walls with a very limited number of slots. As regards the reflections of the forebody expansion, it is not so easy to draw a distinction as to which type of wall is superior. There is still however one point in favour of the perforated wall. This is that since the forebody expansion reflects as a shock originating from near where the wall intersects the end of the expansion, the reflected disturbance is clear of the model sooner than in the case of the slotted tunnel where expansion waves are reflecting from the walls from even the upstream end of the expansion zone.

The results for the perforated tunnel are really an indication that these particular perforated walls are too open to cope with either the leading-edge shock or the forebody expansion. One means of altering the wall characteristics is to converge the walls: this implies an increased outflow and a reduced boundary layer thickness. The effect of converging the walls by 24 minutes is shown in Figure 30. It can be seen that converging has given some improvement for both sets of reflections. As already pointed out, the weak reflections of the leading-edge shock are difficult to determine from the graphs of $\Delta p/H$ against Mach number (Fig. 26) and so not too much notice should be taken of the apparent result that with the walls converged 24 minutes, reflections of the leading-edge shock are virtually eliminated. The improvement with convergence seems to be genuine, however. As regards the more serious shock reflections of the forebody expansion, the small improvement due to convergence is sufficient not to be dismissed as experimental scatter but it is not sufficient to alter the picture materially. It seems likely that a considerable reduction in open-area ratio below the existing value of 22.5% or a much greater amount of convergence will be needed but both these changes would make it much more difficult to obtain a satisfactory axial Mach number distribution in the empty tunnel.

The character of the reflections in the small slotted tunnel, namely shock as shock and expansion as expansion, may appear to indicate that the open-area ratio of the walls is too small for effective wave-cancellation. Another important factor in this case however is probably the limited number of slots, and proper assessment of the possibilities of wave-cancellation in a slotted tunnel will have to await tests with typical multi-slot arrangements.

5.8 Reflections of the Bow Shock and Nose Compression

As already mentioned, Figure 26 shows that the reflections of the bow shock and compression near the nose appear to be stronger for the 0.5% blockage model in the

3ft × 3ft slotted tunnel than for the 0.5% blockage model in the 9ft × 8ft perforated tunnel. The apparent strengths of the reflections of the bow shock in the two cases are plotted against Mach number in Figure 31.

Considering first the results for the slotted tunnel, it will be seen that the strength of the shock reflection is always greater than 0.02 in p/H and for Mach number up to 1.10 it is between 0.03 and 0.04 in p/H. Once again, the variation of strength with Mach number is dependent on several factors but it seems likely that the primary factor which results in the decrease of reflected shock strength with increasing Mach number up to about $M = 1.15$ is the gradual disappearance of the focussing effect. In this case, the pressure holes on the top of the body are 16.25in. away from the top wall, 18in. from the side walls and 19 25in. from the bottom wall of the tunnel. The difference between these figures is of little consequence at $M = 1.05$, say, but is becoming very significant at $M = 1.15$. The best way to see this is to contrast the shape of the perturbation in the $\Delta p/H$ vs Mach number curves for say $x = 4D$, 6D and 7.6D (Figs. 26(a,c,e)). At $x = 4D$, the shock reflection (A) only affects the pressure at the hole over a range of about 0.03 in Mach number but for $x = 7.6D$, the effect is spread over at least about 0.08 in Mach number. It is probable that by $M = 1.15$, the reflections from the different walls are sufficiently well separated when they pass over the top of the body for the strength of the reflection as plotted in Figure 31 to be effectively the strength of the reflection from a single wall. The subsequent increase in this strength with further increase in Mach number may be largely related to the increase in strength of the incident bow wave.

There is evidence in the slotted tunnel results (Fig. 26) of reflected expansion waves ahead of the bow shock reflection. The origin of these cannot be definitely placed. One possibility is that when a strong compression wave system such as the bow shock and nose compression region is incident on the slotted wall, it gives rise not merely to the shock reflections but also to an associated fan of expansion waves. It is on the basis of such an explanation that the peak expansion reflections have also been labelled A in Figure 26. Alternatively, a simpler explanation would be that the reflected expansion waves are due to the ineffectiveness of the slotted walls in cancelling the forward part of the forebody expansion field; this explanation, if correct, would strengthen the argument of the previous section that in a slotted tunnel reflections of the forebody expansion occur from points corresponding to the whole length of this expansion.

In the perforated tunnel, the reflections of the bow shock in the different walls of the tunnel can be easily distringuished above about $M = 1.08$ and so it is probable that the variation of $\Delta p/H$ with Mach number plotted in Figure 31 is a fair indication of the strength of the reflection from either the top wall or the side wall and not from the two in combination; any focussing effect should be absent above $M = 1.08$. It will be seen that at low supersonic Mach numbers the shock is reflecting as an expansion, i.e., as already seen in various other respects, the tunnel is too open to give interference-free data at these Mach numbers. Beyond about $M = 1.10$, the bow shock tends to reflect as a shock but by comparison with the results from the slotted tunnel the perforated walls are evidently giving a good deal of alleviation. It is also possible to think in terms of one reflected wave rather than a whole set of associated reflections as in the slotted tunnel.

The precise variation of strength of the bow shock reflection with Mach number in the perforated tunnel is once again a function of several variables but an important factor in this case is the variation with Mach number of the local open-area ratio of the walls at the points where wave reflection is occurring. For any given Mach number, this open-area ratio is in general not the same for the top wall as for the side walls and also it is not the same for the model in the forward and in the rear positions. This is why the variation in strength of the bow-shock reflections with Mach number for the perforated tunnel has had to be plotted in Figure 31 as a band rather than as a single curve. Individual points within this band as derived by analysis of such curves as those shown in Figure 26 are also given. The band does not indicate scatter; it is analysed below in Section 5.8.1 in terms of the appropriate local open-area ratio.

One other point emerged from the analysis of the bow-wave reflections, applying equally to both the slotted and the perforated tunnels. This was that the results confirm that a simple analysis based on tracing the reflected and incident shocks along the Mach angle of the free stream and assuming that reflection occurs at the wall is not an adequate method of predicting the position of the reflected shock. For example, analysing the bow shock reflections for the 0.5% blockage model in the perforated tunnel would place the bow shock 1.8D ahead of the body nose at $M = 1.07$ and 1.0D ahead at $M = 1.15$ whereas theory would have predicted 0.3D and 0D (i.e. attached) at these Mach numbers. Part of the discrepancy is no doubt due to curvature of the bow shock and also possibly to the bow shock being further ahead than theory would predict. It is also possible, however, that some of the discrepancy is due to the reflection process: reflection may be effectively occurring some distance from the tunnel wall, e.g., at the edge of the tunnel wall boundary layer. When evidence from other tests is available, it will be worth analysing these effects in more detail. For the present, it is worth noting that the simple analysis referred to above would have under-estimated the Mach number at which the reflected shock is clear of the base of the 0.5% blockage model by about 0.04.

5.8.1 Effect of Open-Area Ratio: Perforated Tunnel

Figure 32 has been prepared to show the variation with Mach number in the open-area ratio of the walls at the point where reflection of the bow shock and nose compression occurs for the 0.5% blockage model. It can be seen that in this respect the difference between the model forward and rear test positions is quite significant and that taking into account the results for the two positions and for the top and side walls respectively, one can obtain four points on a curve of reflected wave strength against open-area ratio at a given Mach number. Such curves for both the bow shock and nose compression are given in Figure 33. As would be expected, there is a fair amount of scatter in Figure 33 but the trends appear to be quite unmistakable.

Increasing the open-area ratio at a given Mach number reduces the strength of a shock reflection and tends to turn it into an expansion reflection. Increasing Mach number at a given open-area ratio increases the strength of a shock reflection. These two conclusions have been stated implicitly several times earlier in the paper but Figure 33 is the first time it has been possible to express the statements in quantitative terms.

The precise variation of, say, $\Delta p/H$ with open-area ratio for a given Mach number depends of course on the strength and nature of the incident wave being reflected and

that is why the curves in Figure 33(a) for the bow shock are not necessarily parallel to the curves in Figure 33(b) for the nose compression. One result, however, should be reasonably independent of the strength of the wave being reflected. This is the variation with Mach number of the open-area ratio that is required to cancel the reflected wave completely. This variation has been derived from the curves of Figure 33 and is plotted in Figure 34. It will be seen that the results derived from the bow shock and from the nose compression curves are not quite the same but the order of agreement is reasonable in view of the analysis on which the results are based.

The degree to which the ARA tunnel satisfies the requirements for shock cancellation should be judged by a comparison between Figure 34 and Figure 32 (the rear position is typical of most models). It will be seen that the most serious deviation between the actual and required open-area ratios exists for the side walls which are appreciably too open to cope with the reflections of the bow-shock and nose-compression regions at Mach numbers near $M = 1.10$. During the calibration of the tunnel[6], the open-area ratio of the side walls was appreciably reduced just ahead of this region in order to improve the Mach number distribution in the empty tunnel, and it was indeed suggested in Reference 6 that this reduced open-area ratio could perhaps with advantage have been extended rearward. The present results show that this would be beneficial for better alleviation of the bow shock reflection.

One last point about the curve in Figure 34 is that it should not be taken to apply to any perforated wall: the walls of this perforated tunnel have 0.5in. diameter holes in a plate thickness of 0.187in. and the curve of Figure 34 may strictly apply only to walls of about this ratio of hole diameter/plate thickness. Also it should be remembered that the suction quantities being used at Mach numbers of 1.14 and above are relatively small because the tunnel has a flexible nozzle to generate the supersonic flow. If, for example, a Mach number of 1.20 had to be generated by suction only, the outflow through the walls would be greater and the open-area ratio required for wave cancellation would probably be smaller than shown by Figure 34.

5.8.2 *Effect of Wall Convergence: Perforated Tunnel*

The effects of converging the side walls are illustrated in Figures 35 and 36. The results in Figure 36 are typical of those obtained at other holes and it will be seen that the most obvious result is that converging the walls appears to have given a large reduction in strength of the expansion reflections (B) from the side walls. These are the reflections of the nose compression. This improvement cannot however be taken at its face value because converging the side walls also materially affects the empty tunnel[6] Mach number distribution in the region of the model. Over much of the model, the stream Mach number corresponds reasonably with that based on the static pressure in the plenum chamber but the Mach number near the nose of the model can be significantly lower than this, e.g., for $M = 1.06$, $M_{nose} = 1.043$ and for $M = 1.08$, $M_{nose} = 1.058$. As a result, the bow shock and nose compression waves at a given stream Mach number intersect the tunnel walls further forward when the walls are converged* than when they are parallel and hence the open-area ratio of the wall at the point of reflection is not as great. As already shown, this in itself should

---

* This is confirmed by the fact that, as shown by the results in Figure 36, the Mach number at which any reflected wave crosses any given hole position is higher than when the walls are converged.

reduce the strength of the reflected waves and when allowance has been made for this, Figure 35 shows that the remaining effect which can be ascribed to wall convergence is relatively slight.

It will be realised that if there was any case for operating the tunnel with walls converged, an attempt would have had to be made to modify the open-area ratio distribution along the walls to give a better Mach number distribution, tunnel empty. If this had been successfully accomplished, the open-area ratio effect noted above would have been eliminated and it seems probable that only a small improvement with walls converged would have then been achieved as compared with the present results, walls parallel.

Some further direct evidence as to the effects of wall convergence is required. One way of possibly obtaining this would be to test the small blockage model in the perforated tunnel with the walls converged. This model would be situated sufficiently far back in the working section for the Mach number distribution across the model station to be fairly reasonable whether the walls were converged or not and so the effects of wall convergence would be determined unimpaired by changes in other variables. As shown earlier in Section 5.3, the principal interference effects with the small model are due to the bow shock reflecting as expansion waves and it is this characteristic which it might be hoped wall convergence might improve.

5.9 Summary of Main Effects

The main conclusions of this section can be summarised as follows:

(1) It appears that for Mach numbers close to $M = 1.00$ a blockage correction of the same sign as for an open tunnel is needed. The value of this correction is of the order of $\Delta M = 0.02$ for the perforated tunnel and $\Delta M = 0.01$ for the slotted tunnel and if such a correction is applied the pressure distributions for corrected Mach numbers up to $M = 0.99$ for all the models can be brought into reasonable agreement.

(2) For the models at 0.5% blockage, the rearward movement of the terminal shock with increasing Mach number (with an associated strengthening of this shock) is retarded in both types of tunnel and it seems that this effect is somewhat more pronounced in the perforated tunnel. Beyond an uncorrected Mach number of about $M = 1.03$, the single near-normal terminal shock appears to divide into two with one limb sloping forward and the other limb sloping rearward.

(3) The subsequent wave reflections are much stronger in the slotted tunnel than in the perforated tunnel. At Mach numbers below 1.10, this is partly because the slotted tunnel is very nearly square and a focussing effect of the reflections from different walls is therefore present; the limited number of slots also affects its wave-cancelling properties.

(4) In the slotted tunnel, shocks reflect as shocks and expansions as expansions; there is also the possibility that a strong reflected shock will have an associated fan of reflected expansion waves.

(5) In the perforated tunnel, expansion fields reflect as a single shock originating from near where the wall intersects the end of the expansion region; no serious reflections originate from further forward in the expansion zone.

(6) In the perforated tunnel, incident compression waves can reflect either as shocks or as expansion waves according to whether the open-area ratio is less than or greater than the curve plotted against Mach number in Figure 34. Small improvements can be effected by converging the walls.

An indication of the significance of the interference effects on the overall pressure loadings at zero incidence can be obtained by comparing the pressure distributions at selected Mach numbers with the non-interference distributions from Figure 24. A comparison is made in this way in Figure 37(a-f) for the 0.5% blockage model in the perforated tunnel at a representative selection of Mach numbers. The effects are not insignificant at Mach numbers from 1.0 to 1.04, particularly near the shoulder and over the rear part of the body, but they have become smaller by $M = 1.10$.

6. ANALYSIS OF OTHER PRESSURE DATA

6.1 Base Pressure

Figure 38 gives a comparison between the variation of base pressure with Mach number for the 0.5% blockage models in the perforated and small slotted tunnels, once again compared with the results at 0.06% blockage in the perforated tunnel as a datum. The results for the 0.06% blockage are, incidentally, in very close agreement with the results obtained in free flight and for the small blockage model in the large slotted tunnel. For correlation with the results just discussed the base pressure is plotted as $\Delta p/H$, i.e., as a difference from free-stream static pressure.

The base pressures measured in these different cases do not exactly agree either at low speeds or at high speeds, i.e., where interference effects might be expected to be small. This is thought to be due to differences in the sealing of the model at the base and as a result interference effects have to be judged by considering the Mach number at which variations occur and by the magnitude of these variations, rather than by considering the value of $\Delta p/H$ for a given Mach number.

Figure 38 shows that the variation of base pressure with Mach number near $M = 1.00$ for the models at 0.5% blockage is quite different from that observed for small blockage. It is possible to explain the different variation in terms of the different terminal shock movements for the various models. It seems that when the terminal shock is lying well upstream of the base, the base pressure tends to decrease with Mach number. This trend is evident up to about $M = 0.94$ for the 0.06% blockage model and up to about $M = 1.02$ for the 0.5% blockage model in the perforated tunnel and similarly up to about $M = 1.01$ for the 0.5% blockage model in the small slotted tunnel. Next, when the terminal shock is nearer the base but just upstream of it, the base pressure increases and then, finally, when the terminal shock is lying downstream of the base, the base pressure decreases to a value that is considerably less than at high subsonic speeds. For the model at small blockage, it has already been seen that the terminal shock reaches the base by $M = 1.015$ and so the above succession of changes in base pressure occur relatively rapidly and are complete by about $M = 1.03$.

For the models at 0.5% blockage, the terminal shock does not reach the base until near $M = 1.03$ in the small slotted tunnel or $M = 1.05$ in the perforated tunnels (Fig. 27) and the base pressure data are consistent with these figures, e.g., in the small slotted tunnel the changes in base pressure are complete by about $M = 1.055$ and in the perforated tunnel by about $M = 1.08$. There is however one significant difference between the results for the slotted and perforated tunnels. In the slotted tunnel, the increase in base pressure as the terminal shock passes over the edge of the base is quite marked (about 0.02 in $\Delta p/H$) whereas in the perforated tunnel the effect on $\Delta p/H$ is appreciably less (about 0.01); on the other hand, the effect extends over a much greater Mach number range. This last result is consistent with what was said in Section 5.6 and confirms the impression that in the perforated tunnel, beyond about $M = 1.03$, the single near-normal terminal shock is replaced by a double shock system and consequently a larger Mach number range is needed for this double shock system to pass over the base. The comparative results for the slotted tunnel tend to suggest that this phenomenon does not happen - at least in these tests - in the slotted tunnel where the terminal shock that passes over the base is still a single strong shock.

It is perhaps worth mentioning that one other possible type of explanation for the different variation of base pressure with Mach number near $M = 1.00$ has been investigated and rejected. It was felt originally that it might be due to some upstream influence from the rear end of the working section since at Mach numbers close to $M = 1.0$, if the auxiliary suction and fan pressure ratio are not correctly adjusted, the Mach number distribution in the tunnel downstream of the model will not be constant. Alterations were deliberately made to the combination of auxiliary suction and fan pressure ratio to investigate this but these changes had no effect on the variation of base pressure with Mach number.

It thus seems reasonable to conclude that, as just explained, the different trends near $M = 1.00$ are related to the retarded movement of the terminal shock. The spurious decrease in base pressure for the large models in between $M = 0.96$ and about $M = 1.02$ does not therefore indicate that some disturbance is crossing the base; rather, it is a consequence of the terminal shock lying too far upstream of the base. With a boat-tailed afterbody, these errors near $M = 1.0$ would of course apply to the afterbody pressures and hence to the drag as well as just the base pressure. In some experiments, therefore, these particular effects could determine the limiting Mach number beyond which the tunnel results were thought to be unreliable.

At higher Mach numbers, the base pressure is affected when reflected waves cross the base of the model. Figure 38 suggests that these effects are very much greater in the slotted tunnel than in the perforated tunnel. For example, the measured base pressure terms of $\Delta p/H$ for the 0.5% blockage model in the small slotted tunnel appear to be about 0.05 low at Mach numbers near $M = 1.15$: this corresponds to the speed at which the expansion reflections of the forebody-expansion cross the base. In the perforated tunnel, on the other hand, the reflected-wave effects on base pressure once the terminal shock has passed appear to be definitely less than $|0.01|$ in $\Delta p/H$.

6.2 Wing Pressures

The results obtained for a pressure point near the wing root trailing edge were very similar to those at a corresponding position on the top of the body and so need not be discussed here.

The results obtained for a pressure point at 0.95c and 0.7 × semispan are however very interesting and are plotted in Figure 39. This hole is situated 7.45D downstream of the body nose and 1.88D out from the model centre line. Broadly speaking, therefore, the results should be comparable with those obtained for the 7.6D hole on the top of the body (Fig. 26e) and a comparison of the two figures shows that the agreement is remarkably close. This is, in fact, the most important conclusion from Figure 39 as, without this evidence, it might have been argued that deductions from the body pressures need not have borne much relation to developments on the wing and need not therefore have given a reliable indication of possible interference effects on the overall forces and moments.

Small differences in detail are to be expected between Figure 26(e) and Figure 39. As regards reflections from the top wall, the wing hole should correlate best with what is observed on the body at the station slightly further upstream, i.e. nearer 7.2D, whereas as regards reflections from the side walls the wing hole results should correlate with a position further downstream on the body, between 7.6D and 8.0D. One result of this is that the shock reflections of the forebody expansion, C_g and C_T , which are evident as separate perturbations in the results for the body hole (Fig. 26c) are only evident as one perturbation in the results for the wing hole in Figure 39. Other similar but less important examples could be quoted.

As regards the actual strength of the reflected waves, these appear to be of the same order over the wing as above the body but since data for only one hole are available it would not be profitable to analyse these in detail.

7. CORRELATION OF PRESSURE AND OVERALL FORCE RESULTS

In conclusion, some examples can be quoted of where the interference effects discussed in the analysis of the pressure measurements can be seen to have influenced the overall force and moment results. These will now be discussed briefly.

7.1 Blockage Effects

These were deduced from the body pressures and Figure 39 shows that similar effects are present on the wing. They are largest for the 0.5% blockage model in the perforated tunnel for which the correction is of the order of 0.01 in Mach number at $M = 0.95$ and 0.015 at $M = 0.99$. This correlates fairly well with the comparison in Figure 19 of the zero-lift drag of the 2½in. and 7in. models in the perforated tunnel which showed that for the larger model the early part of the drag rise appeared to be delayed by about 0.01 in Mach number. The lift and moment results also tend to show the same characteristics but somewhat less clearly.

7.2 Terminal Shock Movement

Apart from its effect on base pressure, this has not had a very pronounced effect upon the overall results for the present wing-body combination but this is purely because the rear part of the body is parallel. However, one important result from the pressure analysis is that the delay in shock movement appears to be related to where the walls intersect the wing expansion field and so, whatever the configuration, this phenomenon should not materially affect the pressures over a wing unless it is

very highly swept back. Its principal effects will be on afterbody pressures and on the flow over a tailphane or fin (see Section 7.3.2).

7.3 Reflected Waves

The two most serious consequences of the reflected waves interfering with the flow field around the model are their effects on drag and on the flow over any tail surface placed behind the wing.

7.3.1 Effects on Drag

The results for the perforated and small slotted tunnels as plotted in Figures 19 and 14 are in good qualitative agreement with effects deduced from the pressures and in particular from the pressures for the hole on the wing, as plotted in Figure 39.

In qualitative terms, it has often been noted that for a model in a slotted tunnel the measured drag at Mach numbers just above $M = 1.00$ is too low, while later, at Mach numbers near, say, $M = 1.10$, the measured drags are too high, whereas in a perforated tunnel the second of these effects is not observed. This difference can be related to the fact that strong expansion reflections originating from the forward part of the forebody are present in the slotted tunnel but not in the perforated tunnel. This can be seen by correlating the results in Figures 39, 14 and 19.

In detail, in the slotted tunnel, the drag at Mach numbers between $M = 1.00$ and 1.05 for the 0.5% blockage model is too low and this is associated partly with the reflection of the leading-edge shock crossing the aft part of the wing and partly with the reflections of the forebody expansion crossing the forward part of the wing. The excess drag measured between about $M = 1.05$ and $M = 1.12$ is associated with the reflections of the forebody expansion crossing the aft part of the wing and the fact that the drag is too low at Mach numbers between $M = 1.12$ and 1.20 is associated with the reflections of the bow shock and nose compression passing over the wing. As expected from the analysis of the pressures, therefore, the drag is significantly in error throughout the range from $M = 1.0$ to $M = 1.2$ and the more serious effects appear to be related to the strong expansion reflections crossing the wing.

In the perforated tunnel the drag as measured for the 0.5% blockage model is too low up to about $M = 1.08$ and this appears to be largely due first to the blockage effect noted above and then later to the strong shock reflections originating from the end of the forebody expansion. The differences above $M = 1.08$ are small and are presumably related to the passage of the other reflected expansion waves across the wing.

7.3.2 Effects on the Flow over a Tailplane

This problem has been studied by a special test made in the perforated tunnel. The model arrangement for this test is shown in Figure 40. The 2½in. model was mounted above the rear part of the 7in. model thus simulating a high tailplane arrangement. It was tested in two alternative longitudinal positions. In its forward position, the base of the 2½in. model was at the same station as the base of the 7in. model; in the rear position, its base was 5in. further aft. The point of

testing the pseudo-tailplane in two fore-and-aft positions was that differences between the characteristics in the two positions should be largely a function of the tunnel interference effects since the changes in downwash and dynamic pressure with such a small change in axial position should be relatively slight. The actual test results showed that this argument did not remain quite true in practice because, when in the rear position, the flow over the wings of the small model became influenced by the flow around the base of the large model.

Some typical results from this test are shown in Figure 41. The normal force measurements on the small model have been analysed to give effective values of downwash which are plotted against Mach number for different incidences of the main model. For these particular results, the two models were set at the same incidence, i.e. they refer to effectively $\eta_T = 0^\circ$; results from a second series of tests with $\eta_T = 3^\circ$ appeared to tell roughly the same story as regards interference effects.

The effective downwash for $\alpha = 0^\circ$ should be virtually zero and with the tailplane in the forward position this is shown to be true up to $M = 0.98$ and at the highest test Mach number (1.18). With the tailplane in the rear position, the effective downwash at Mach numbers up to $M = 0.98$ is about 0.35° and this difference is thought to be due to the influence of the flow around the base of the large model.

In the present context, it is more important to note that with the tailplane in the forward position an effective downwash of about 0.15° is produced near $M = 1.00$ to 1.02 and a downwash of about 0.45° near $M = 1.10$. Similar effects can be observed for the tailplane in the rear position at somewhat higher Mach numbers, e.g., near $M = 1.04$ and $M = 1.16$ respectively. The delaying of the effects to higher Mach numbers with the tailplane in the rear position is consistent with interpreting the effects on the basis of reflected waves interfering with the flow over the tailplane. The additional changes with Mach number apparent in the downwash derived from the tailplane in the rear position do not correlate with corresponding effects for the forward position and therefore are probably due to changes in the flow expansion around the base of the large model.

The interference near $M = 1.00$ to 1.04 which leads to a maximum downwash of about 0.15° would seem to be related to the movement of the terminal shock across the tailplane. In magnitude it is of the same order as might have been expected on the basis of the pressure measurements. From Figure 27 the pressure rise across the terminal shock is of the order of 0.025 in p/H and the flow deflection through a shock of this strength would be expected to be not more than 0.1° to 0.2°.

The more serious effect is the 0.45° change in downwash which occurs near $M = 1.10$ to 1.16 , according to tailplane position. The most likely explanation for this is that when it happens the tailplane is ahead of the reflection of the forebody expansion from the bottom wall and behind the corresponding reflection from the top wall. This has been confirmed by a quantitative analysis based on the pressure measurements of Figure 26, etc. Also, the magnitude of the effect, i.e. about 0.45°, correlates well with the observed strength of these reflections (at $M = 1.10$, for example, the flow deflection through a shock with a pressure rise of about $\Delta p/H = 0.015$ would be expected to be about 0.45°). The Mach number range over which this spurious downwash is present is, therefore, a function of the relative position of both the forebody and tailplane with respect to the top and bottom walls of the tunnel. If both the

body centre line and the tailplane had been on the centre line of the tunnel, this effect would not have been present; similarly, the further the tailplane is displaced from the tunnel centre line, the greater the Mach number range over which the downwash is in error.

It is also of interest to compare results obtained from different model incidences, particularly in view of the fact that no analysis has yet been made of the pressures measured at non-zero incidences. The downwash results in Figure 41 suggest that the nature of the interference effects remains substantially the same over the incidence range shown, i.e., $\alpha = -3^{\circ}$ to $+6^{\circ}$, but that incidence evidently has some effect on the strength and possibly position of the reflections of the forebody expansion field. The results at $M = 1.10$ for the tailplane in the forward position suggest that these effects become less important with increasing positive incidence but analysis of the pressure results will be needed before this can be properly explained. Broadly speaking, however, the effect on $\partial\epsilon/\partial\alpha$ seems to be less than the effect on ϵ at given α.

No corresponding experiment has been performed in the small slotted tunnel. Since the nature of the wave reflections is radically different, it is difficult to forecast what the corresponding picture to Figure 41 would look like. The reflected waves are stronger and the possibility of flow deflections of the order of 1° or more exists, but on the other hand the Mach numbers at which a tailplane would be cut by reflections from the top and bottom walls respectively would not be as different as in the perforated tunnel.

8. CONCLUDING REMARKS

From the results so far obtained, it is apparent that much useful information on interference effects is being obtained from the current programme and more is to be hoped for as the tests planned are completed. The proposed extension of the tests to models of higher blockage ratios should assist in the assessment of the interference effects on overall forces, which have in general proved to be small: clearer understanding of the larger effects obtained in some cases at higher incidence can also be looked for. The analysis of the body pressure measurements has shown the nature of the wave reflection interference effects at zero incidence for particular slotted and perforated wall tunnels. Similar analysis is required of pressures at incidence, and of the wave-cancelling properties of other tunnels, particularly the RAE 8ft x 6ft tunnel with many-slotted walls. In addition, as some of the most serious interference effects are on drag and on the flow over the rear part of the body, tests with different afterbody shapes and tailplane arrangements would be useful.

ACKNOWLEDGEMENTS

Acknowledgement is made of the assistance and advice of staff in the different facilities concerned with the programme, both in obtaining the test data and in the preparation of this paper. Acknowledgement is made in particular to Mr. E.P. Sutton of Cambridge University for his part in planning the programme, to Messrs. P.G. Hutton, J.G. Wingfield and K. Rollins of ARA for the perforated-tunnel results, to Messrs. D.J. Harper and C.N. Hall of PAE for the large slotted tunnel results, and to Mr. G.H. Greenwood of RAE for the free-flight results.

REFERENCES

1. Roe, F.E. — *Some Aspects of Transonic Tunnel Operation in Industry.* Jour. Roy. Aero. Soc. Vol. 62, January 1958.

2. Sutton, E.P. — *Wing Tunnel Interference Effects at Transonic Speeds in a Slotted Working Section for Bodies With and Without Wings.* M.O.S. Unpublished report.

3. O'Hara, F. — *The Assessment of Results Obtained in Transonic Wind Tunnels.* Jour. Roy. Aero. Soc. Vol. 62, January 1958.

4. Taylor, R.A. McDevitt, J.B. — *Pressure Distributions at Transonic Speeds for Parabolic-Arc Bodies of Revolution Having Fineness Ratios of 10, 12 and 14.* NACA Tech. Note 4234, March, 1958.

5. Hills, R. — *Design and Operational Problems of the Electrically-Driven Transonic Wind Tunnel.* Jour. Roy. Aero. Soc. Vol. 62, January 1958.

6. Haines, A.B. Jones, J.C.M. — *The Centre Line Mach Number Distributions and Auxilliary Suction Requirements for the ARA 9ft × 8ft Transonic Wind Tunnel.* ARA Report No. 2, April 1958.

7. Vessey, H.F. — *Transonic Wind Tunnel Testing Techniques: Historical and General Introduction.* Jour. Roy. Aero. Soc. Vol. 62, January, 1958.

8. Sutton, E.P. et alii — *Performance of the 36in. x 35in. Slotted Transonic Working Section of the RAE Bedford 3ft Wind Tunnel.* M.O.S. unpublished report.

9. Sutton, E.P. — *The Development of Slotted Working Section Liners for Transonic Operation of the RAE Bedford 3ft Wing Tunnel.* ARC R & M 3085.

10. Kirk, J.A. — *Design and Operational Problems of the Transonic Jet-Driven Wind Tunnel.* Jour. Roy. Aero. Soc. Vol. 62, January 1958.

11. Squire, L.C. Standbrook, A. — *The Influence of a Model on Plenum Chamber Indication of Mach Number in a Slotted Wall Wind Tunnel.* ARC Current Paper 395.

12. R.Ae.S. — Royal Aeronautical Society Data Sheets.

13. Maeder, P.F. Wood, A.D. — *Transonic Wind Tunnel Test Sections.* Z.A.M.P. Vol. VII, 1956.

14. DuBose, H.C. — *Experimental and Theoretical Studies on Three-Dimensional Wave Reflection in Transonic Test Sections. Part II: Theoretical Investigation of the Supersonic Flow Field About a Two-Dimensional Body and Several Three-Dimensional Bodies at Zero Angle of Attack.* AEDC TN-55-43 (AD-83539), March, 1956.

15. Page, W.A. — *Experimental Study of the Equivalence of Transonic Flow about Slender Cone-Cylinders of Circular and Elliptic Cross Section.* NACA TN4233, April, 1958.

16. Rogers, E.W.E. Hall, I.M. — *Some Experiments with Static Tubes at Transonic Speeds in a Slotted-Wall Wind Tunnel.* ARC 20,306, 14th July, 1958.

17. Spiegel, J.M. et alii — *Measurements of the Effects of Wall Outflow and Porosity on Wave Attenuation in a Transonic Wind Tunnel with Perforated Walls.* NACA TN4360, August, 1958.

18. Berndt, S.B. — *Theoretical Aspects of the Calibration of Transonic Test Sections.* FFA Report 74, 1957.

TABLE I

Principal Dimensions of the Models

Body diameter	*Span*	*Aerodynamic mean chord*	*Wing area*	*Maximum X-sectional area*	*Body length*
1.75	9.4	3.6	31	3.2	17.5
2.50	13.5	5.2	64	6.5	25
5.0	26.9	10.3	256	26.1	50
7.0	37.7	14.4	502	51.2	70

(dimensions in inches and square inches)

TABLE II

Details of the Tunnels

Tunnel	*Working section dimensions (in.)*	*Total open-area ratio (%)*	*Detail of walls*	*Ref.No.*
Aircraft Research Association	108 x 96	22½	Perforated; 0.5in. diameter holes	5,6
RAE, Bedford	96 x 96	-	Supersonic tunnel, solid walls	
RAE, Farnborough	96 x 72	11	All four walls slotted, total of 24 slots	7
RAE, Bedford	36 x 35	10	One slot at centre of each wall, half slot at each corner	8
RAE, Bedford	35 x 27	10	6 slots in 35 inch wall; 27 inch side walls are solid	9
De Havilland	24 x 24	10	5 slots in each of top and bottom walls	10
National Physical Laboratory	21 x 20	4.2	10 slots in each of top and bottom walls	
RAE, Farnborough	24 x 18	11	as 96in. x 72in. tunnel	7

TABLE III

Proposed Tests

Tunnel	*Model diameter (in.)*	*M**	*Area ratio (%)*	*Reynolds no. based on* $\bar{c} \times 10^{-6}$
ARA 108in. x 96in.	7 5 2½	> 1.3 1.19 1.07	0.5 0.25 0.06	5** 4 2
RAE, Bedford 96in. x 96in.	7	> 1.3	0.55	Range 2 to 6
RAE, 96in. x 72in.	7 5 2½ 1¾	> 1.3 > 1.3 1.09 1.06	0.75 0.38 0.09 0.05	÷5 2 3 2 1 1
RAE, 36in. x 35in.	2½ 1¾	> 1.3 1.17	0.52 0.25	2 1 2 1
RAE, 35in. x 17in.	2½	> 1.2	0.69	1
De Havilland 24in. x 24in.	1¾	> 1.3	0.55	÷1
NPL, 21in. x 20in.	1¾	> 1.3	0.76	1
RAE, 24in. x 18in.	1¾	> 1.3	0.75	1

M* Mach number at which reflection of bow wave is clear of model base
** Tests completed are underlined

TABLE IV

Details of Free-Flight Tests

2 Models: 5in. diameter, one transition free and one fixed: measuring body pressures.

1 Model: 1¾in. diameter, transition fixed, with tapered sting added: measuring body pressures.

2 Models: 5in. diameter, to measure zero-lift drag and base-pressure.

1 Oscillating model to measure aerodynamic centre and lift-curve slope.

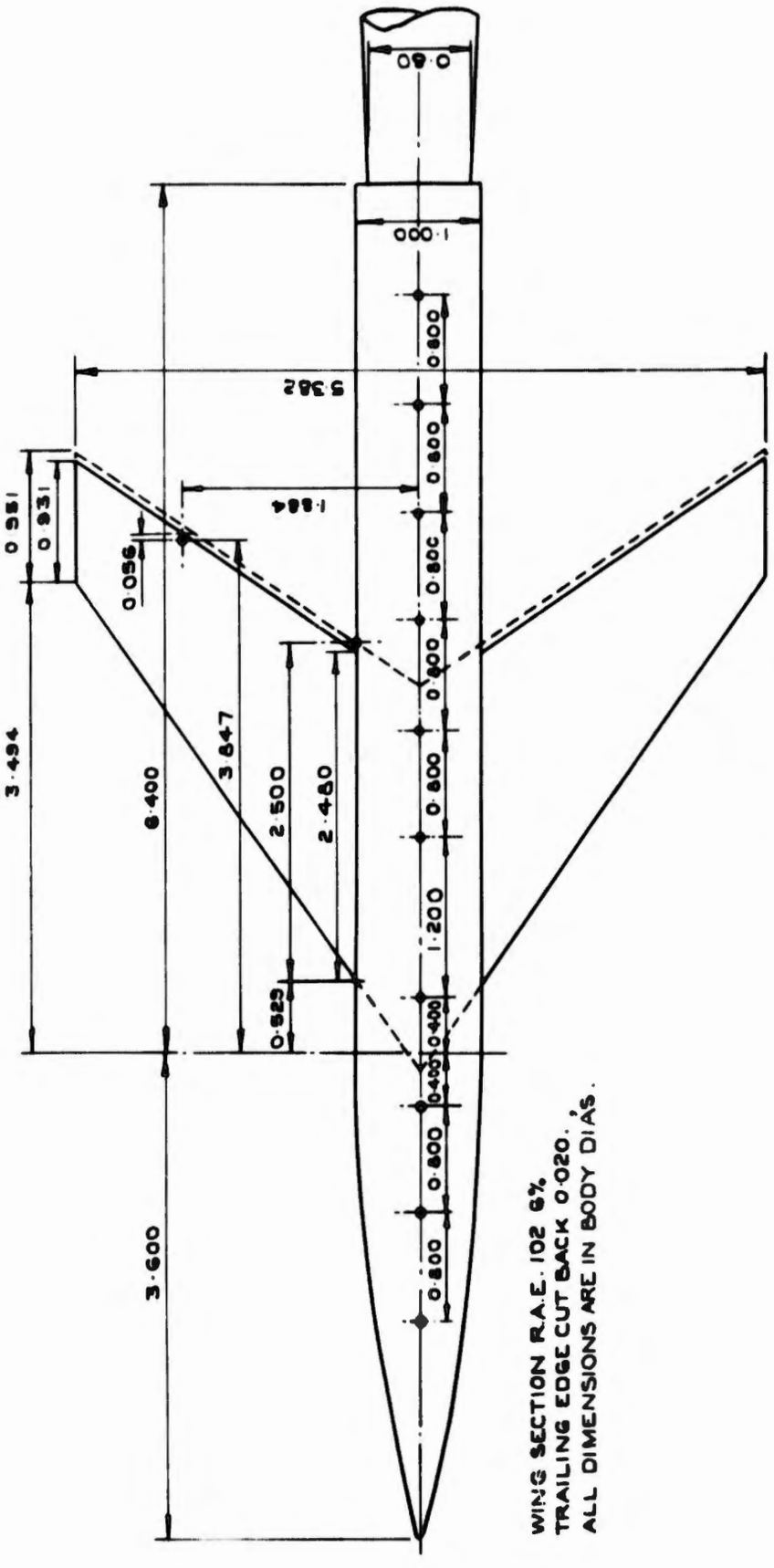

Fig.1 Details of interference model

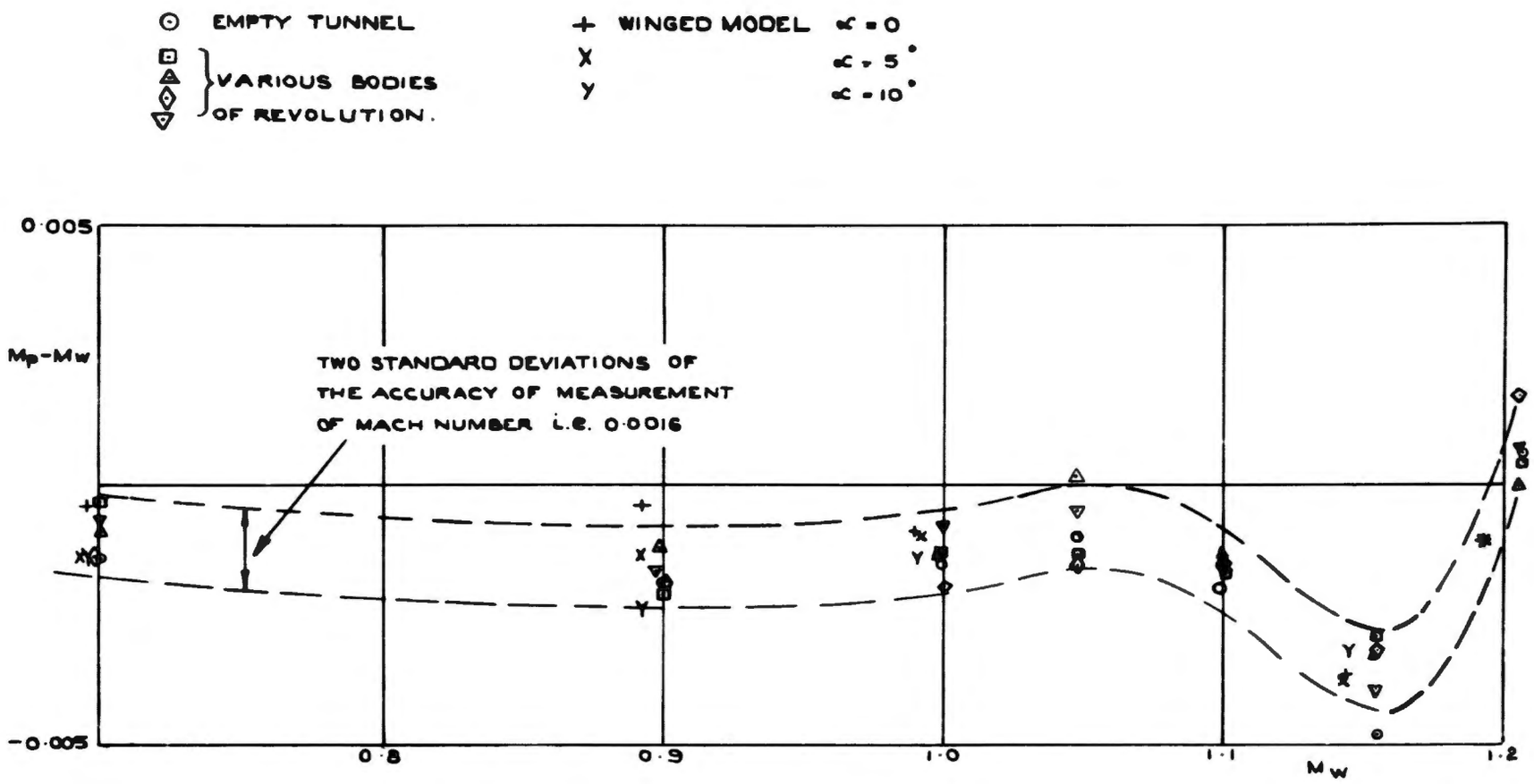

Fig.2 Effect of models on plenum Mach number

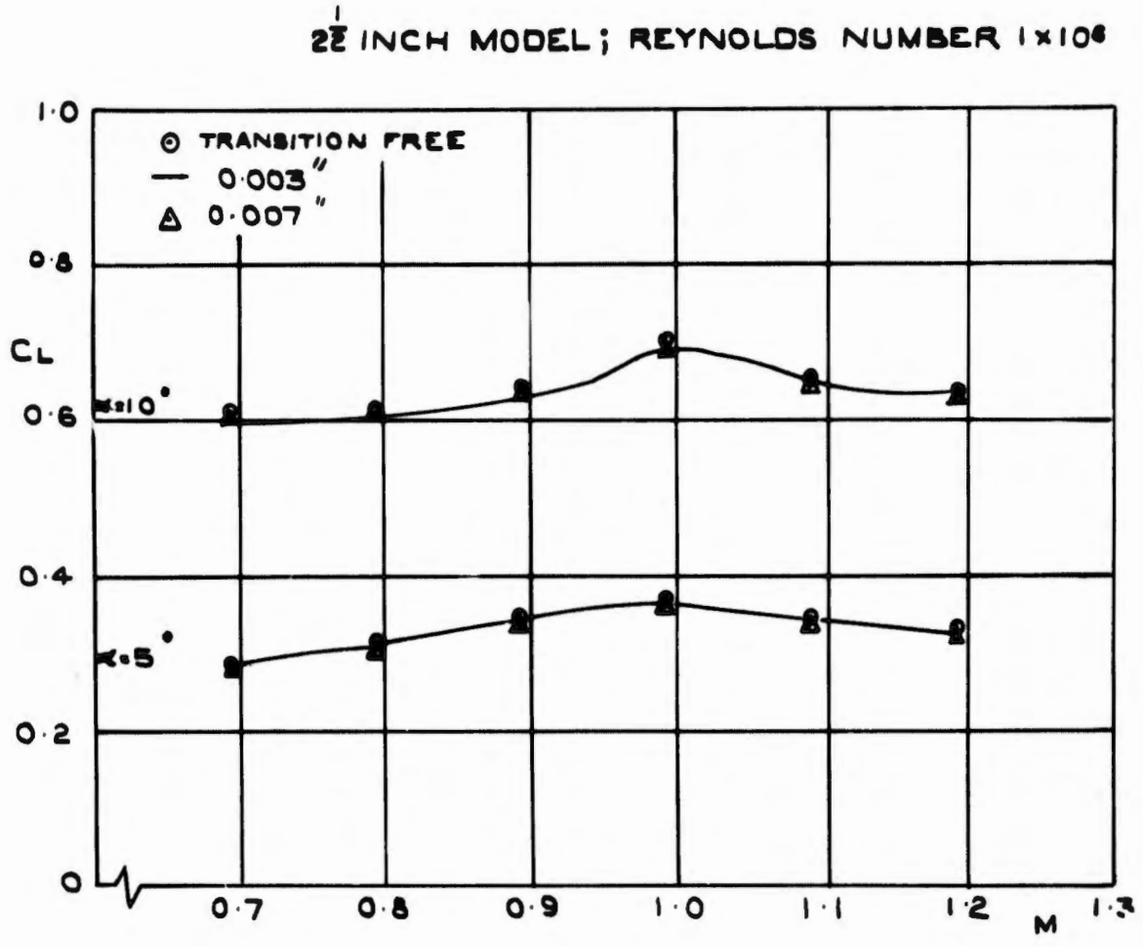

Fig.3 Effect of roughness size on lift

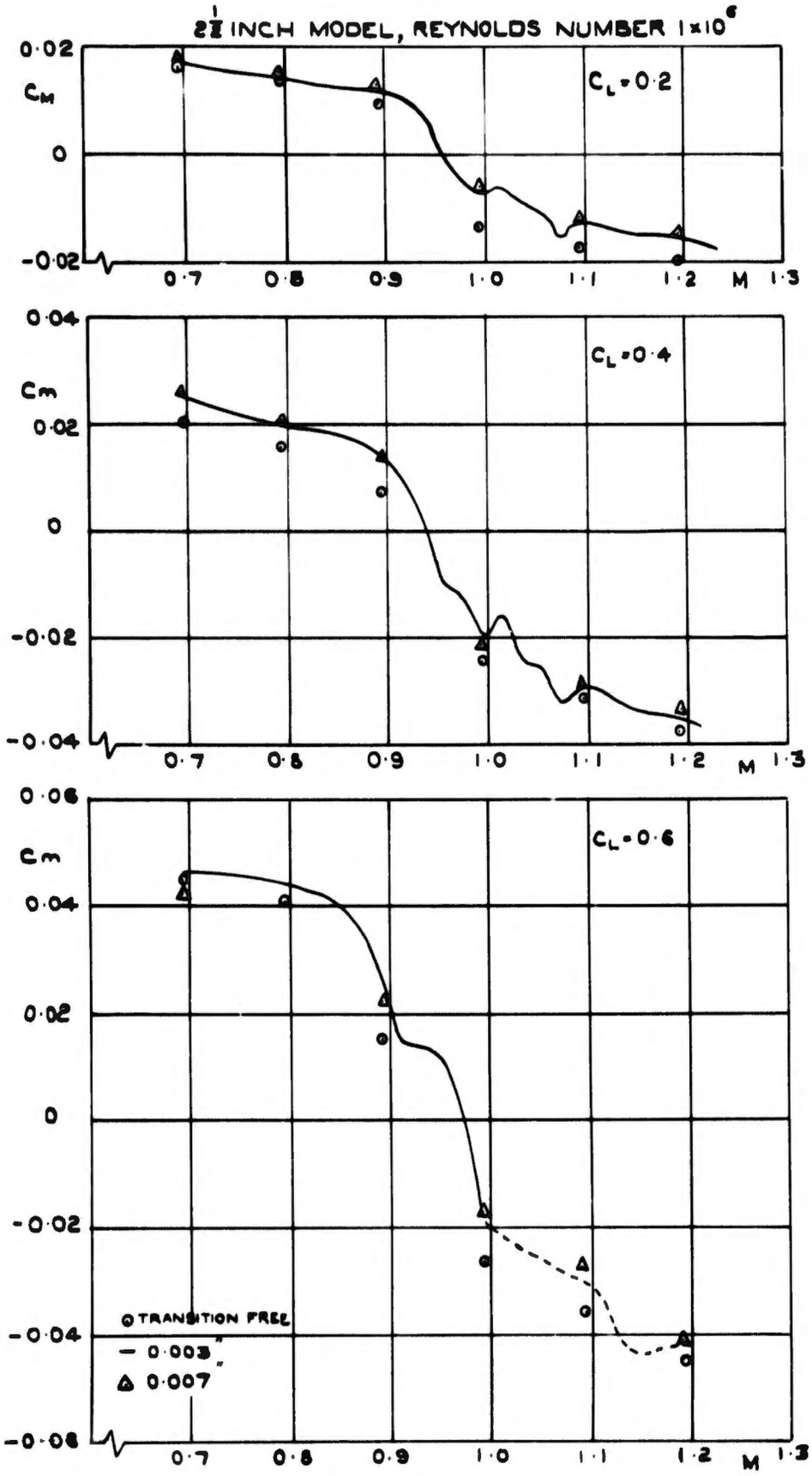

Fig.4 Effect of roughness size on pitching moment

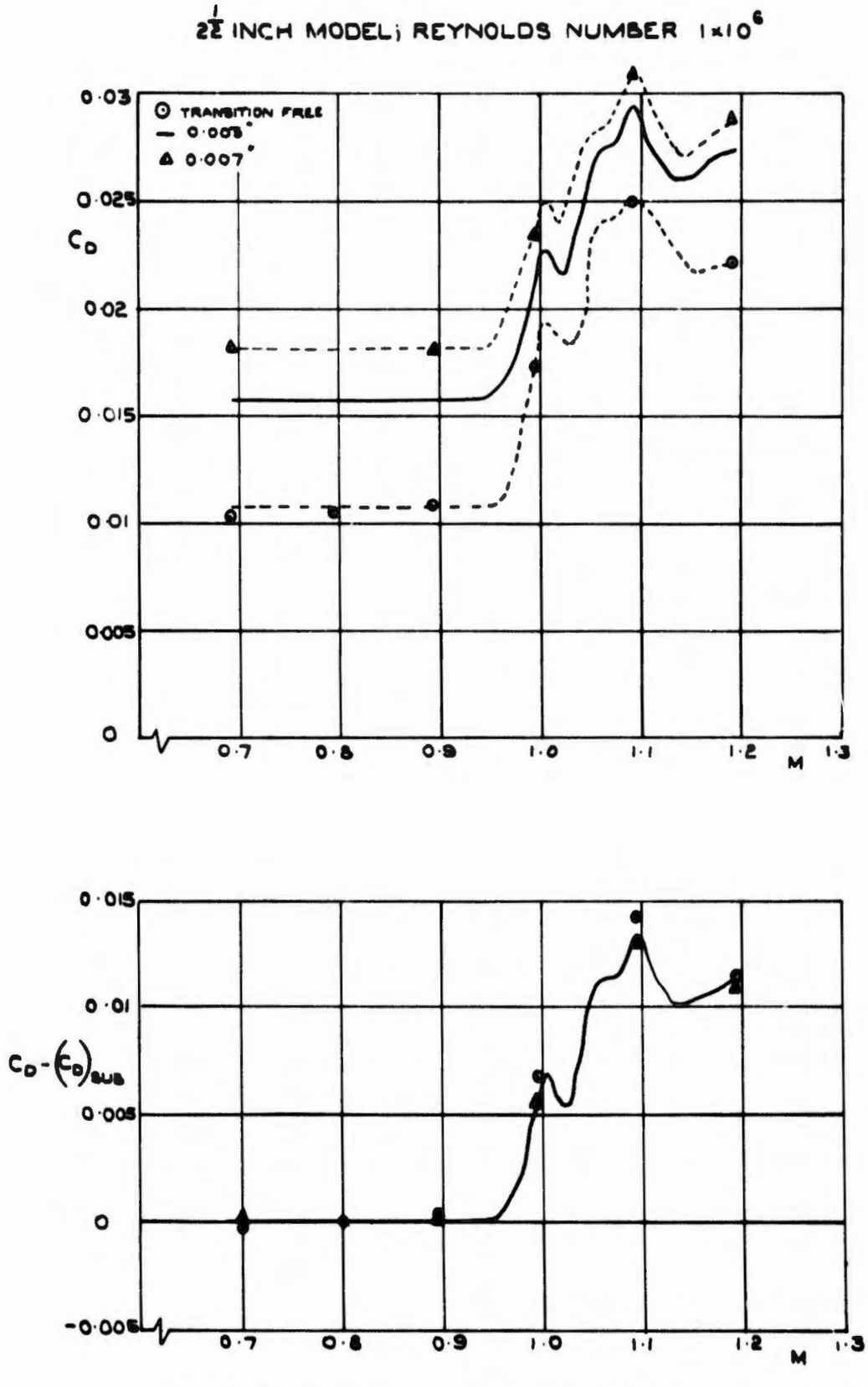

Fig.5 Effect of roughness size on zero-lift drag

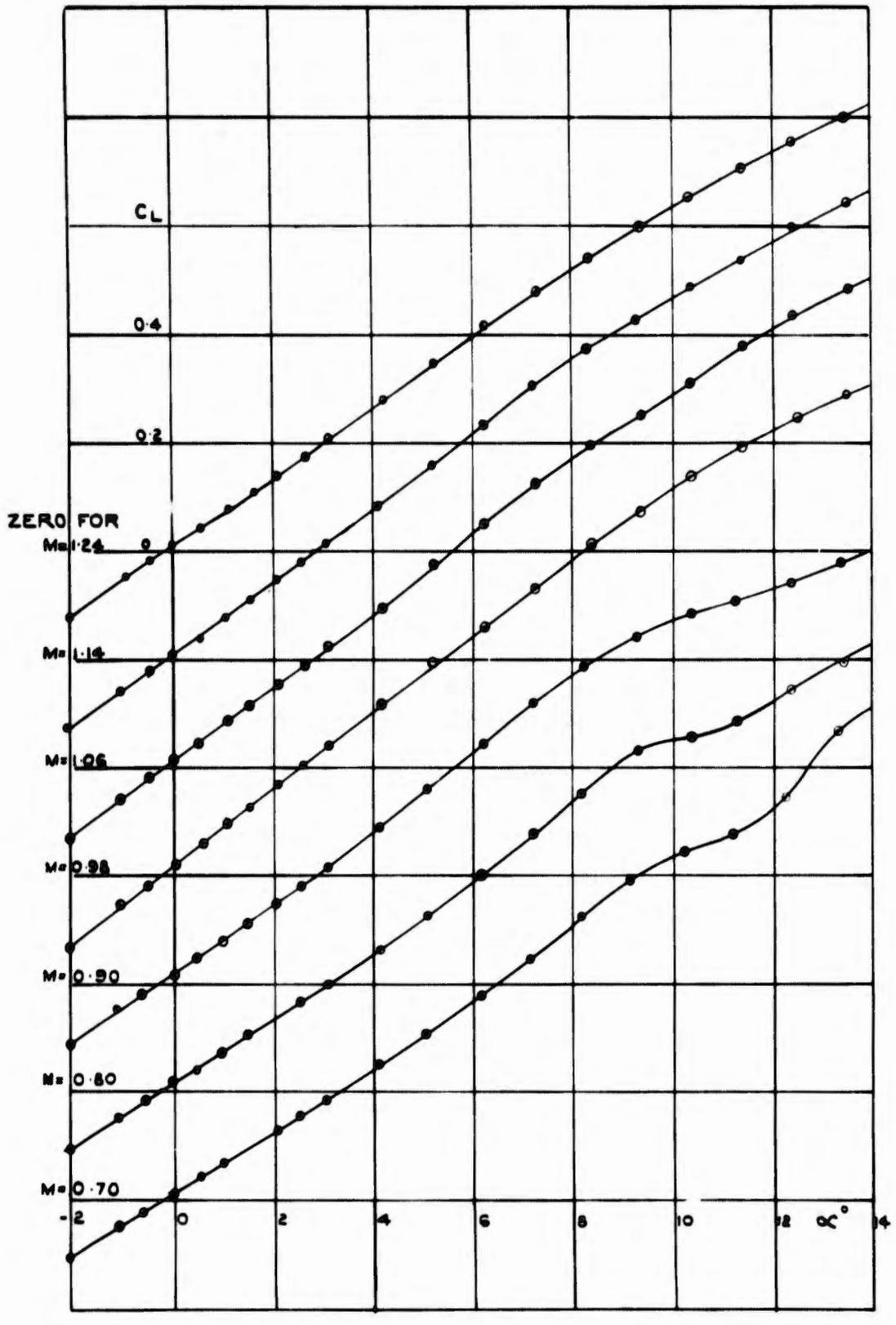

Fig.6 Variation of lift with incidence; 2½in. model in perforated tunnel; Reynolds number 2×10^6

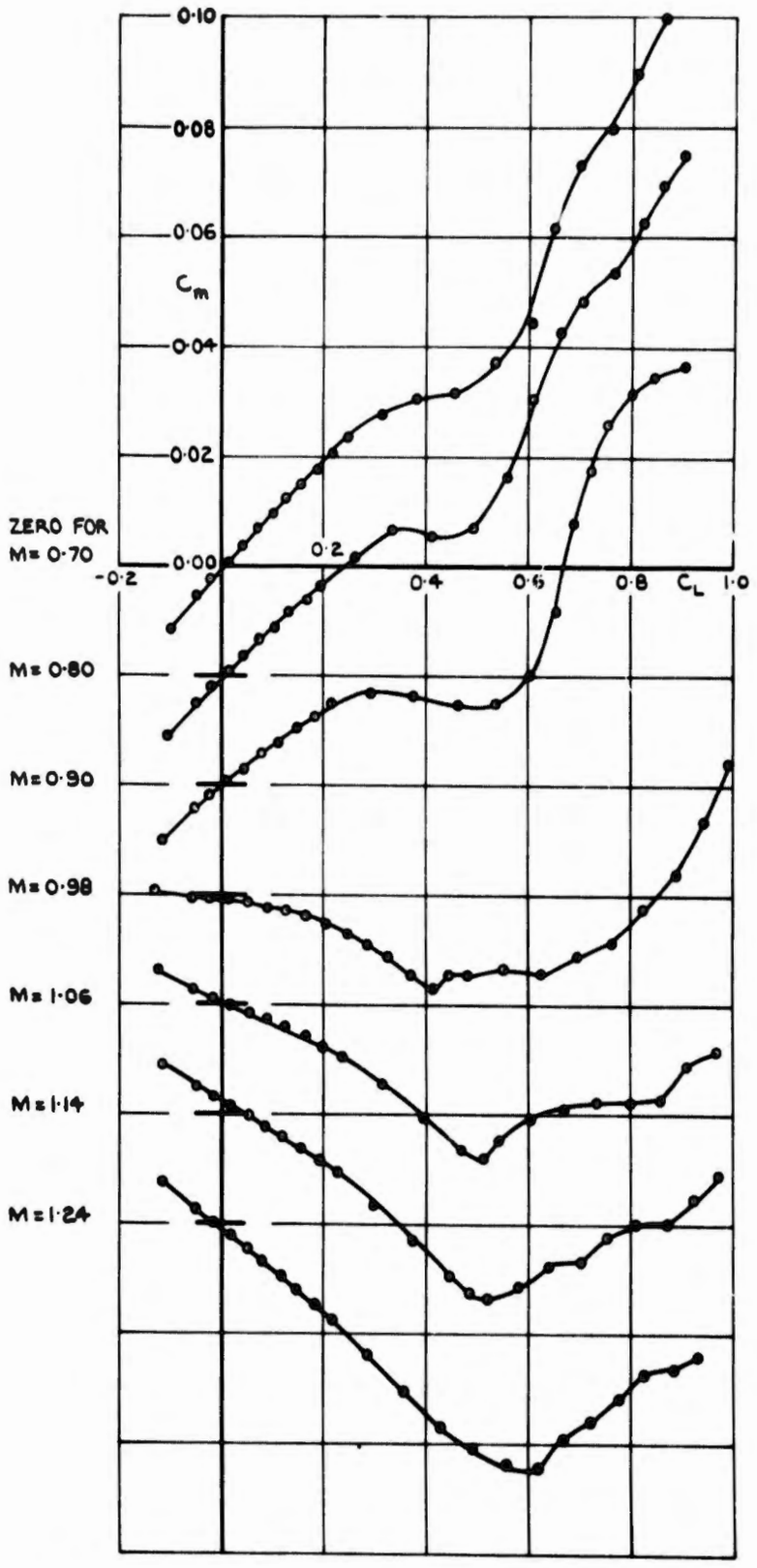

Fig.7 Variation of pitching moment with lift; 2½in. model in perforated tunnel; Reynolds number 2×10^6

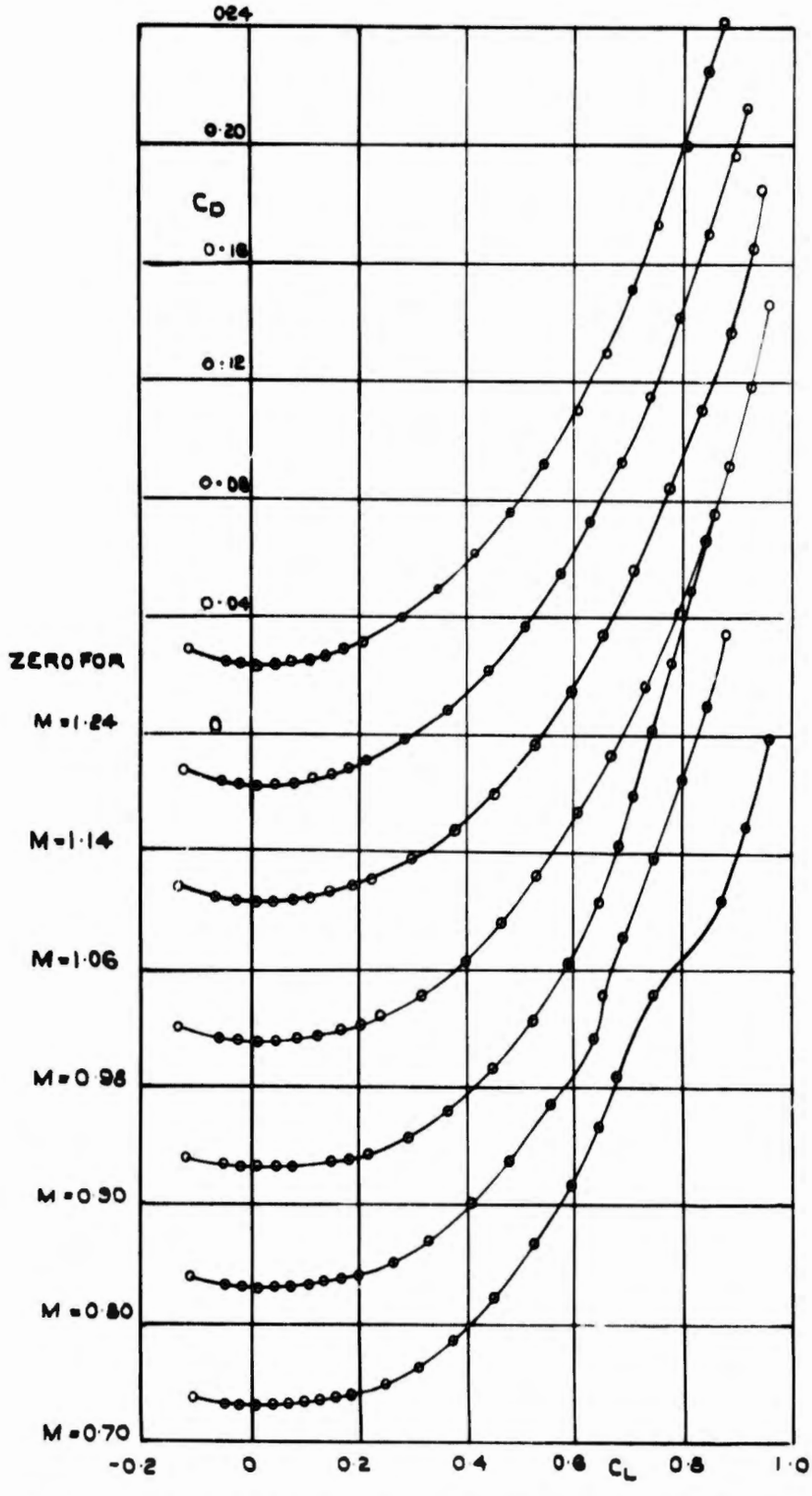

Fig.8 Variation of drag with lift; 2½in. model in perforated tunnel; Reynolds number 2×10^6

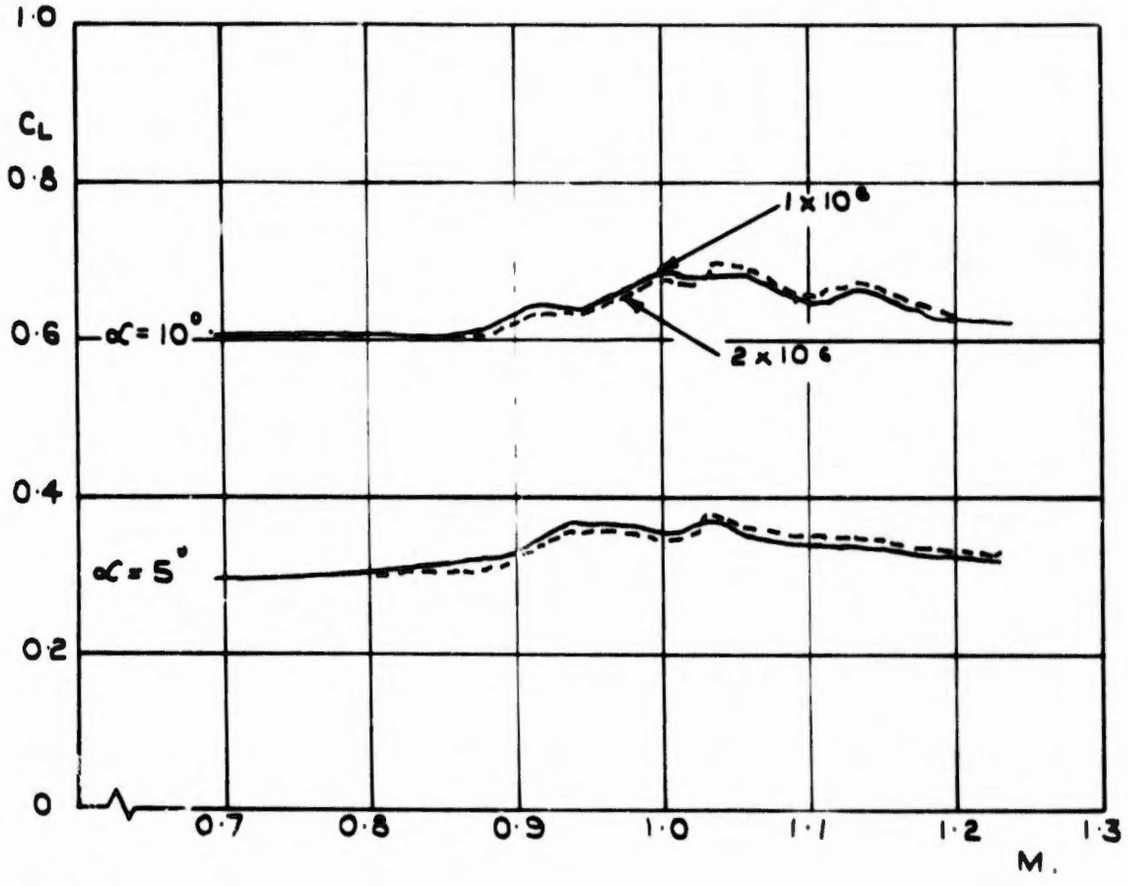

Fig.9 Effect of Reynolds number on lift; 2½in. model in small slotted tunnel

BLANK PAGE

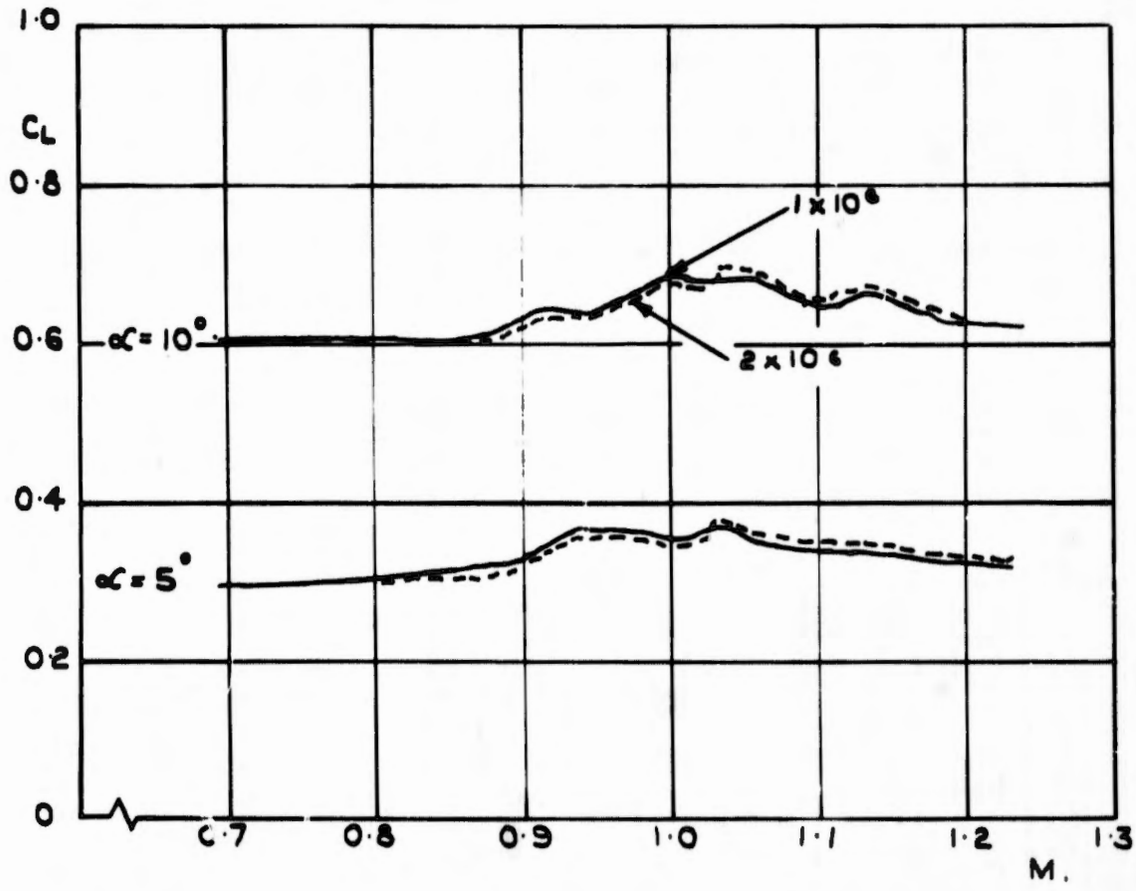

Fig.9 Effect of Reynolds number on lift; 2½in. model in small slotted tunnel

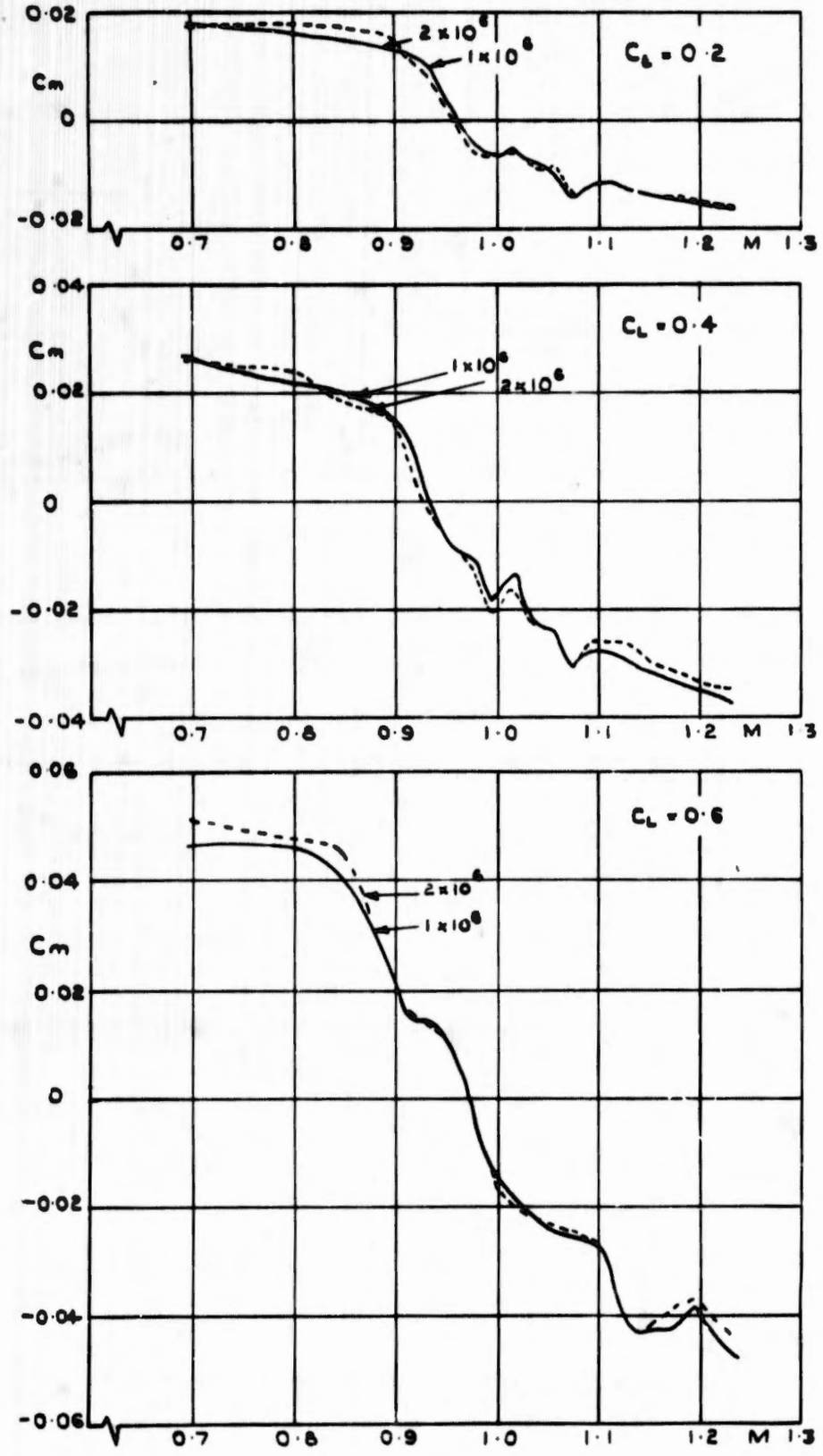

Fig. 10 Effect of Reynolds number on pitching moment; 2½in. model in small slotted tunnel

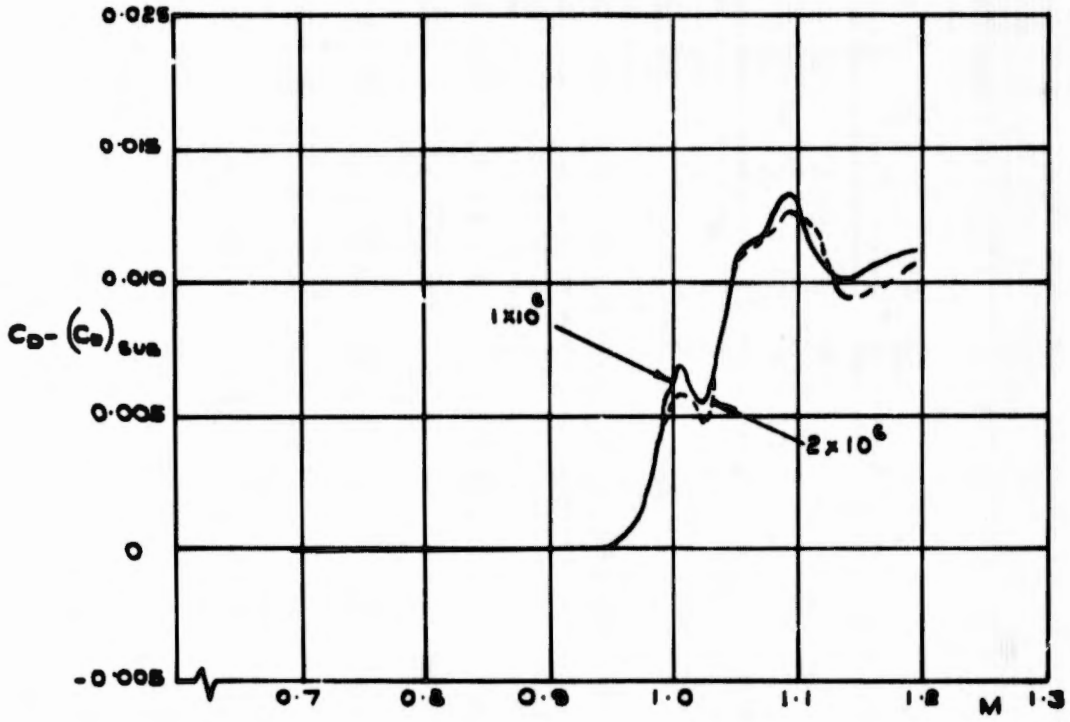

Fig.11 Effect of Reynolds number on zero-lift drag; 2½in. model in small slotted tunnel

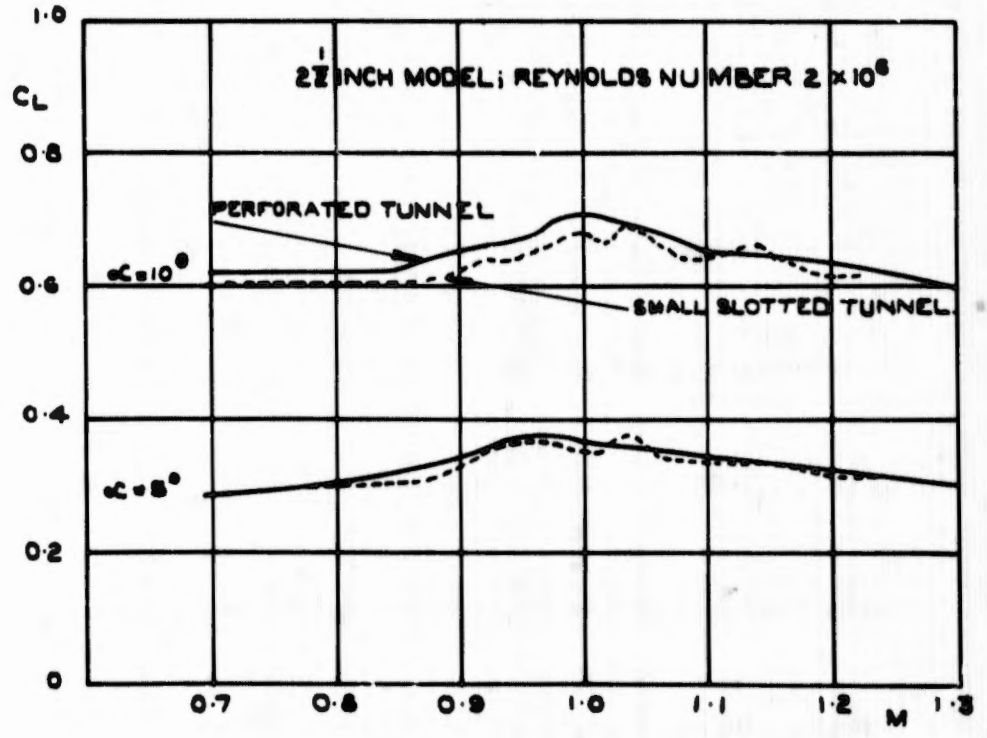

Fig.12 Comparison of lift of 2½in. model in perforated and small slotted tunnels

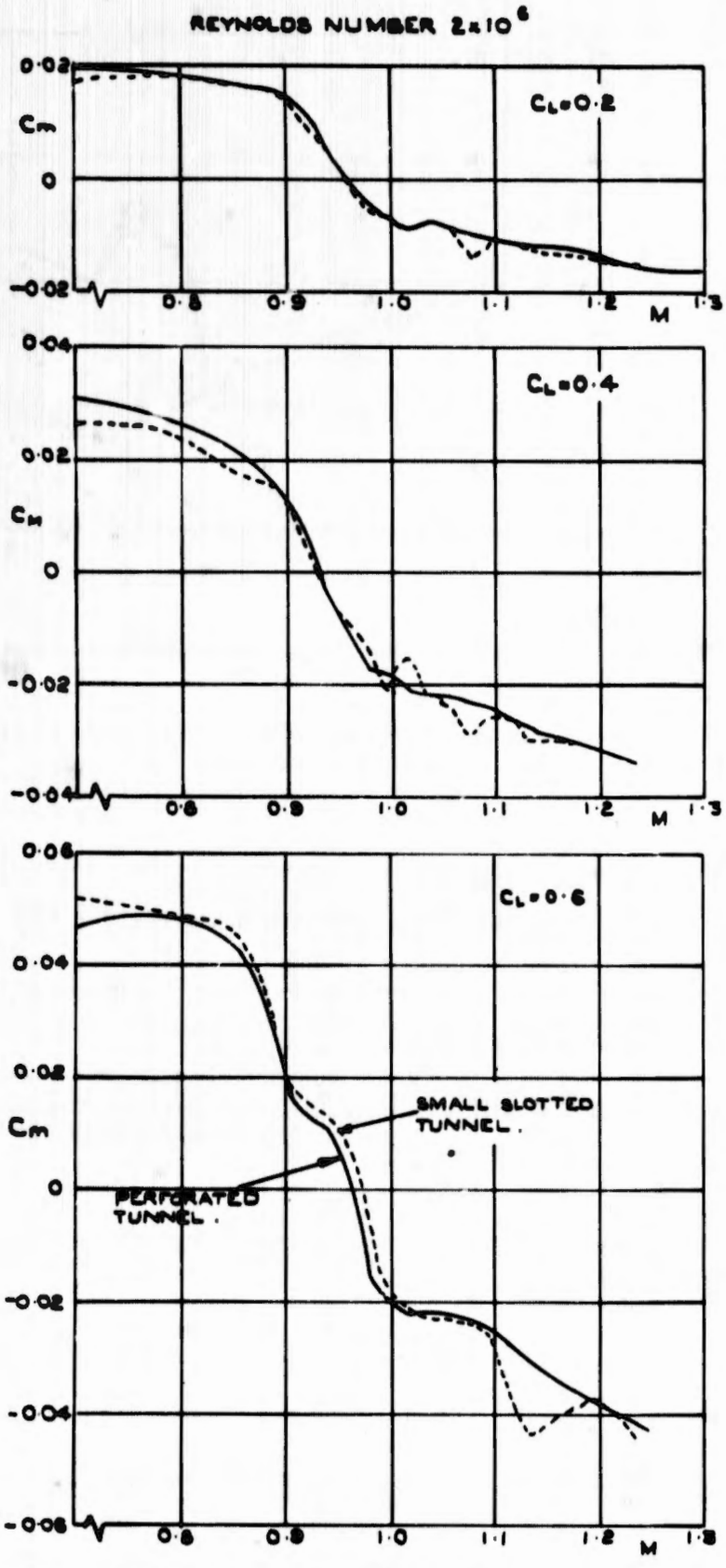

Fig. 13 Comparison of pitching moment of 2½in. model in perforated and small slotted tunnels

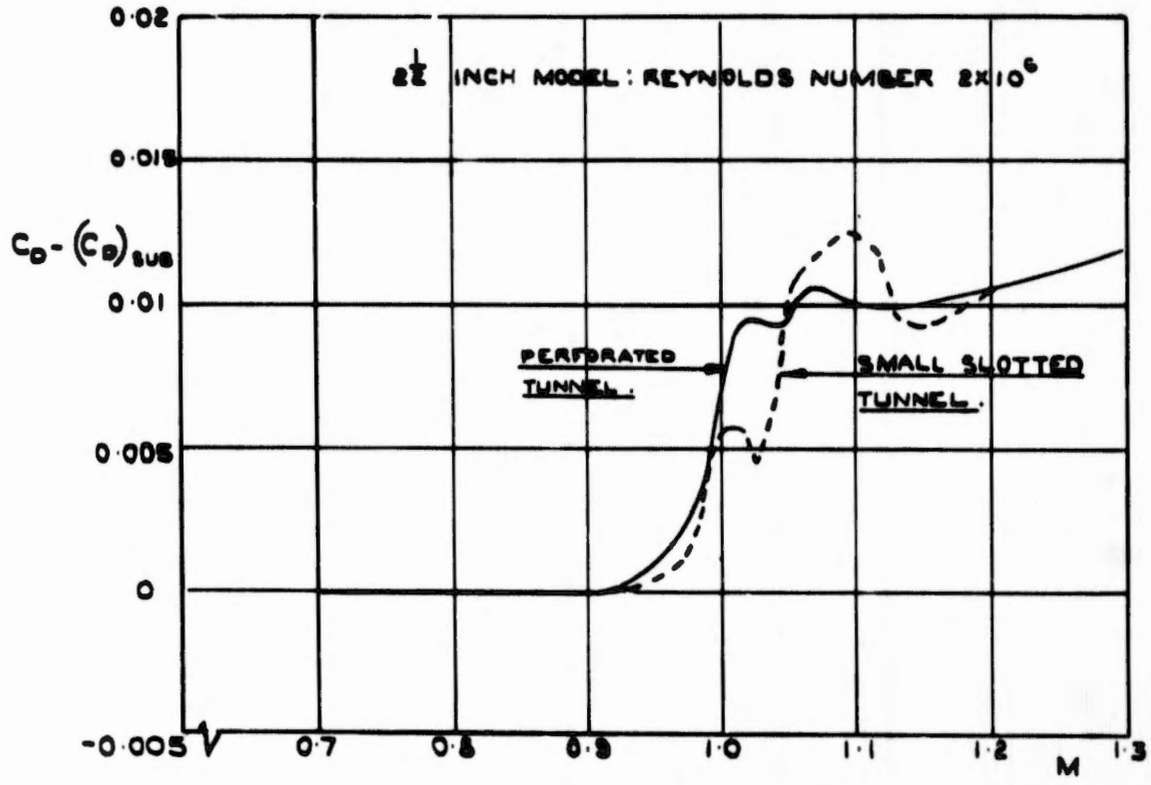

Fig.14 Comparison of zero-lift drag of 2½in. model in perforated and small slotted tunnels

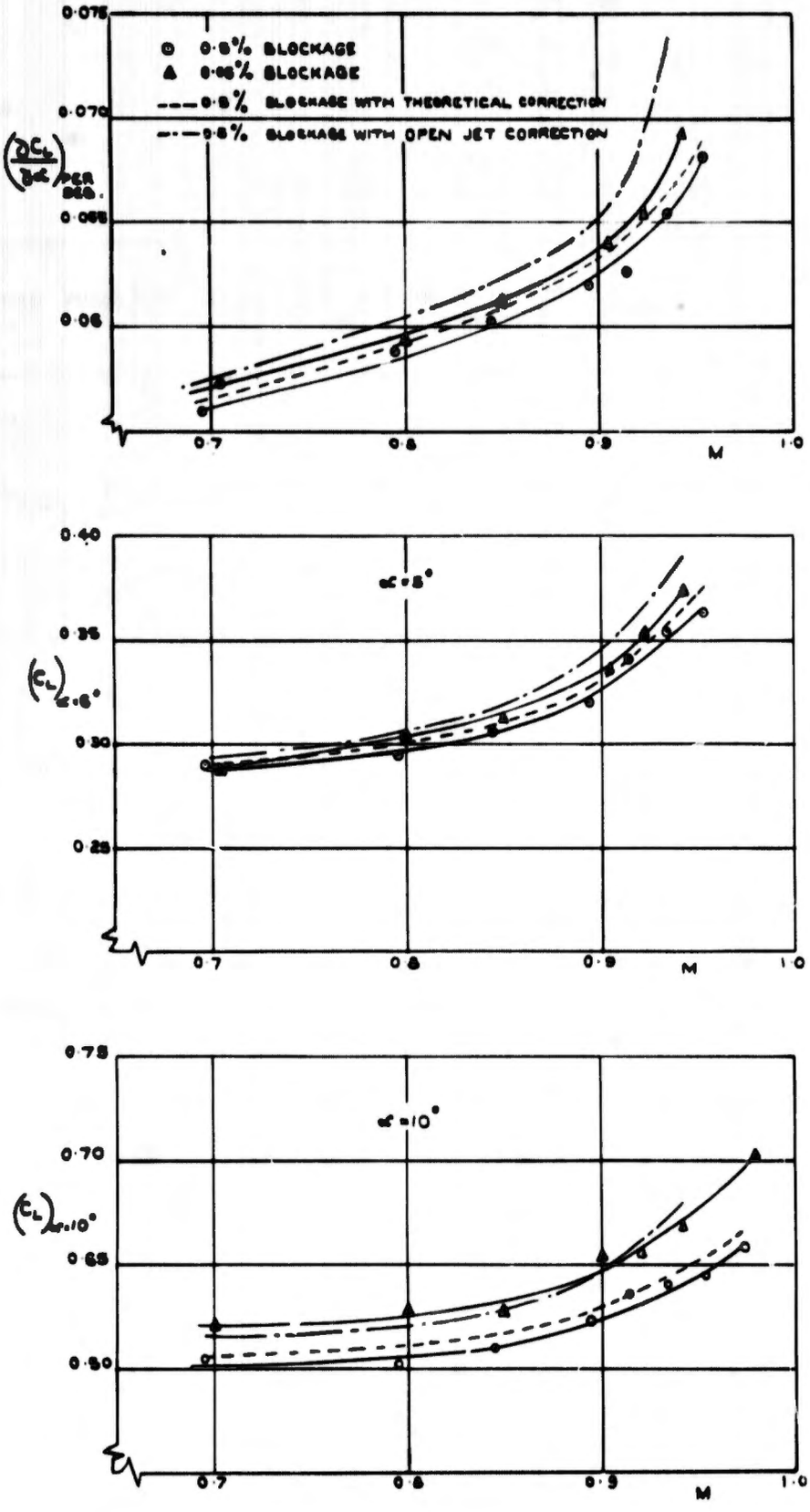

Fig.15 'Corrected' lift of 2½in. model

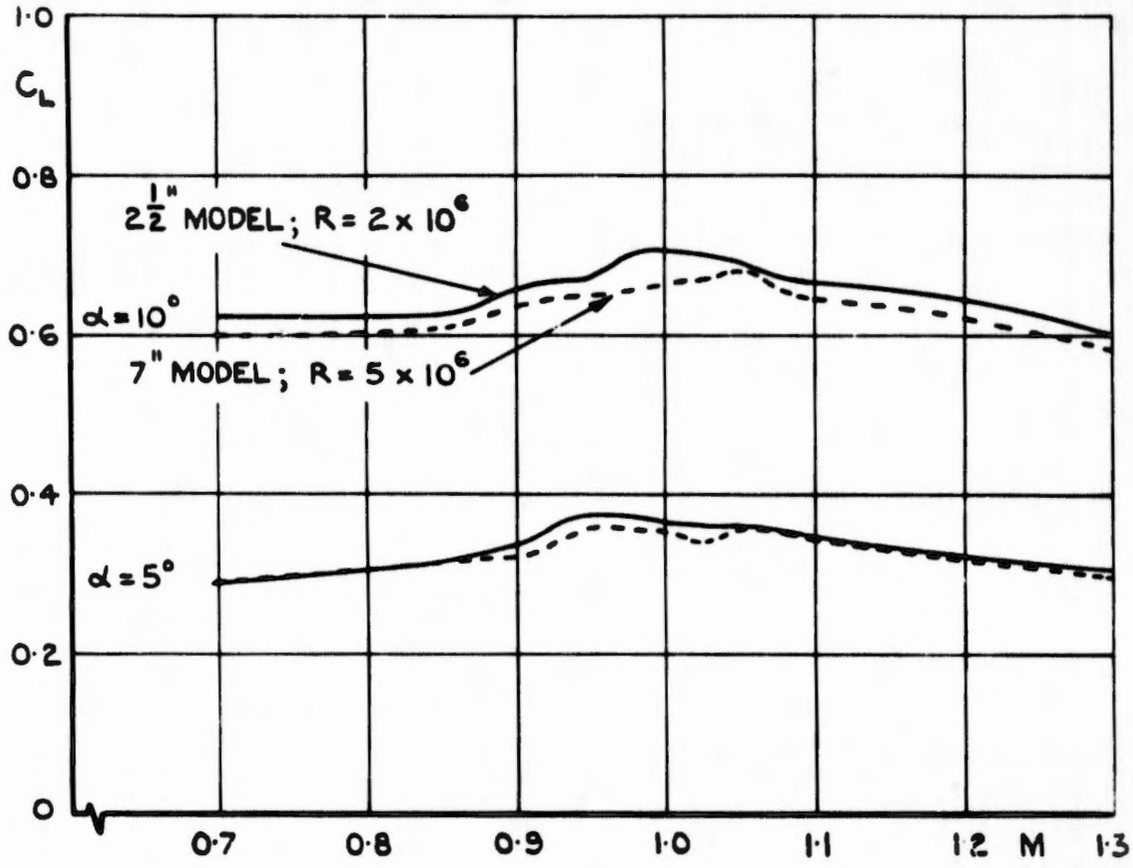

Fig.16 Comparison of lift of 2½in. and 7in. models in perforated tunnel

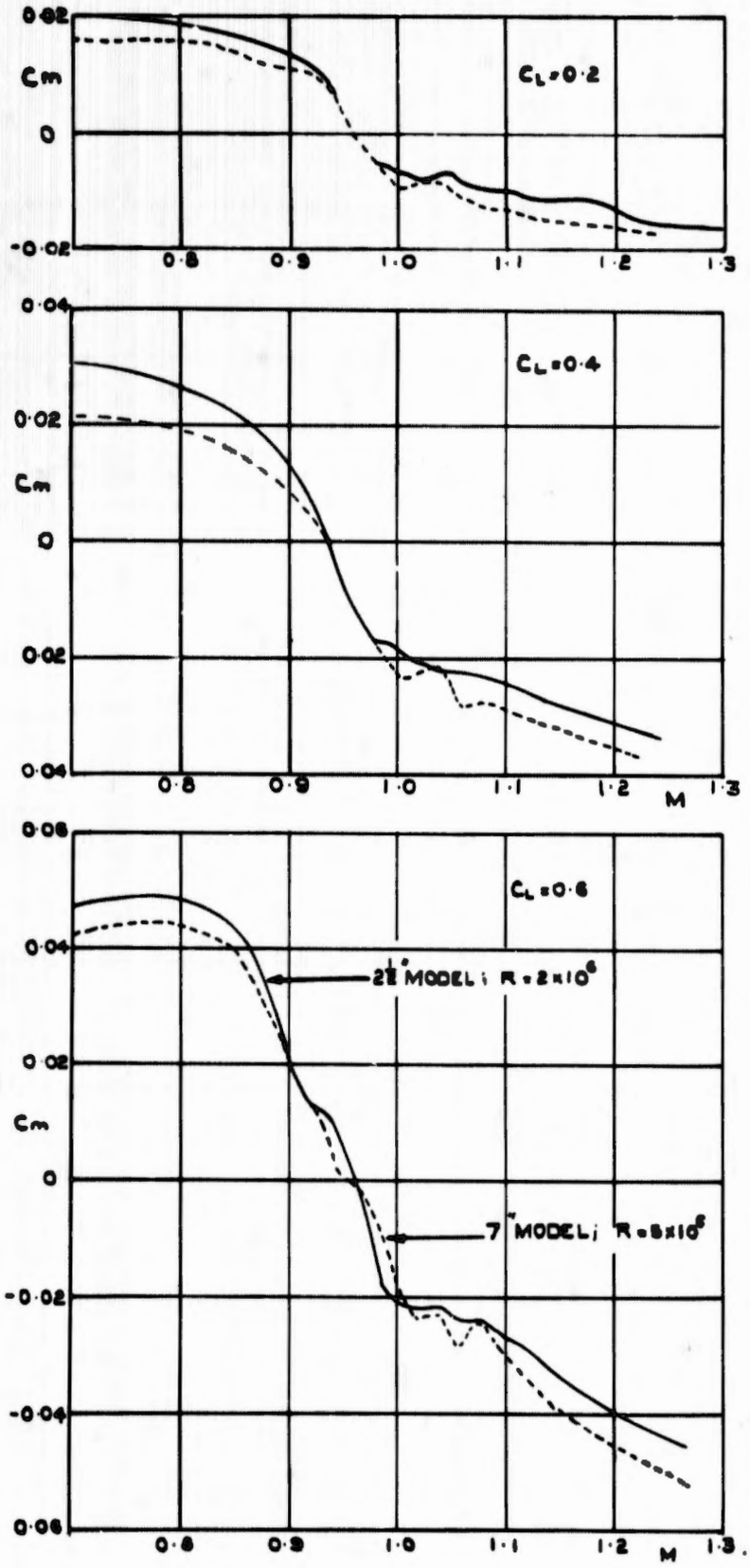

Fig.17 Comparison of pitching moment of 2½in. and 7in. models in perforated tunnel

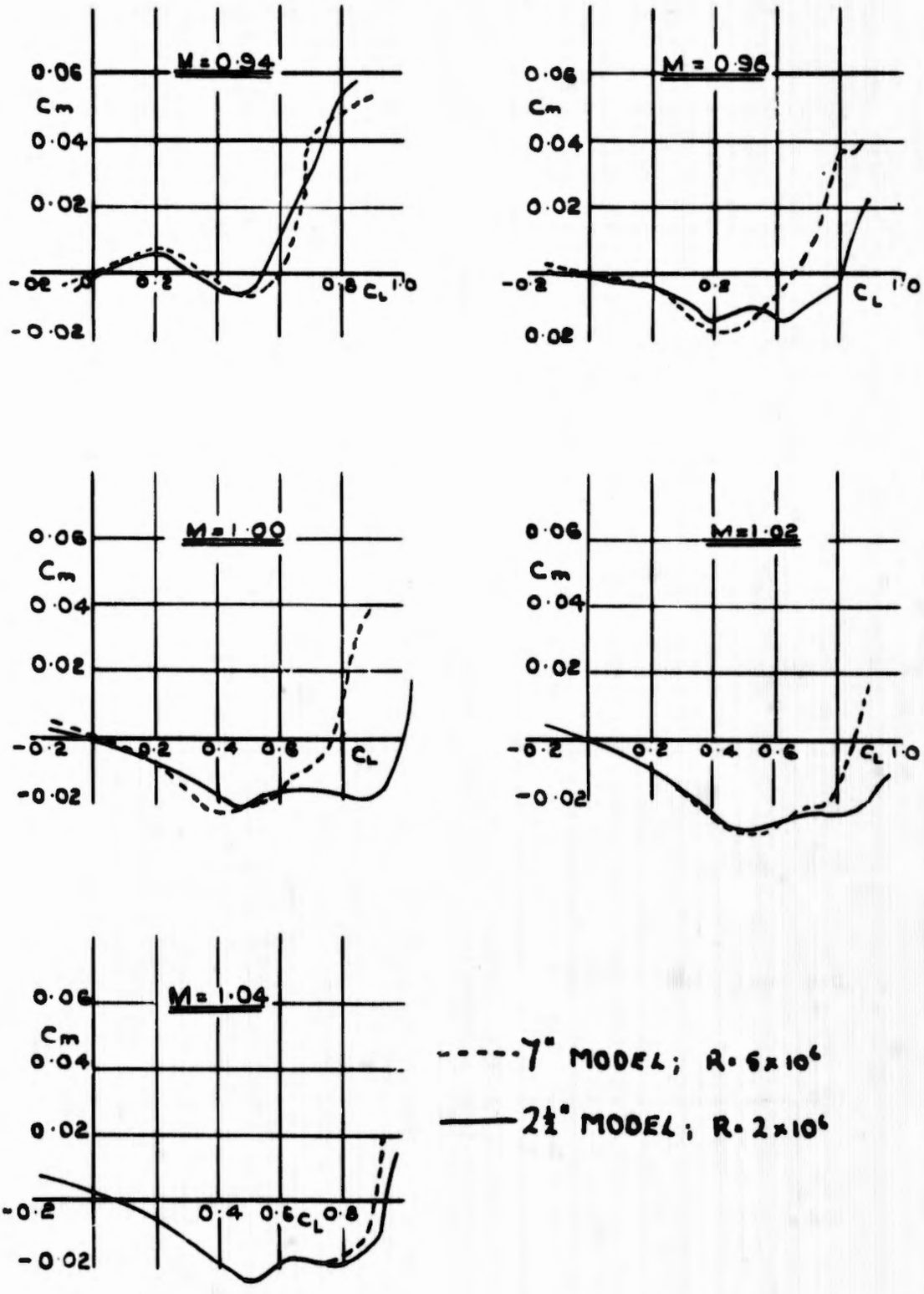

Fig. 18 Comparison of C_m and C_L curves of 2½in. and 7in. models in perforated tunnel

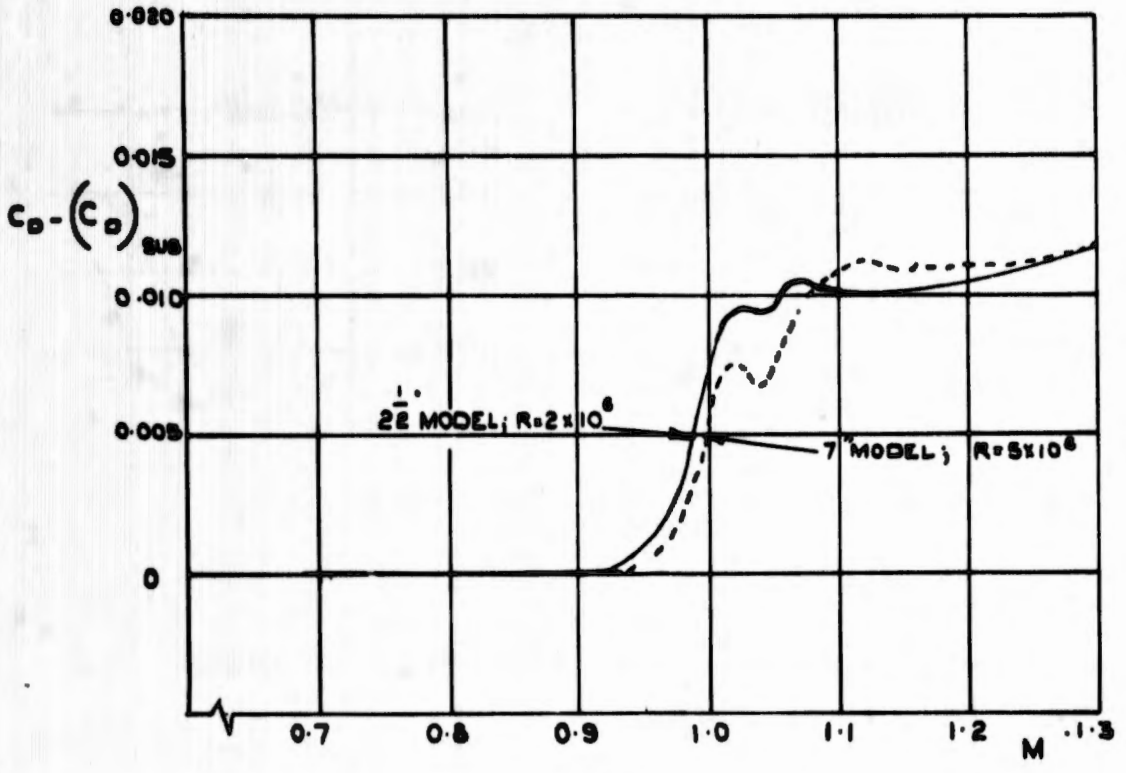

Fig.19 Comparison of zero-lift drag of 2½in. and 7in. models in perforated tunnel

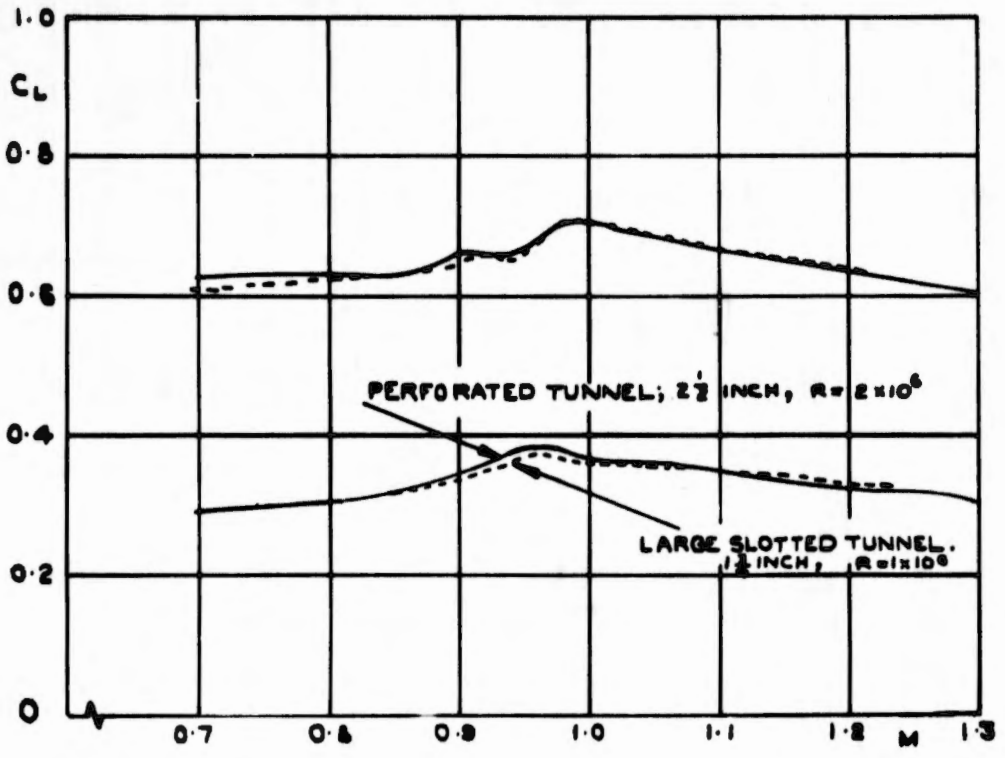

Fig.20 Comparison of lift at small blockage in two tunnels

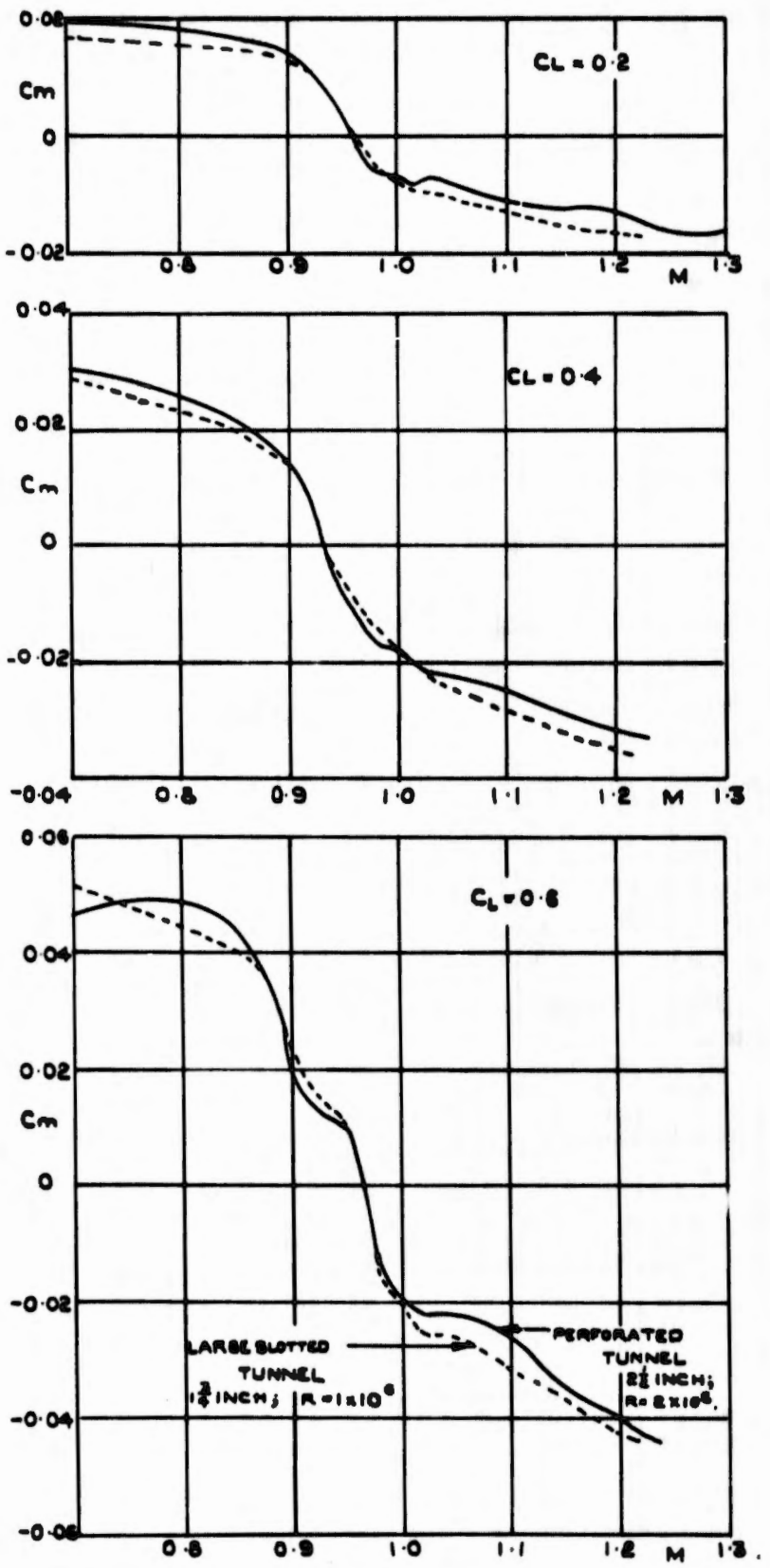

Fig. 21 Comparison of pitching moment at small blockage in two tunnels

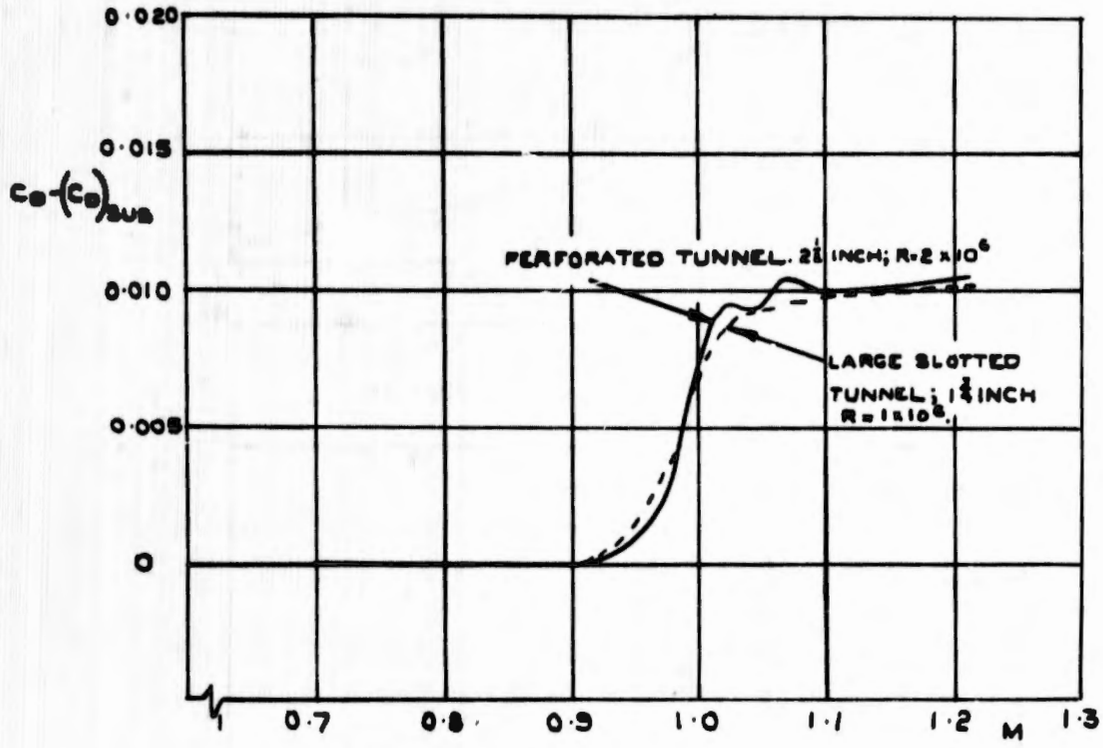

Fig.22 Comparison of zero-lift drag at small blockage in two tunnels

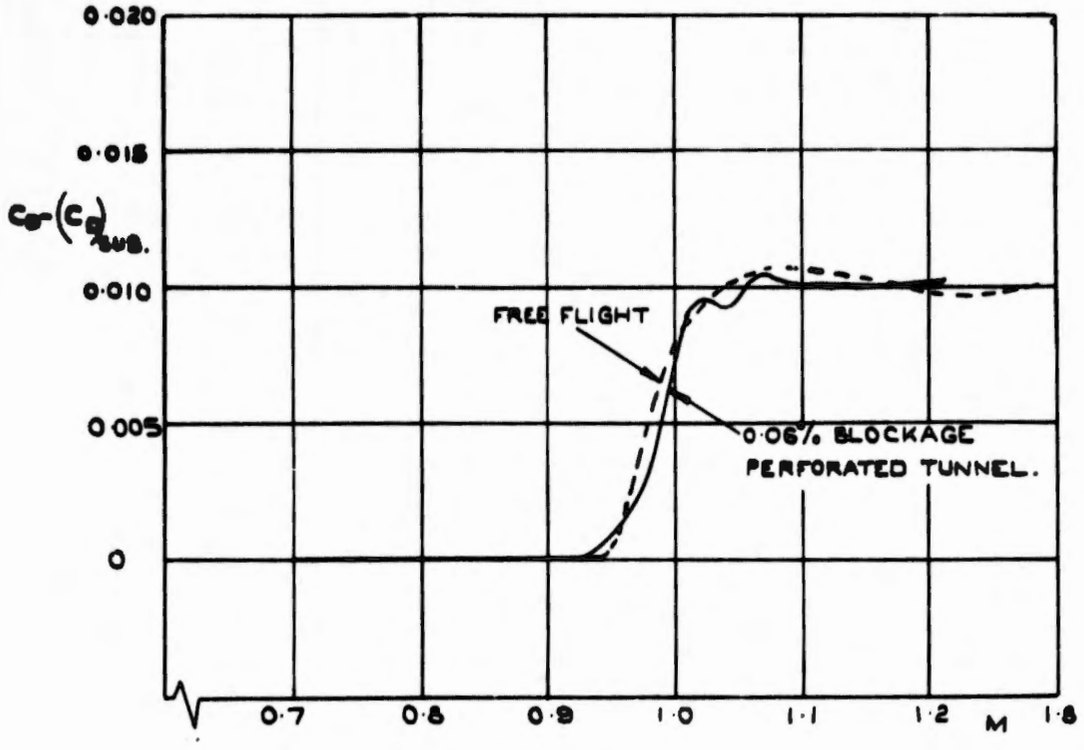

Fig.23 Comparison of tunnel and free-flight zero-lift drag

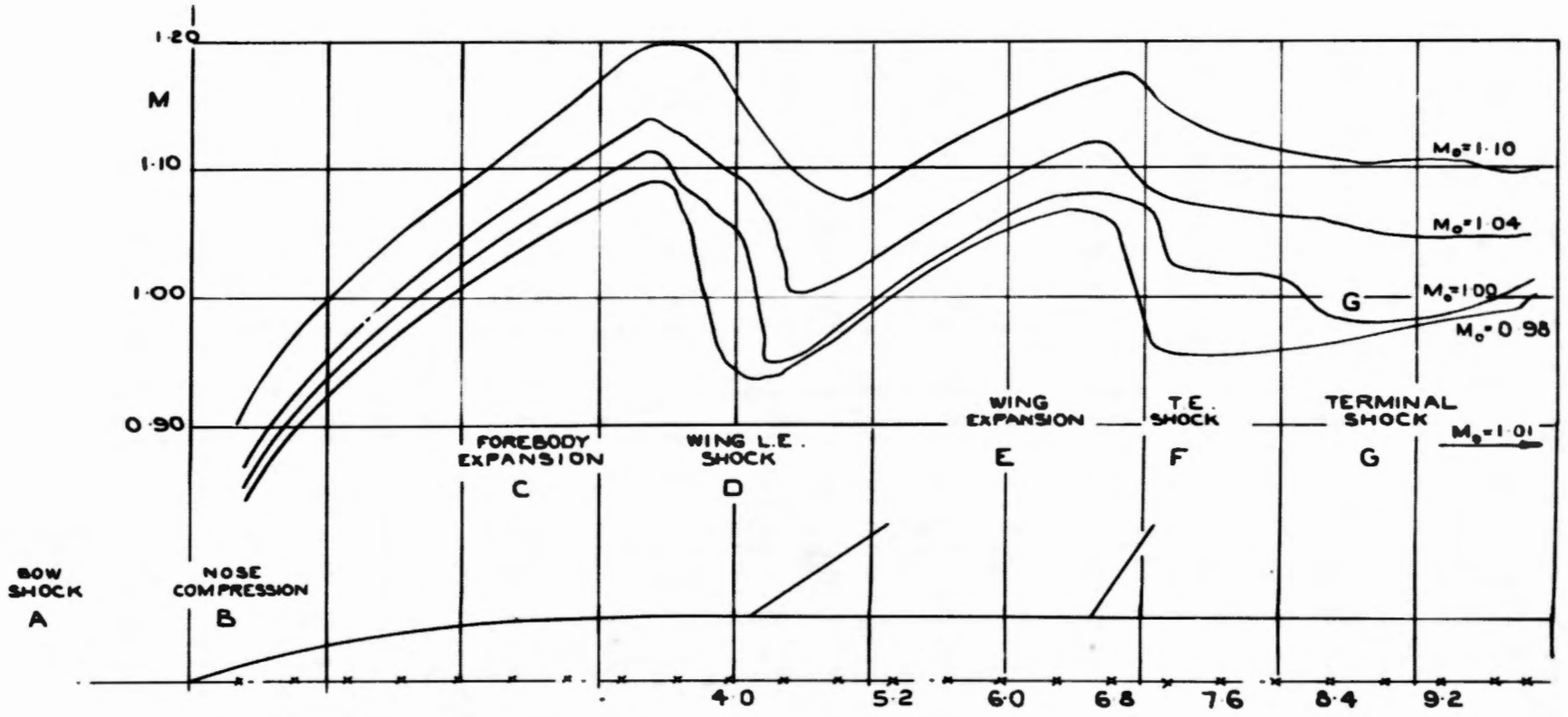

Fig.24 Specimen body pressure distributions and hole positions (top body centre line); $\alpha = 0^\circ$

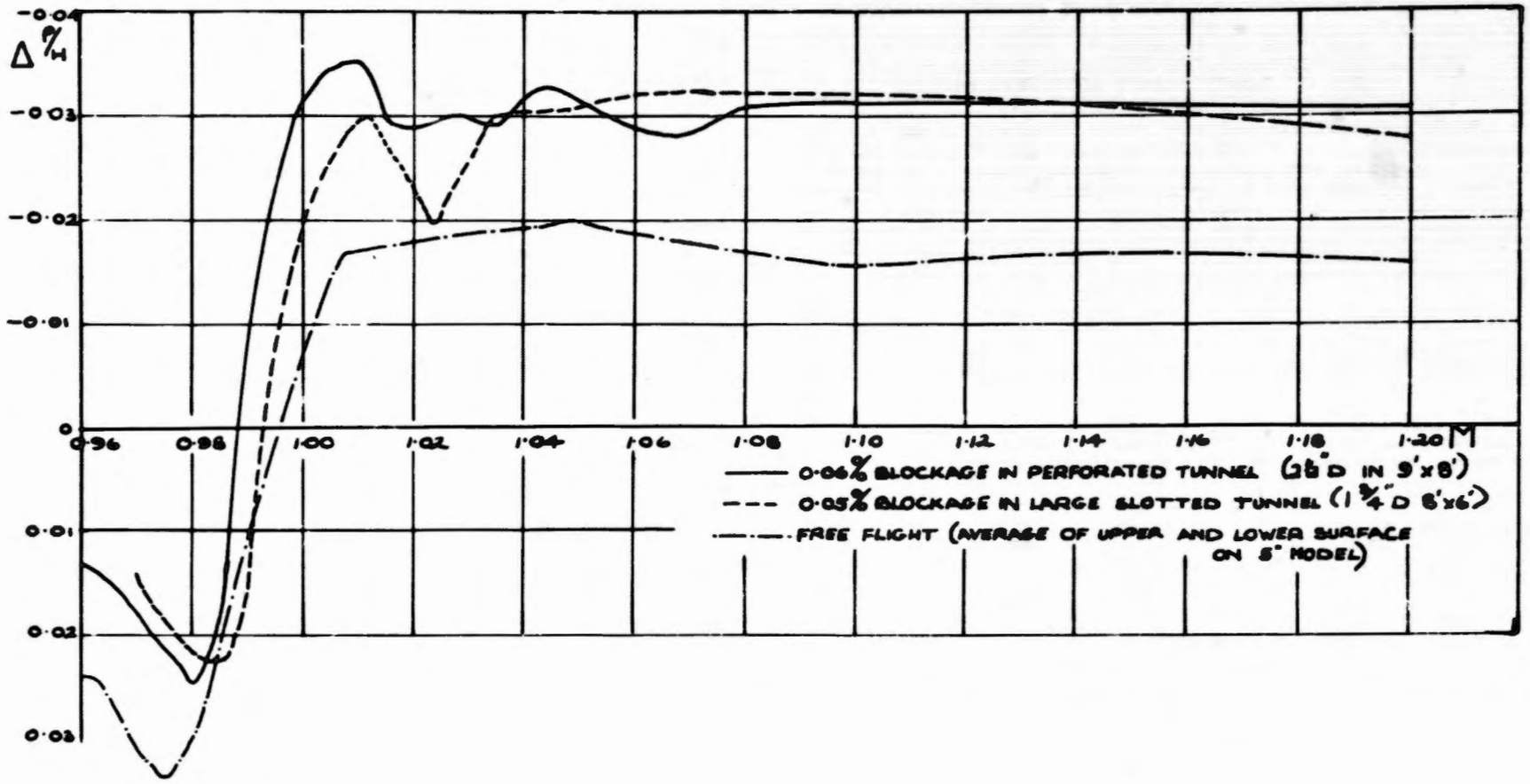

Fig. 25 Comparison of pressures for tunnel models at small blockage with free flight
(a) x = 4D

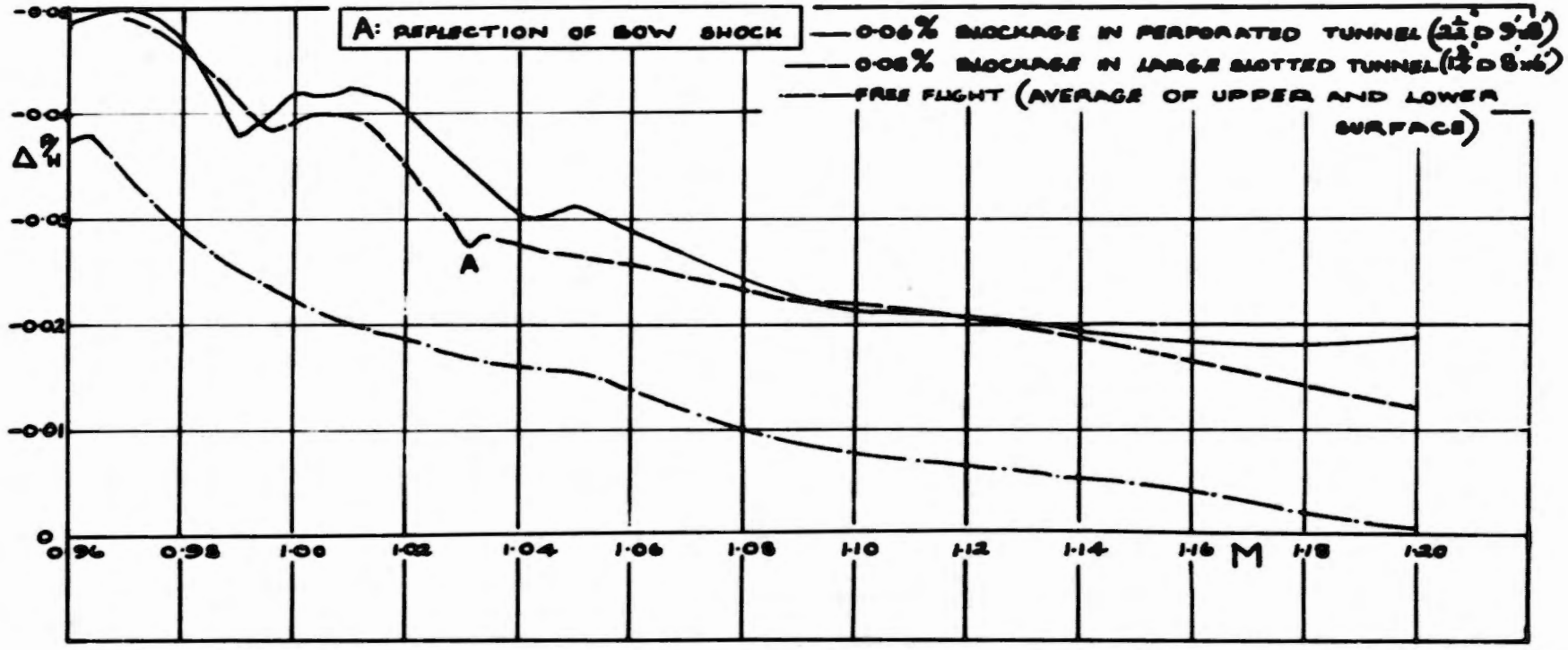

Fig. 25 Comparison of pressures for tunnel models at small blockage with free flight
(b) x = 6.0D (near peak of wing expansion)

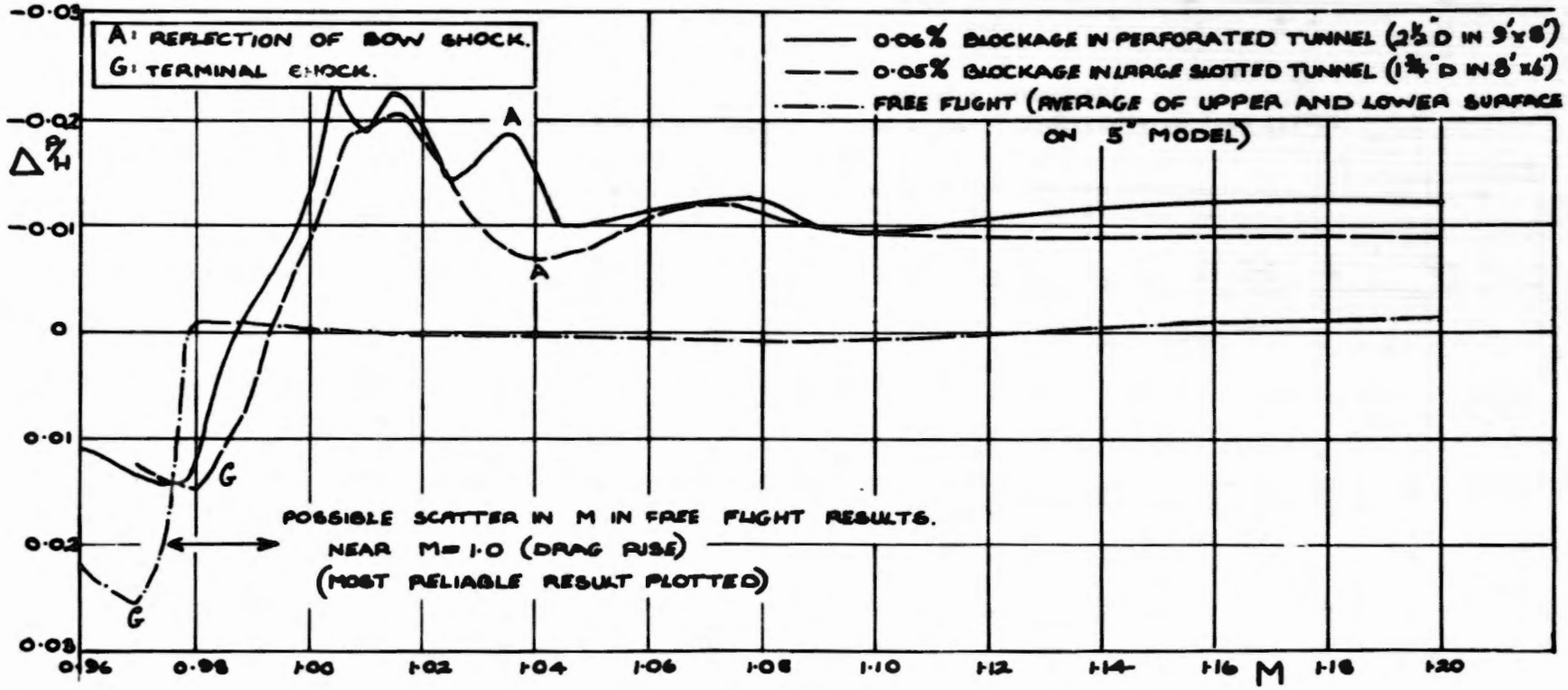

Fig.25 Comparison of pressures for tunnel models at small blockage with free flight
(c) x = 7.6D (downstream of wing)

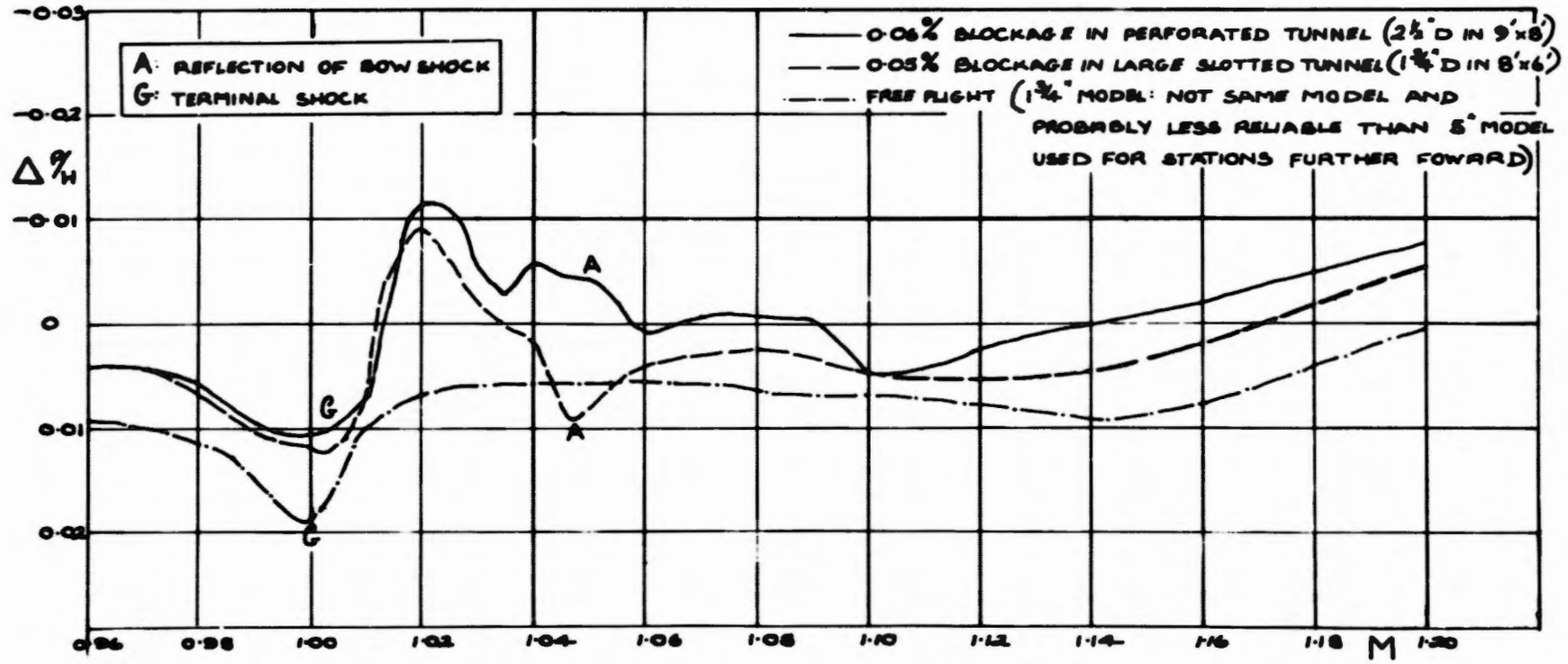

Fig. 25 Comparison of pressures for tunnel models at small blockage with free flight
(d) x = 9.2D (towards rear of body)

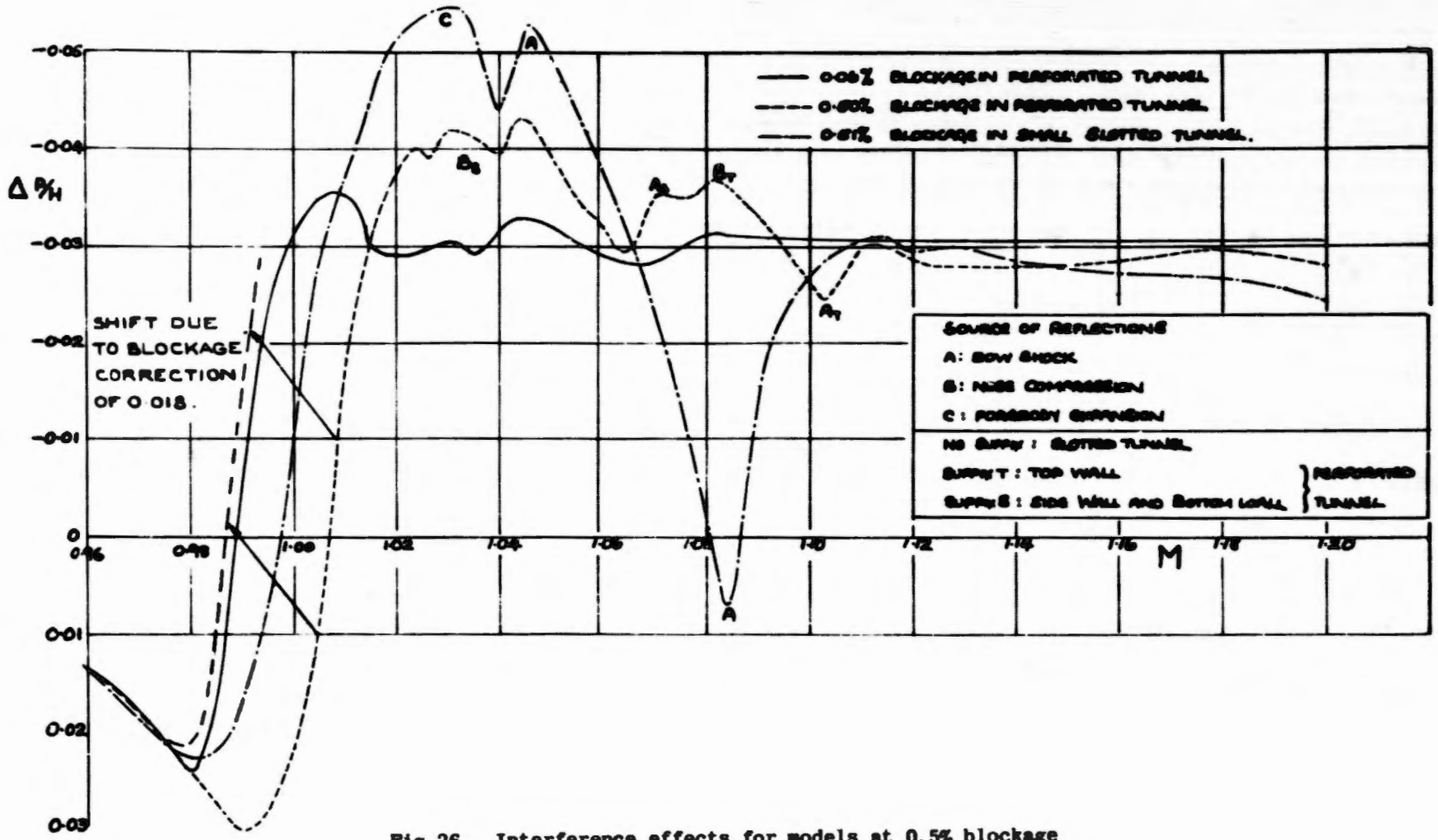

Fig.26 Interference effects for models at 0.5% blockage
(a) x = 4D (just ahead of wing root)

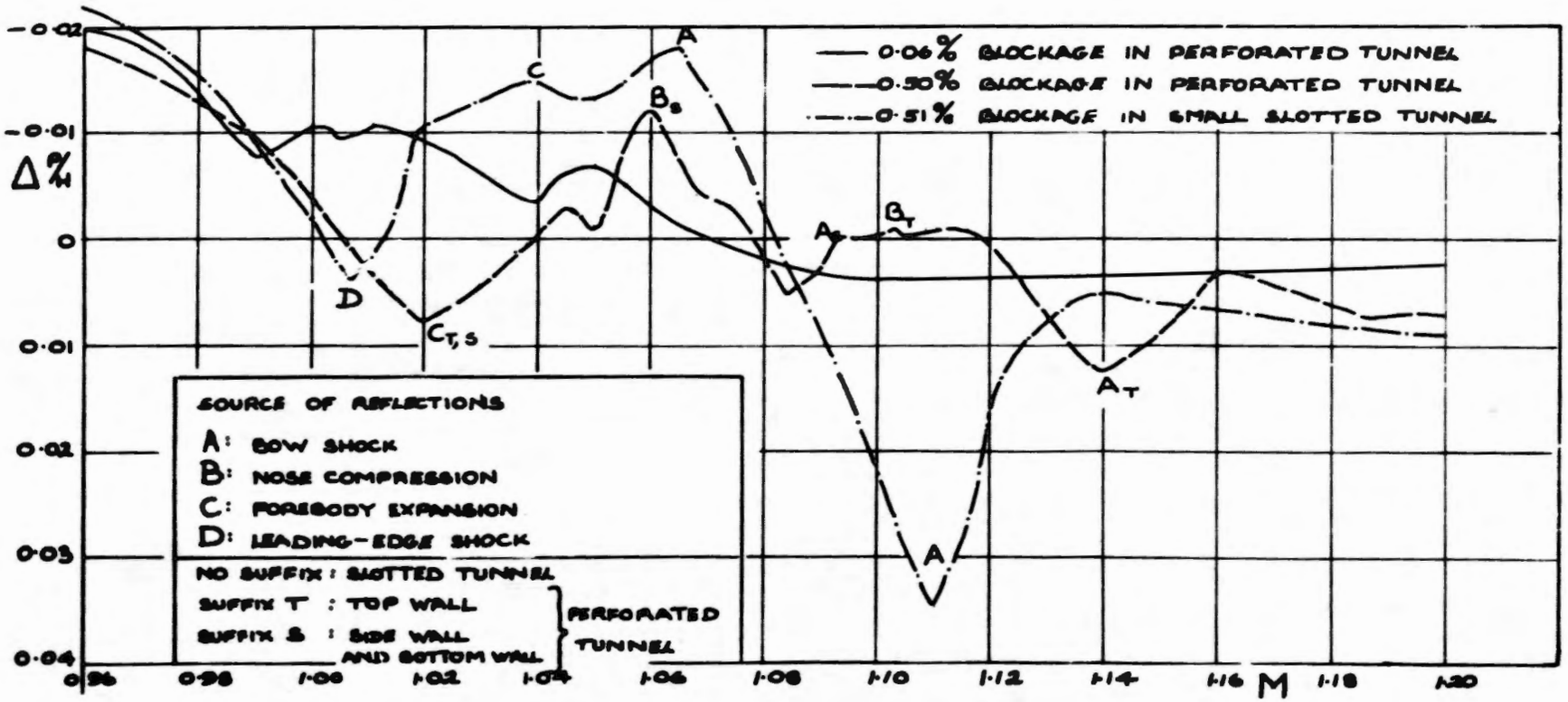

Fig.26 Interference effects for models at 0.5% blockage
(b) x = 5.2D

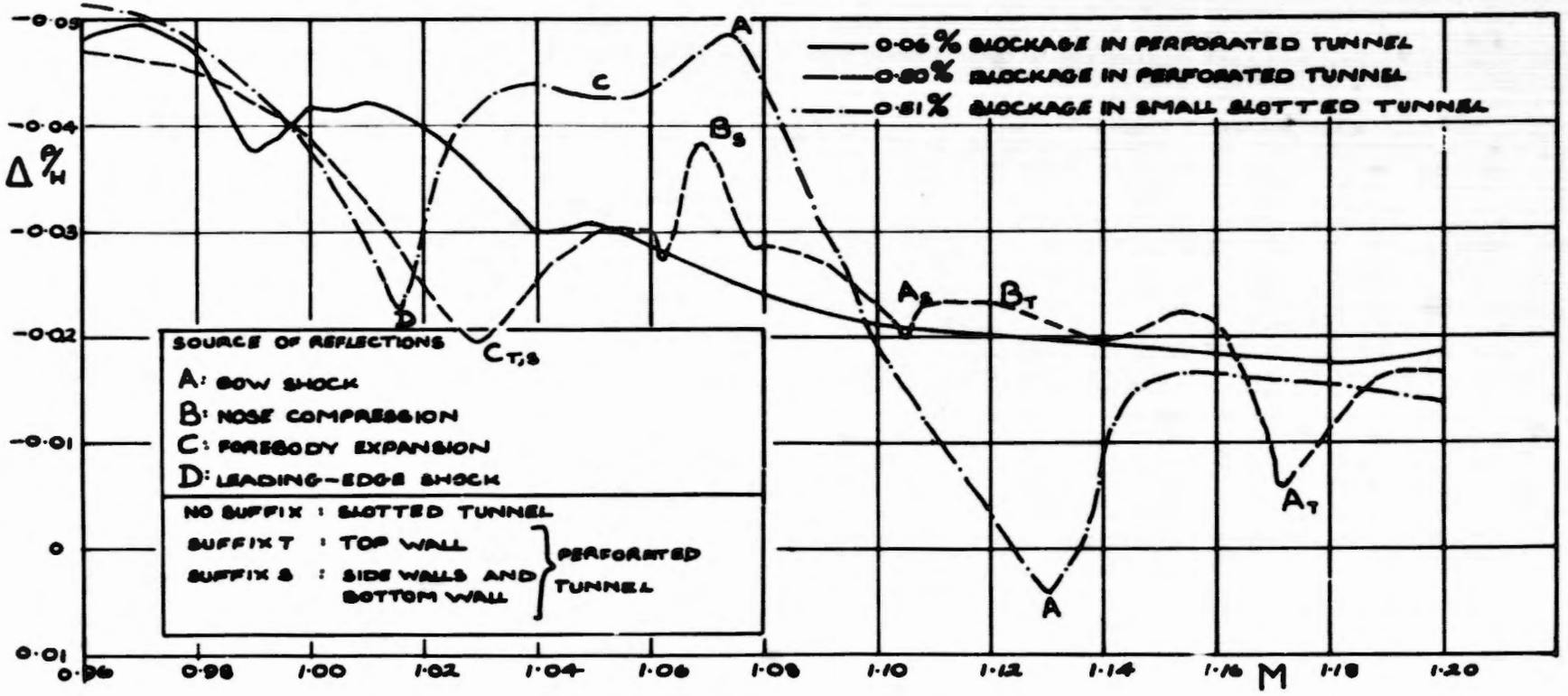

Fig. 26 Interference effects for models at 0.5% blockage
(c) x = 6.00

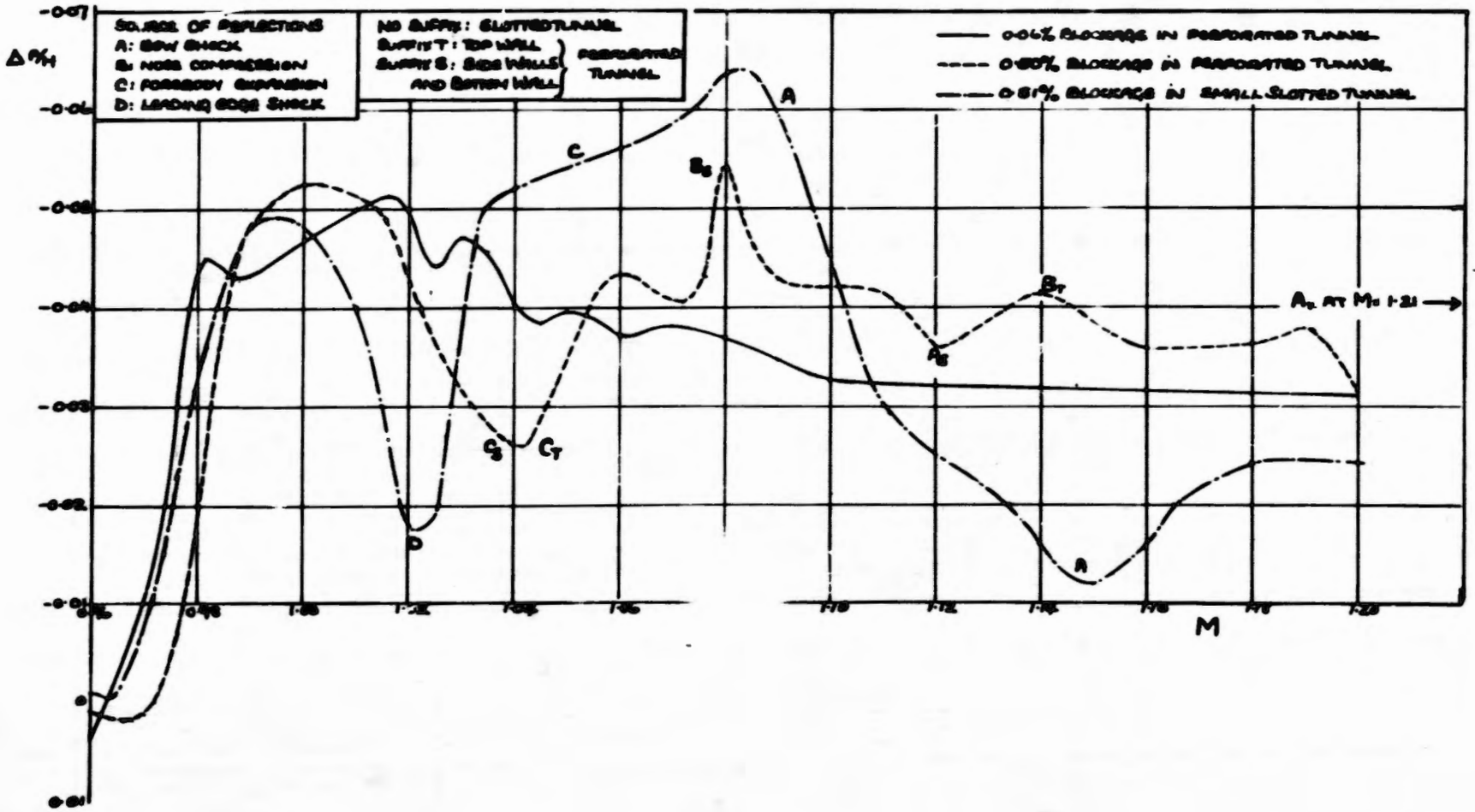

Fig. 26 Interference effects for models at 0.5% blockage
(d) x = 6.8D (near wing root T.E)

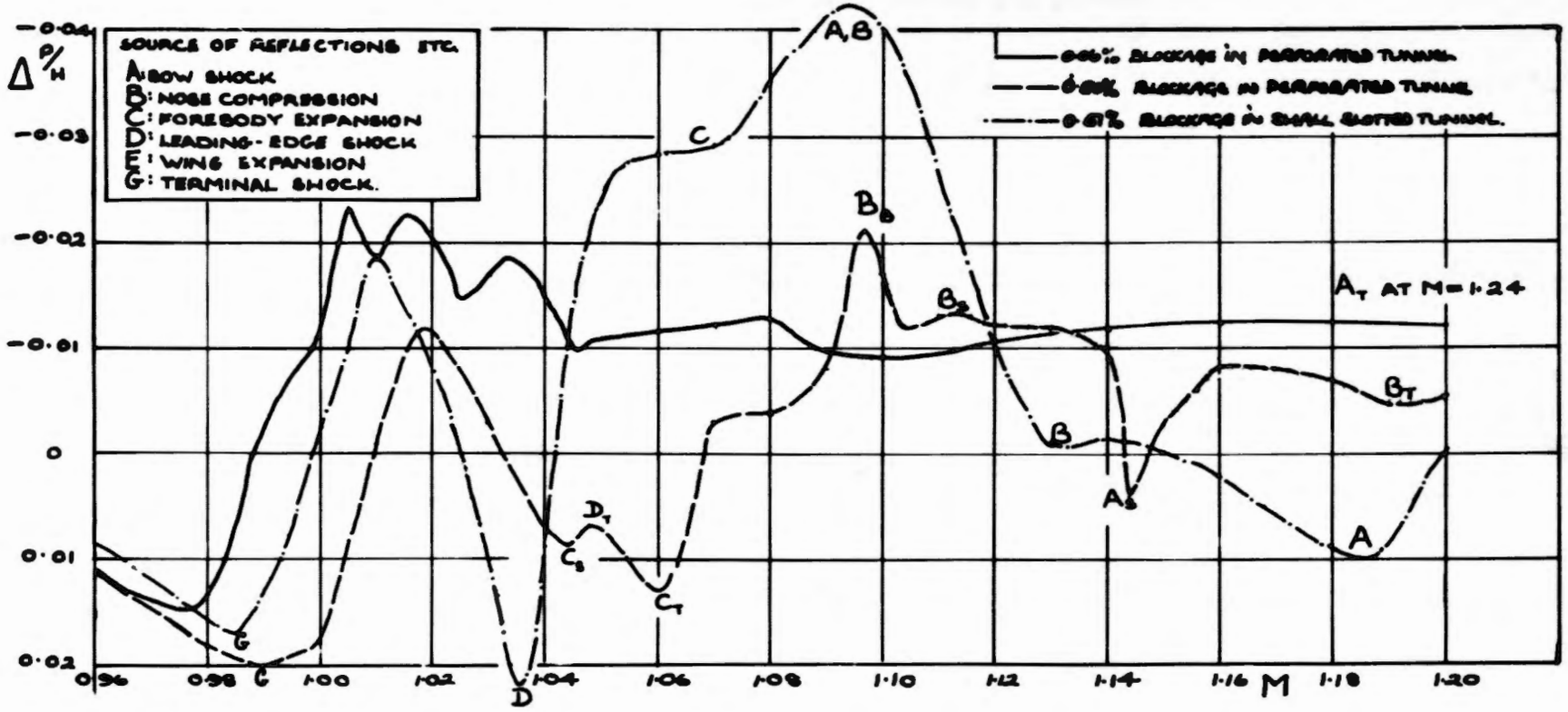

Fig. 26 Interference effects for models at 0.5% blockage
(e) x = 7.6D

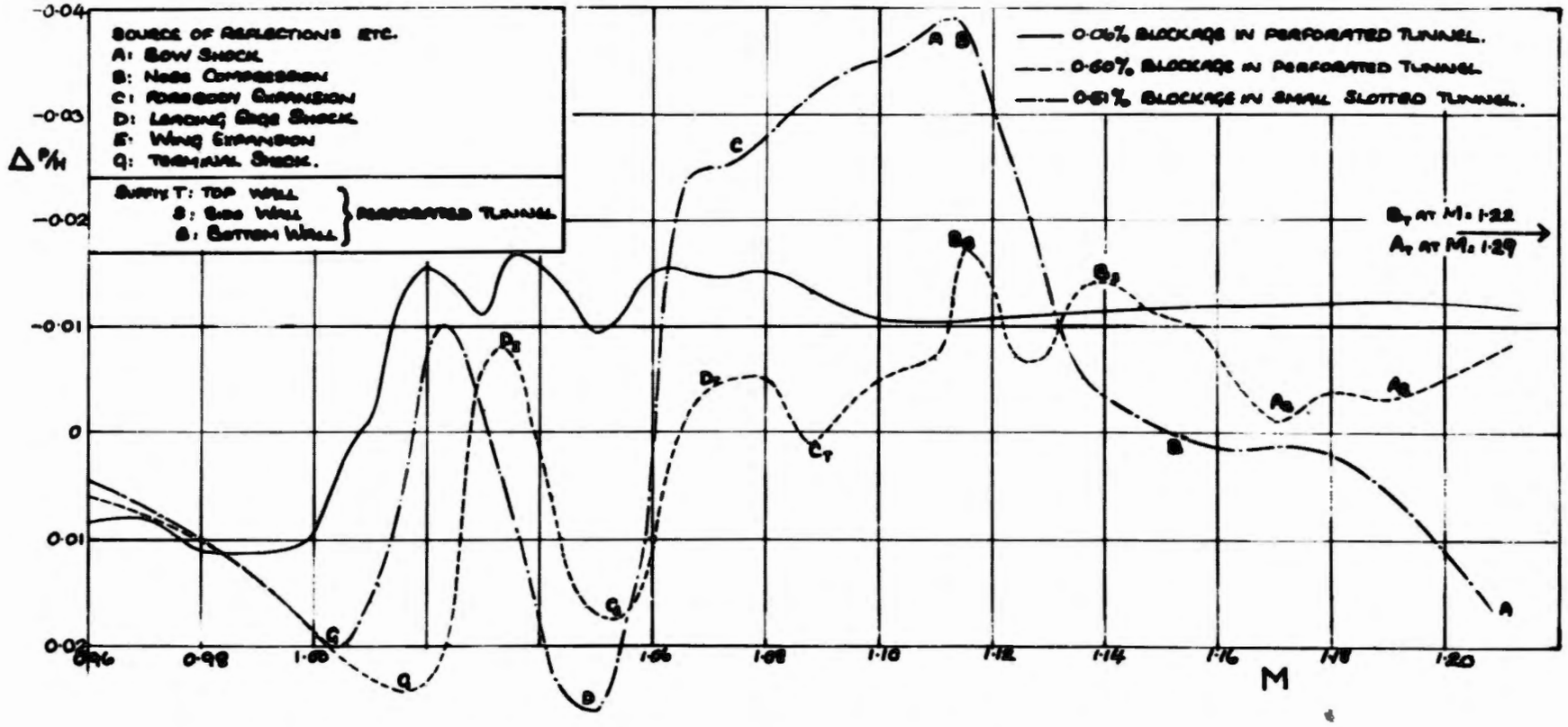

Fig. 26 Interference effects for models at 0.5% blockage
(f) x = 8.4D

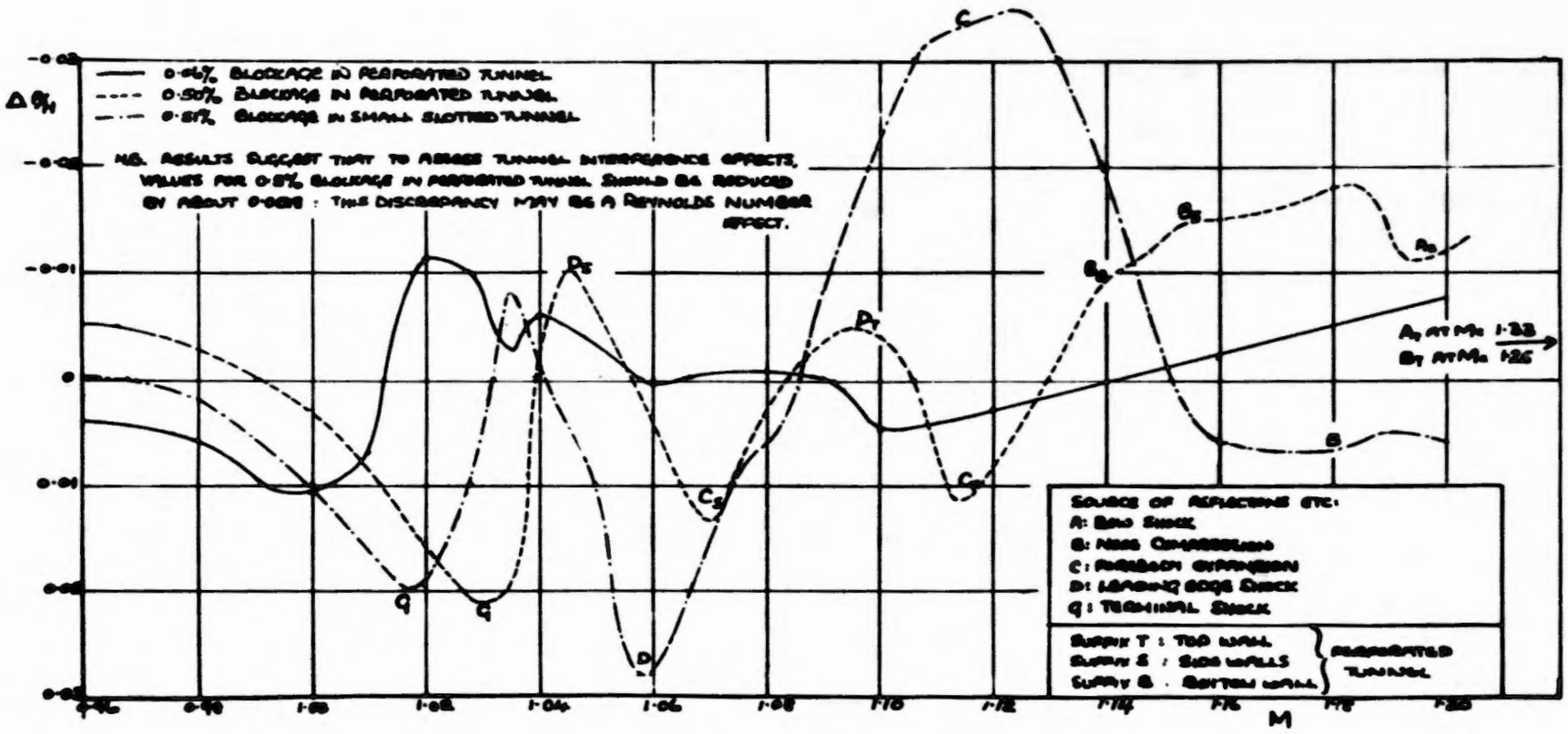

Fig. 26 Interference effects for models at 0.5% blockage
(g) x = 9.2D

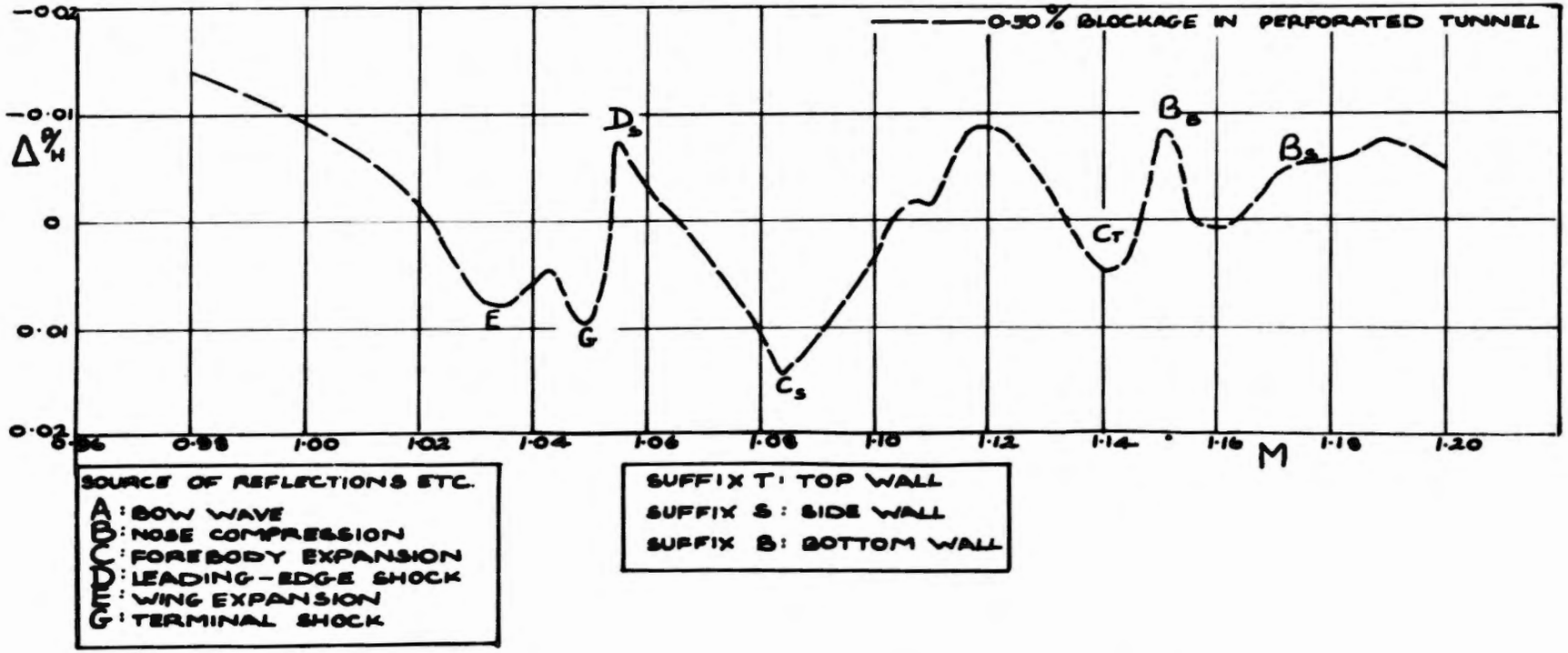

Fig.26 Interference effects for models at 0.5% blockage
(h) x = 9.83D

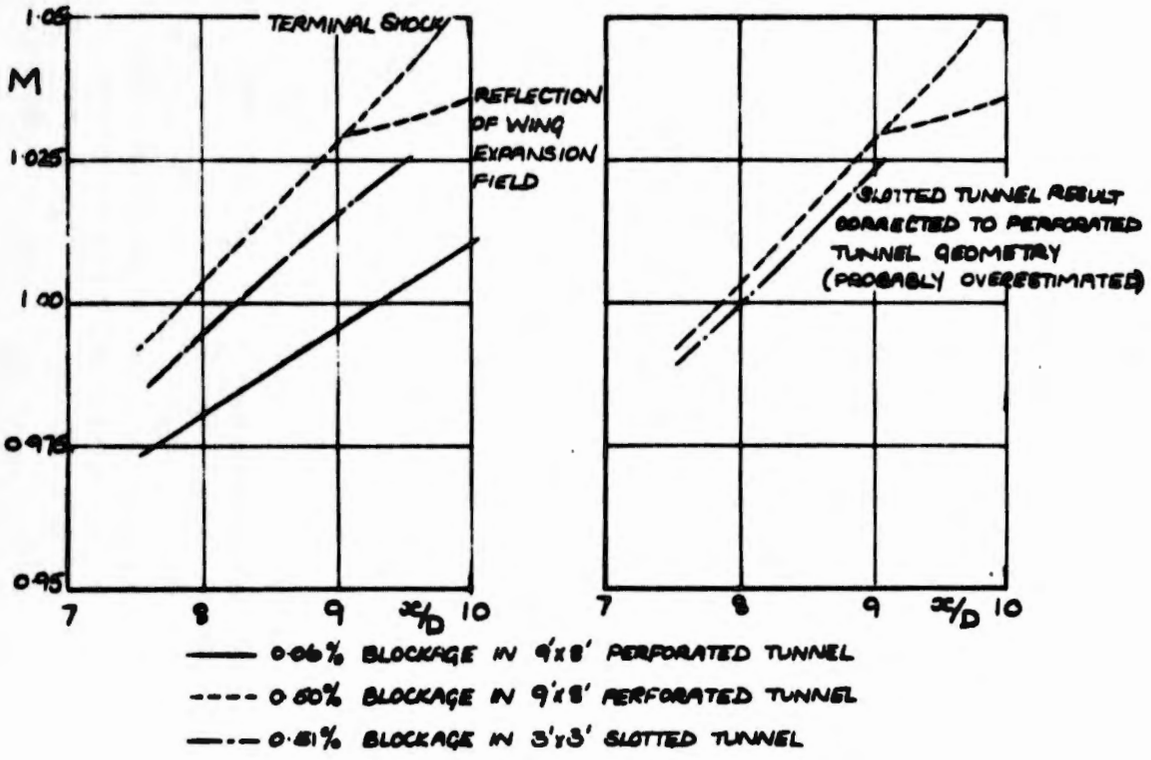

(a) Movement of terminal shock down body (also reflection of wing expansion field)

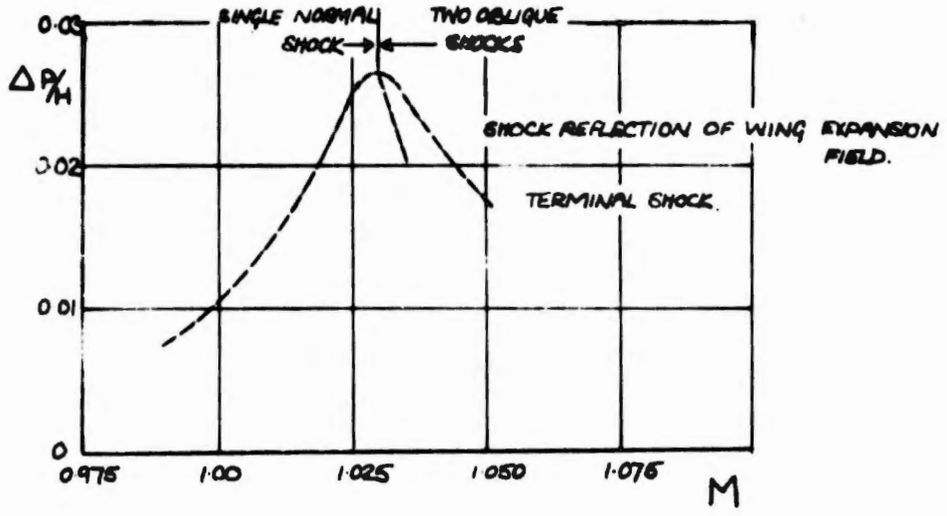

(b) 'Strength' of terminal shock (results from slotted and perforated tunnels agree; no data from slotted tunnel for $M > 1.02$)

Fig.27 Terminal shock effects

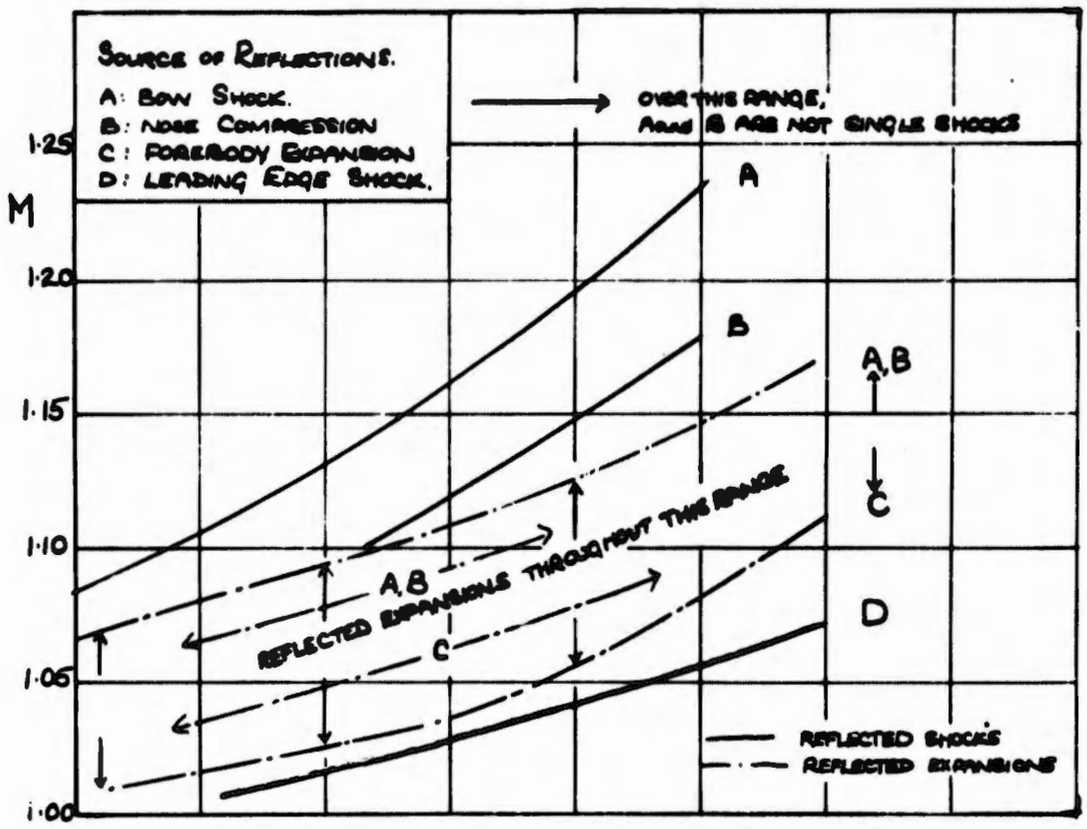

(a) Small slotted tunnel

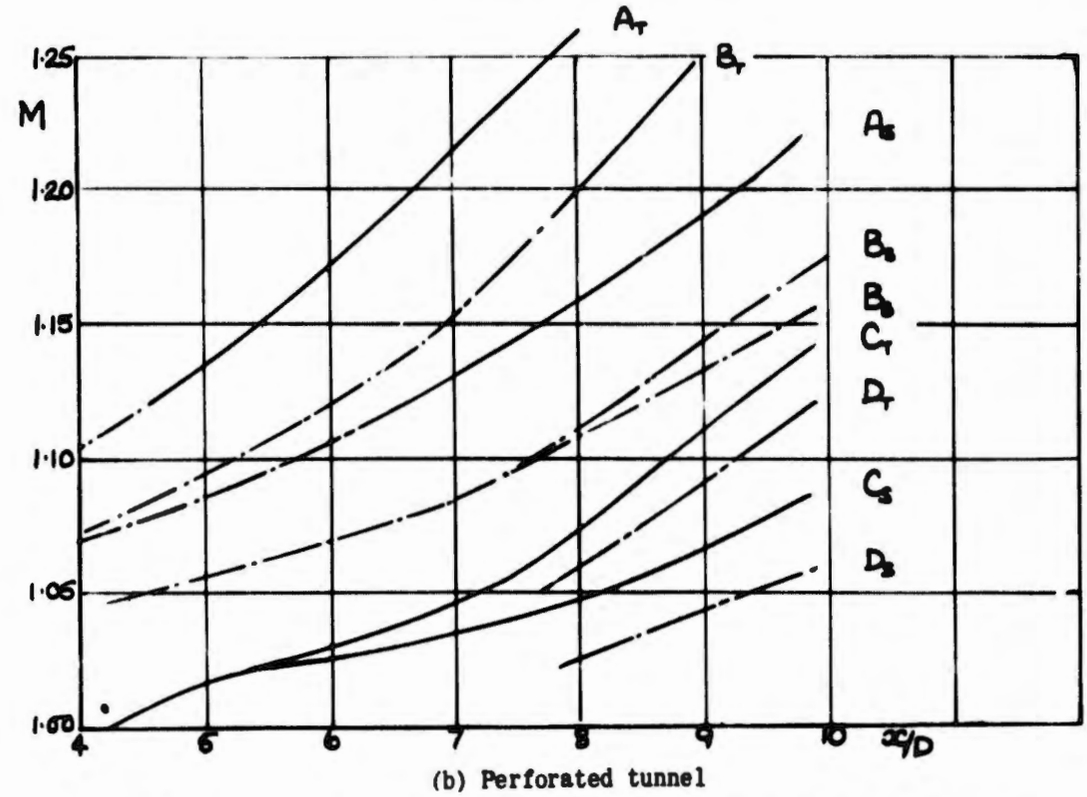

(b) Perforated tunnel

Fig. 28 Passage of reflected waves down bodies of 0.5% blockage models

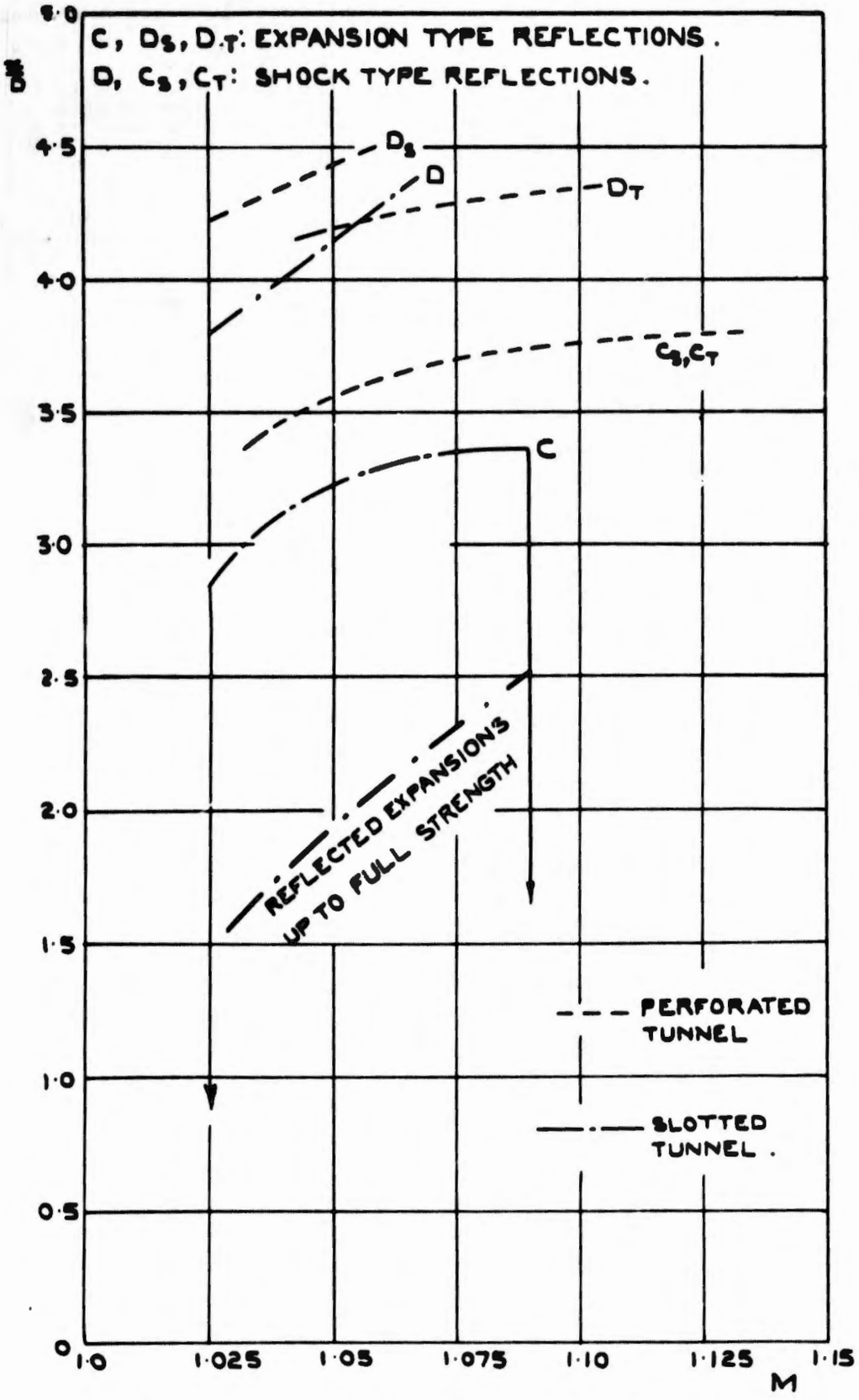

Fig. 29 Apparent position of sources of reflected disturbances

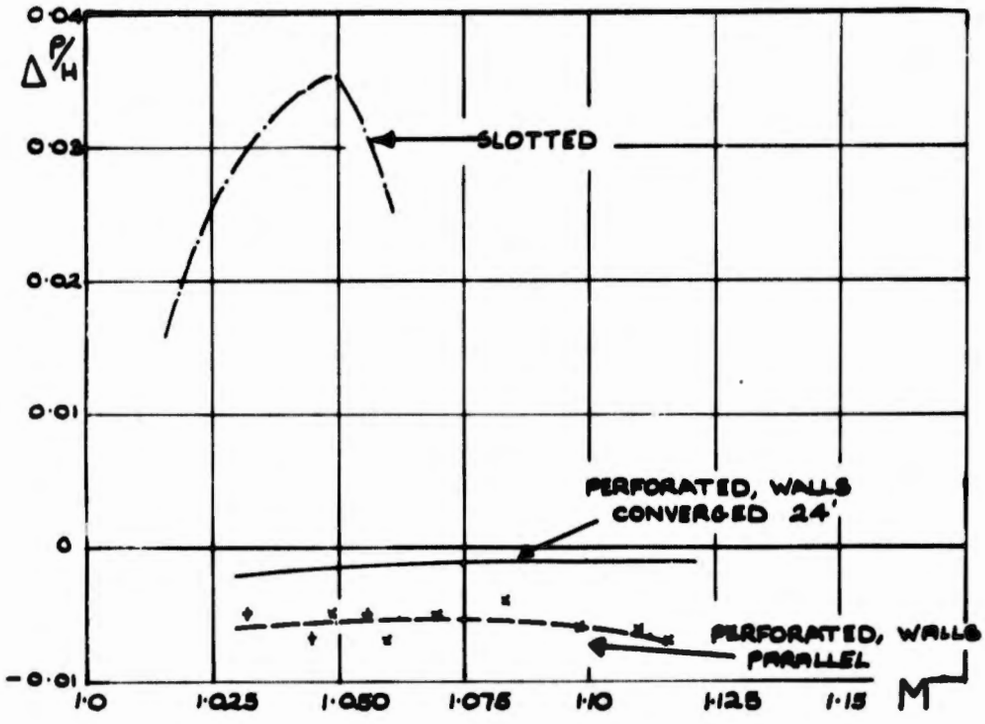

(a) Leading-edge shock

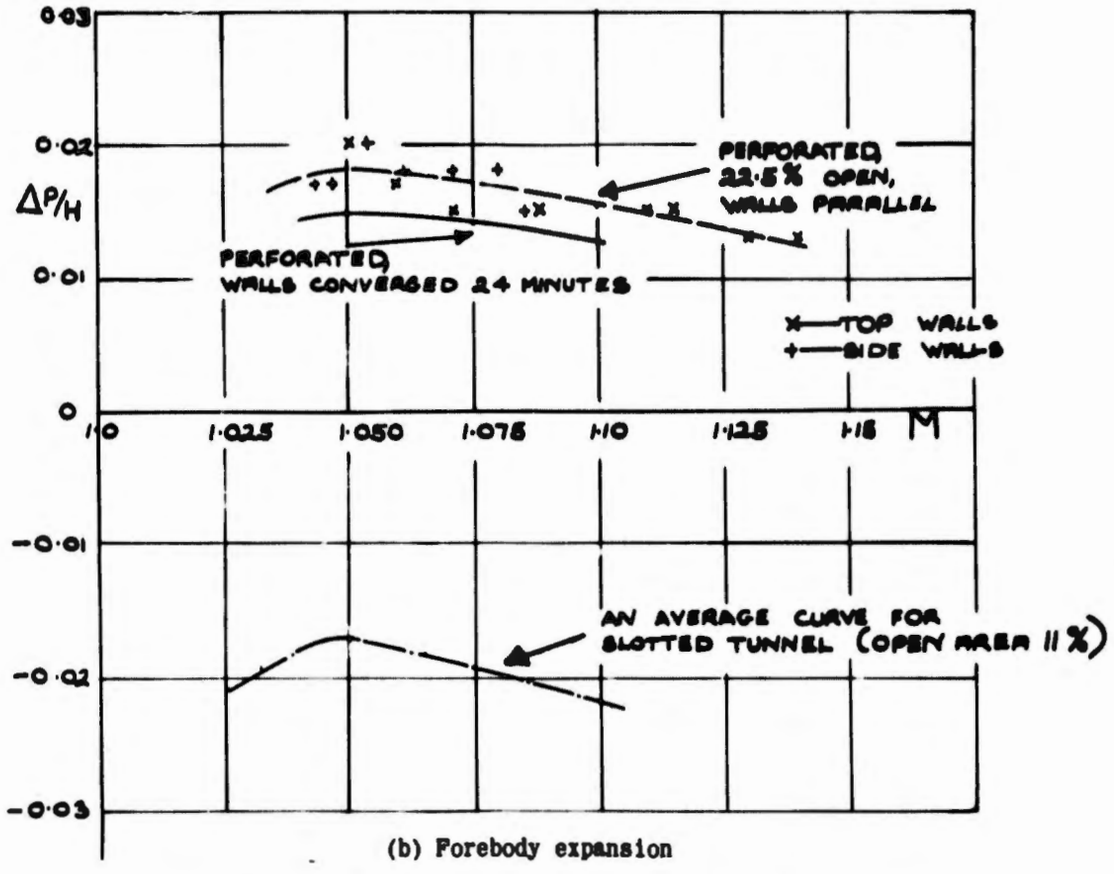

(b) Forebody expansion

Fig.30 Strength of reflected waves

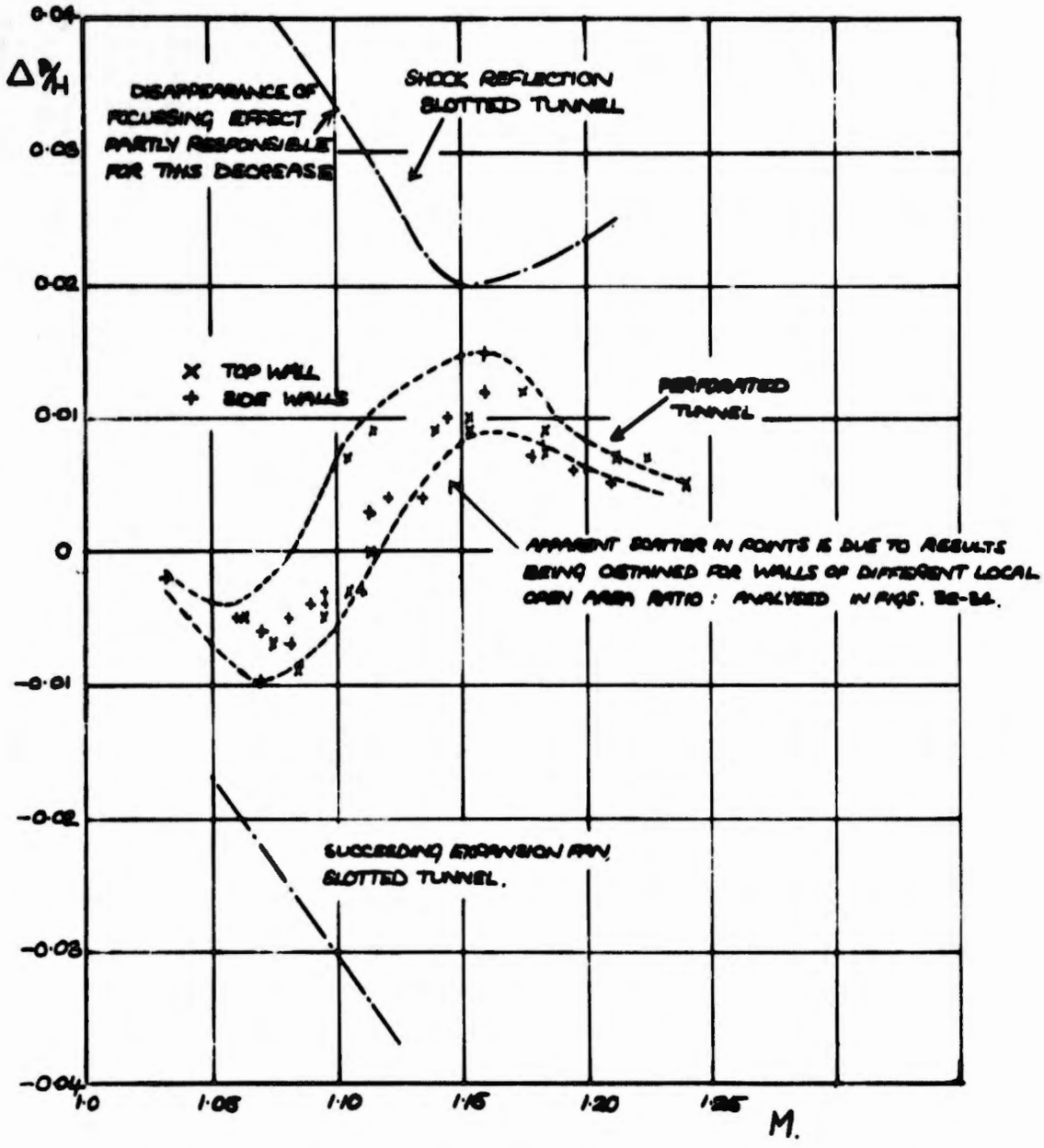

Fig.31 Strength of bow-wave reflections; comparison of 3ft × 3ft slotted and 9ft × 8ft perforated tunnels; 0.5% blockage

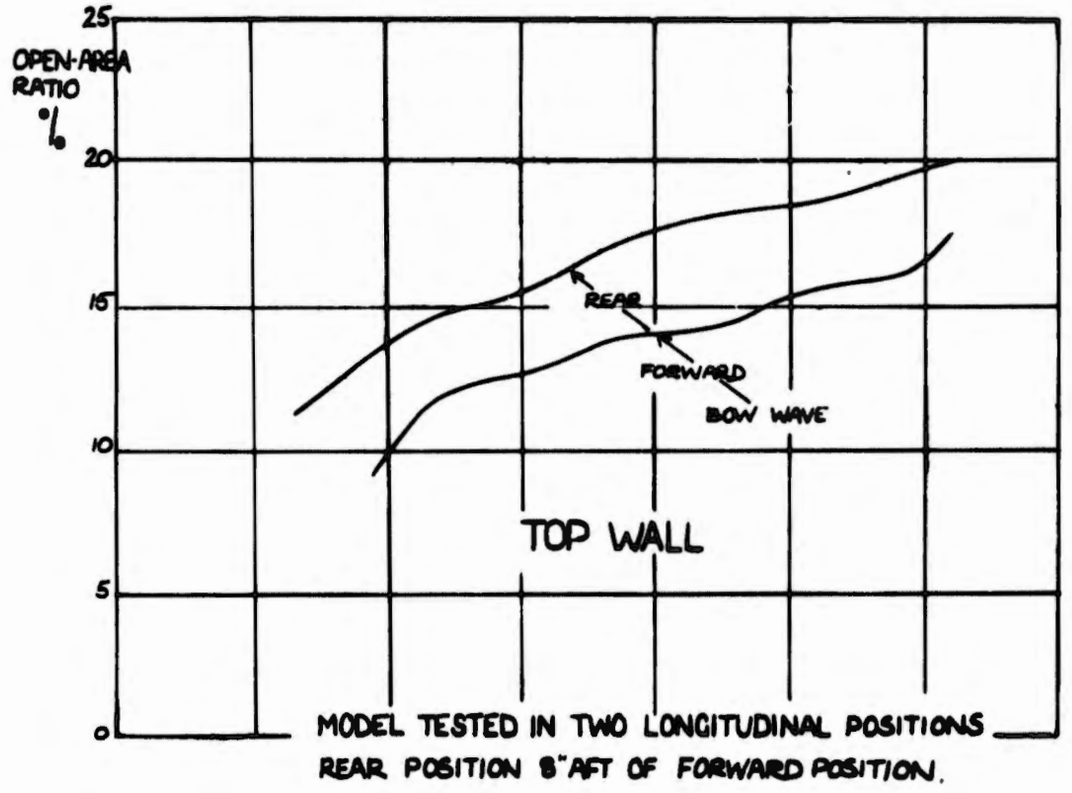

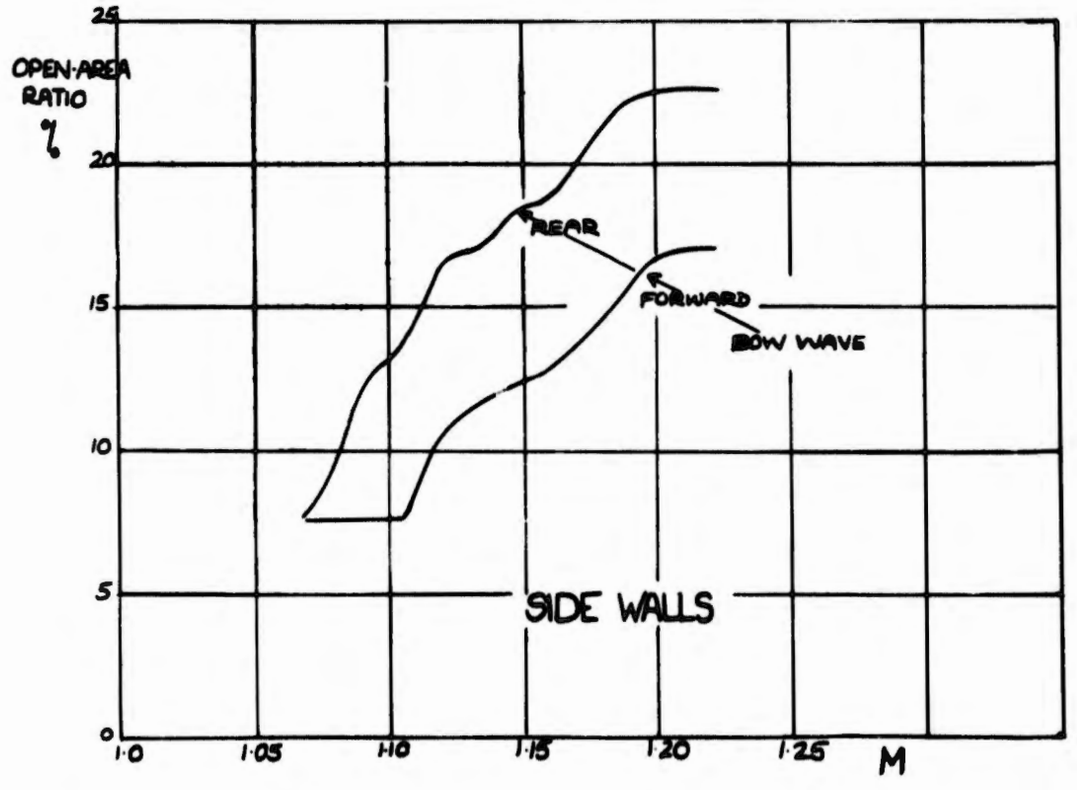

Fig.32 Open-area ratio at point of wave reflection; perforated tunnel; 7in. model

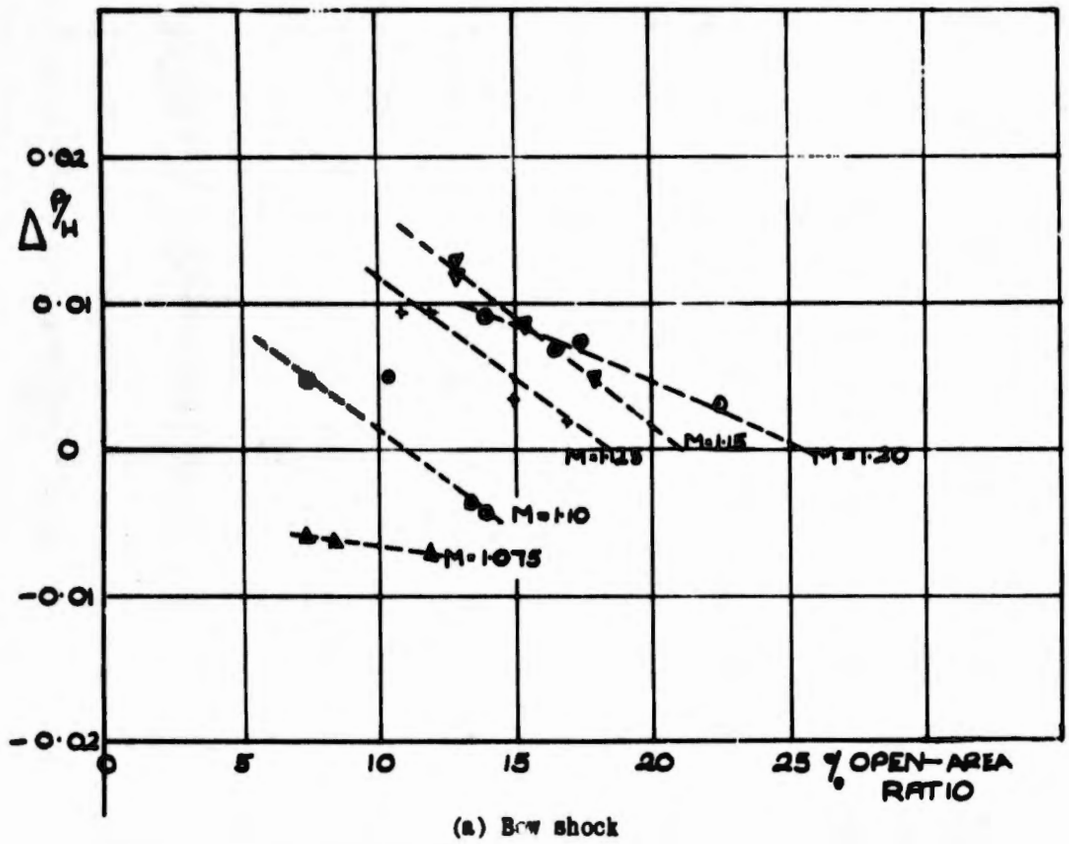

(a) Bow shock

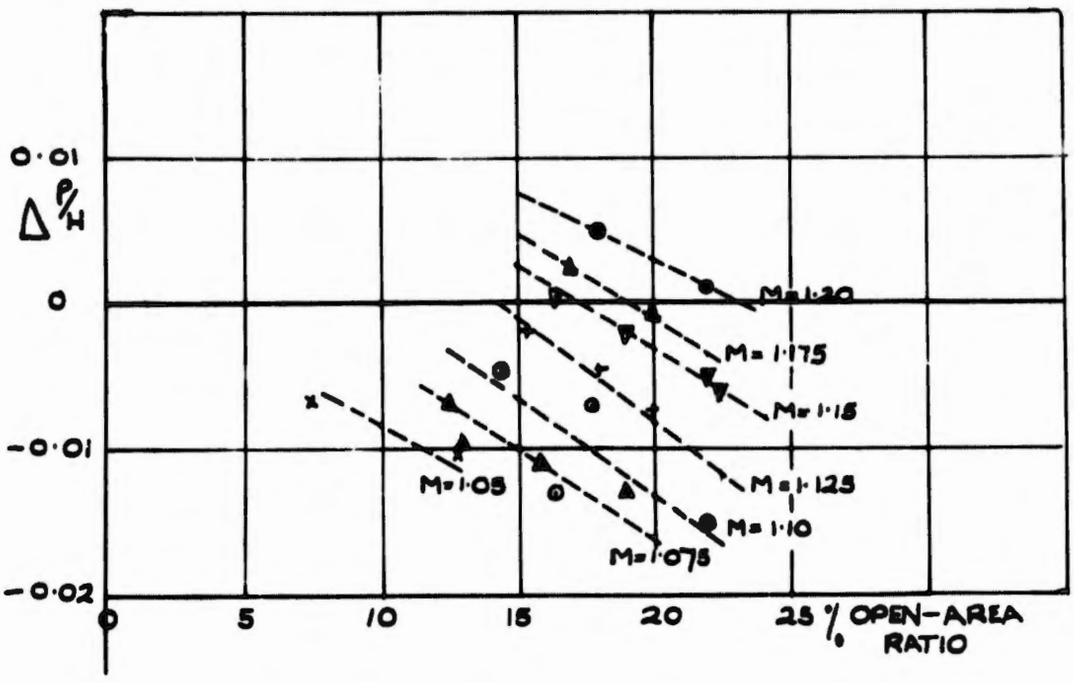

(b) Nose compression

Fig.33 Strength of reflections of incident compression waves as function of open-area ratio and Mach number; perforated tunnel, walls parallel

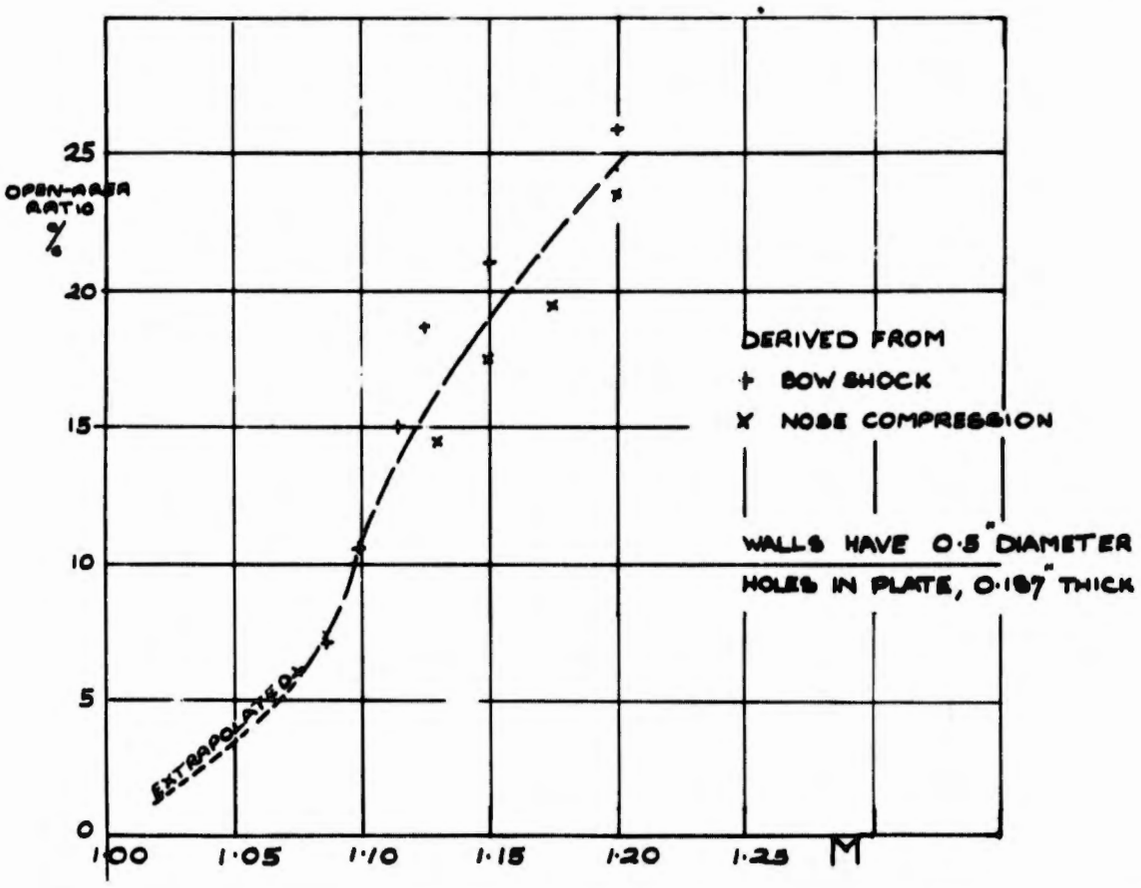

Fig.34 Open-area ratio required for cancellation of reflections of incident shock waves; perforated tunnel, walls parallel

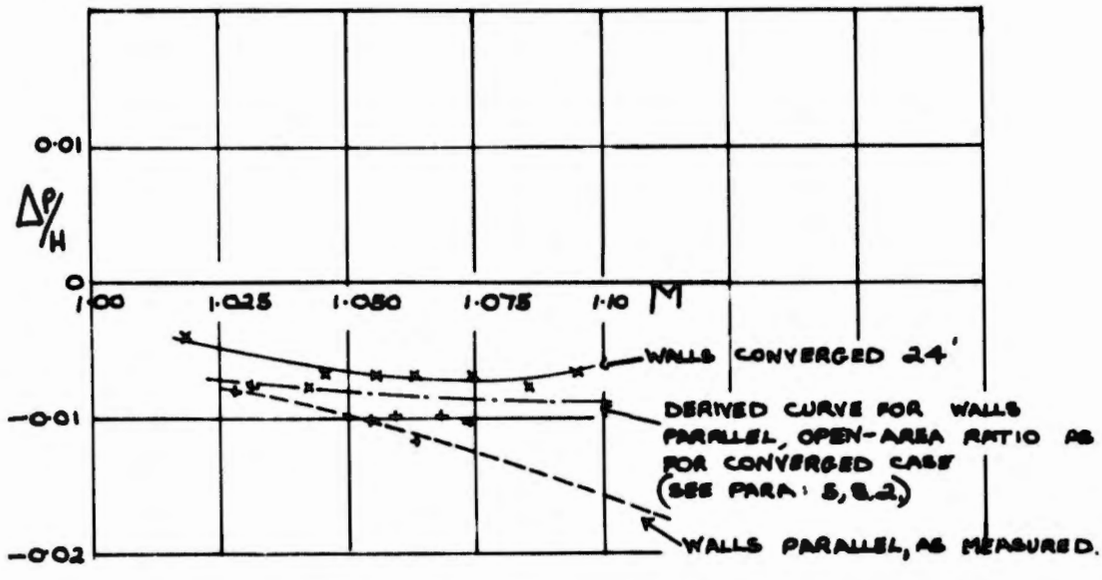

Fig.35 Effect of 24ft convergence of side walls on strength of reflection of nose compression in side walls (model in rear position)

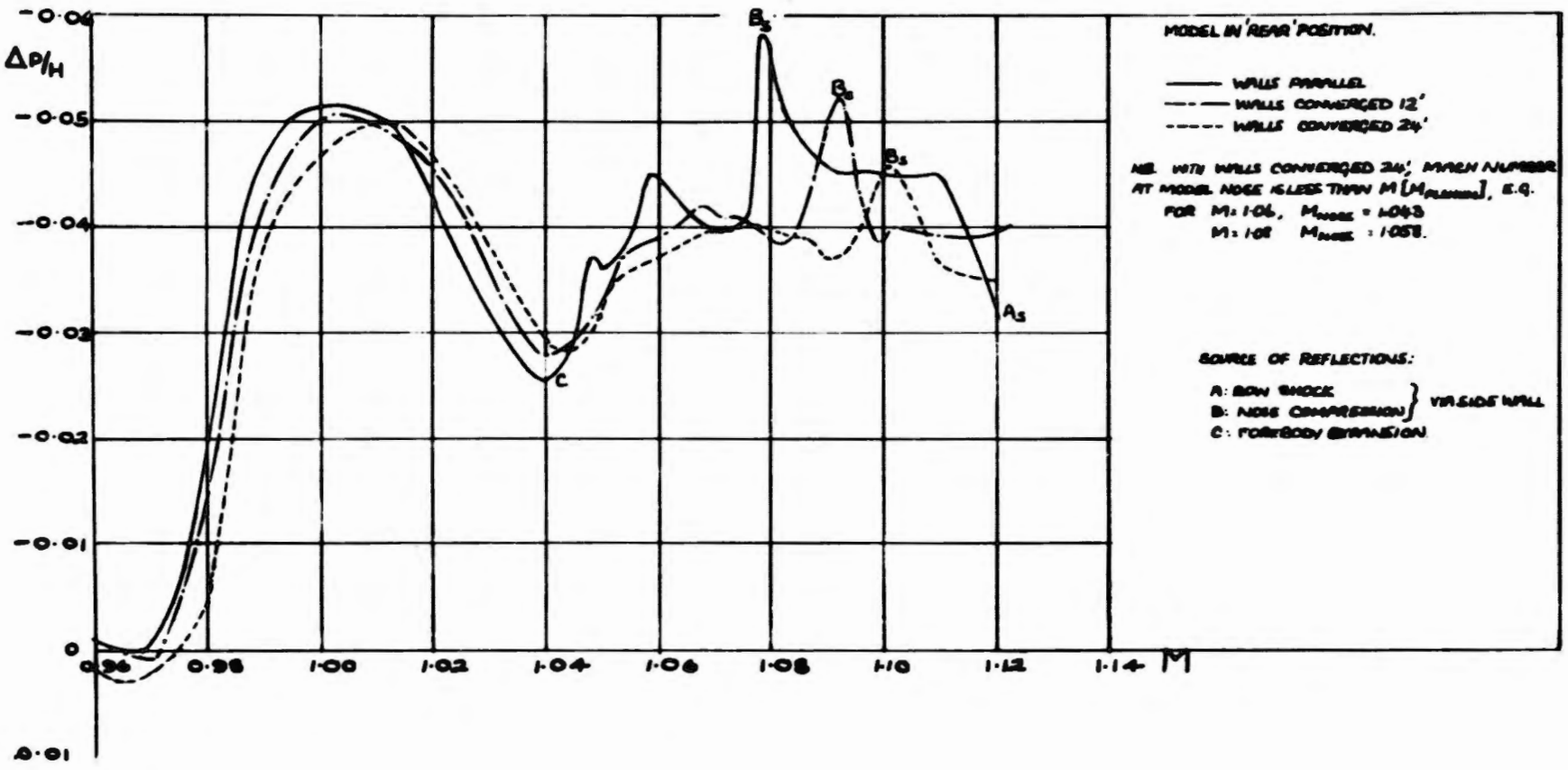

Fig.36 Effect of side wall convergence on body pressures at x = 6.8D; 0.5%; blockage model in perforated tunnel

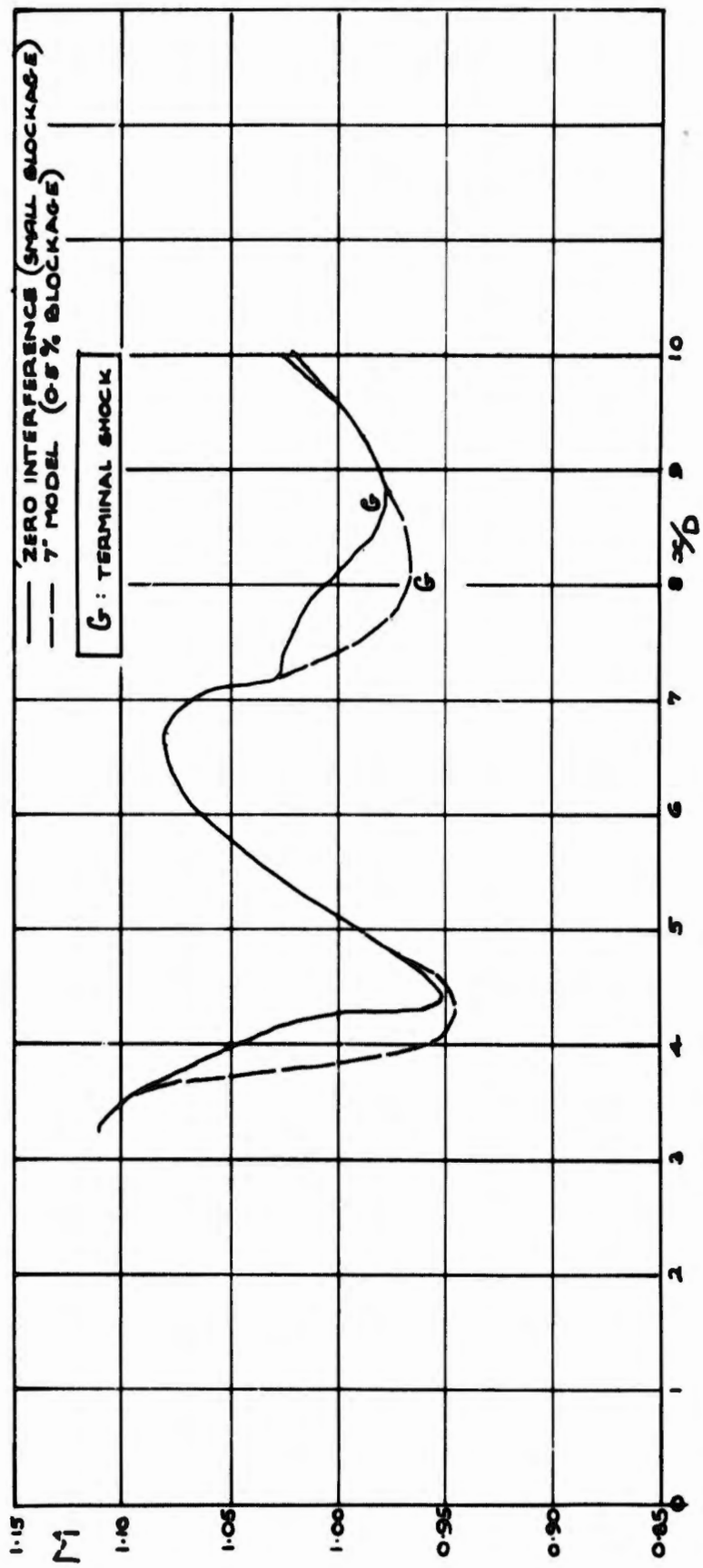

Fig.37(a) Interference effects at M = 1.00; perforated tunnel

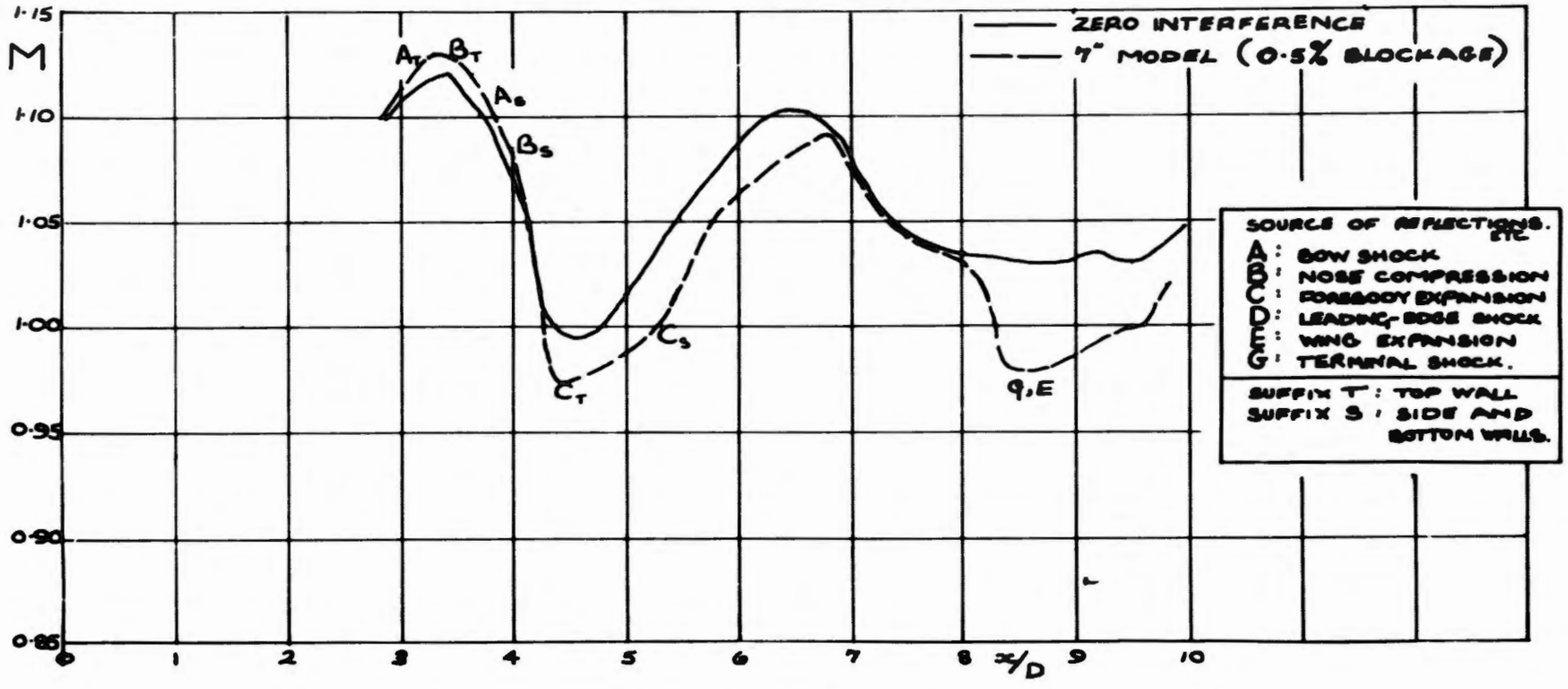

Fig.37(b) Interference effects at M = 1.02; perforated tunnel

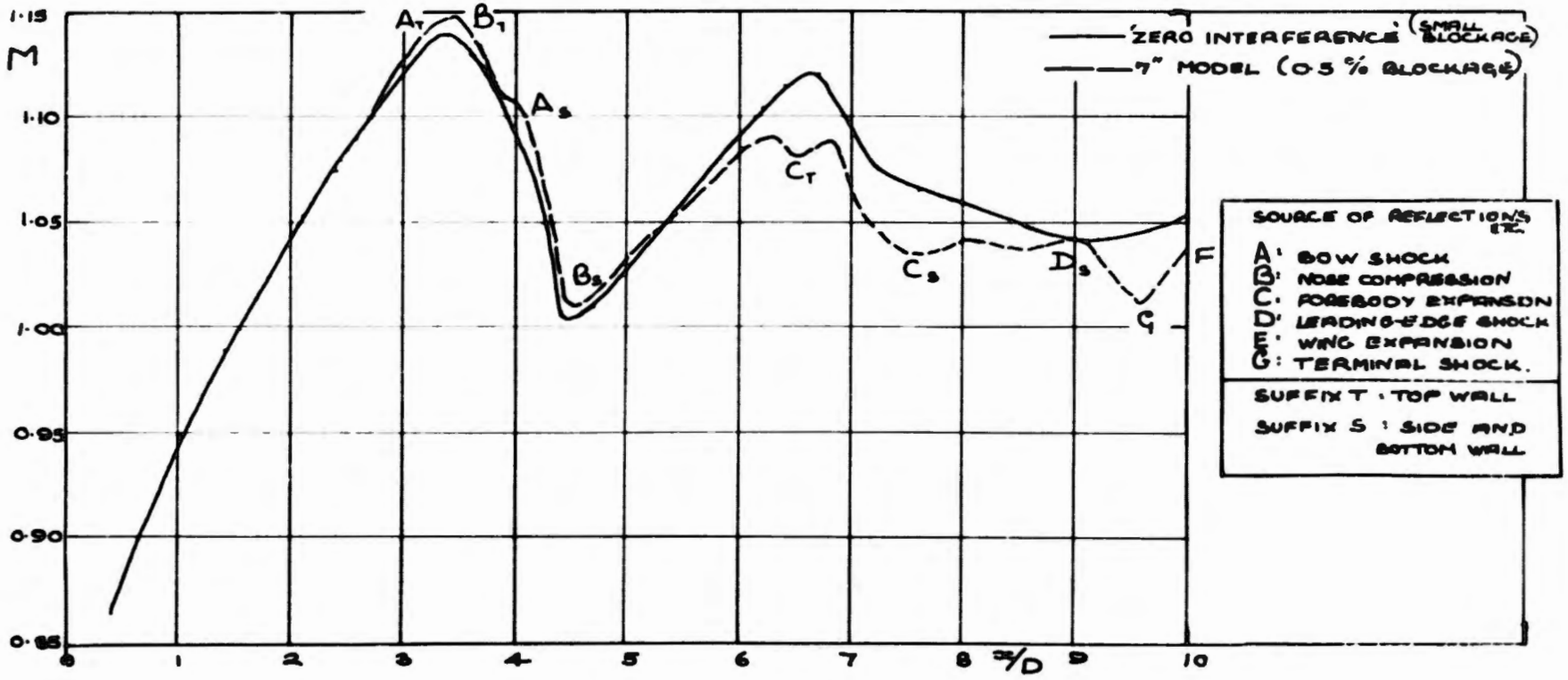

Fig.37(c) Interference effects at M = 1.04; perforated tunnel

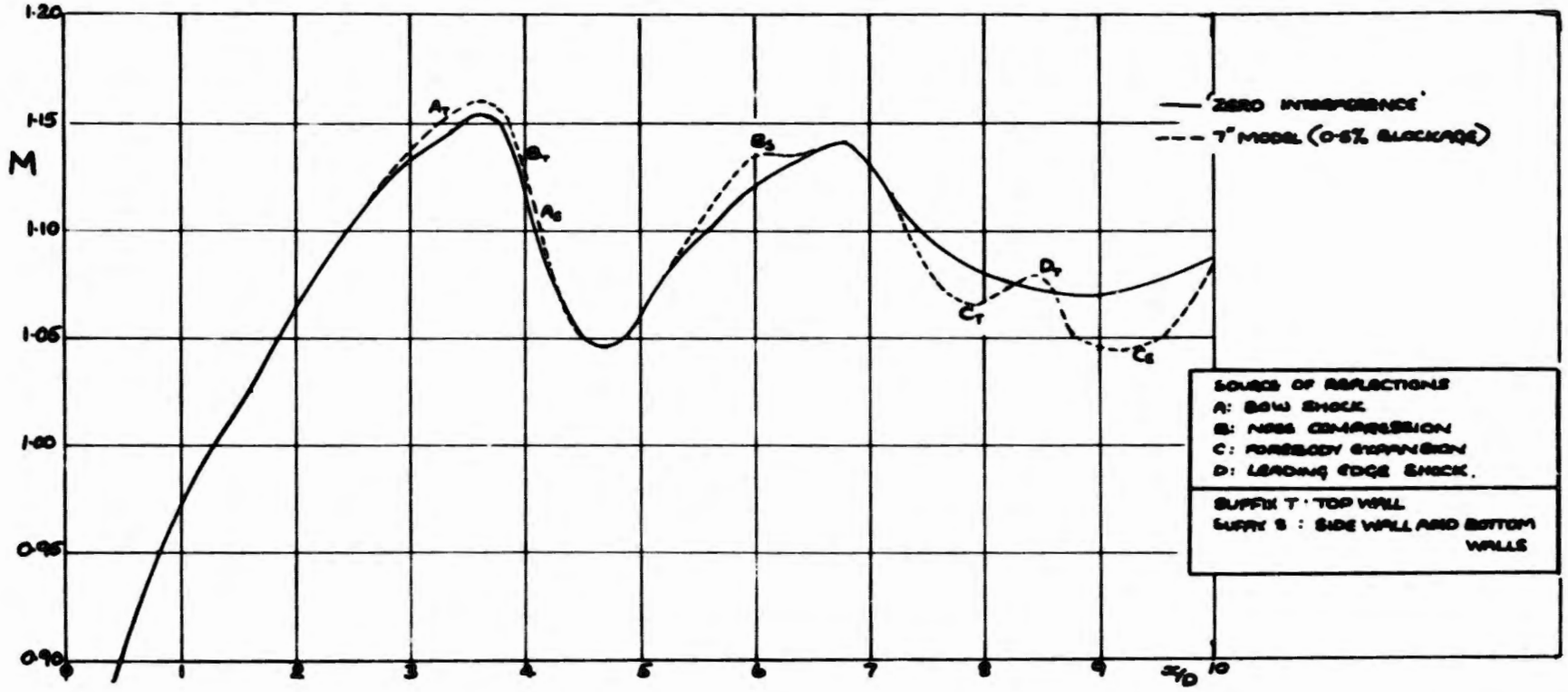

Fig.37(d) Interference effects at M = 1.07; perforated tunnel

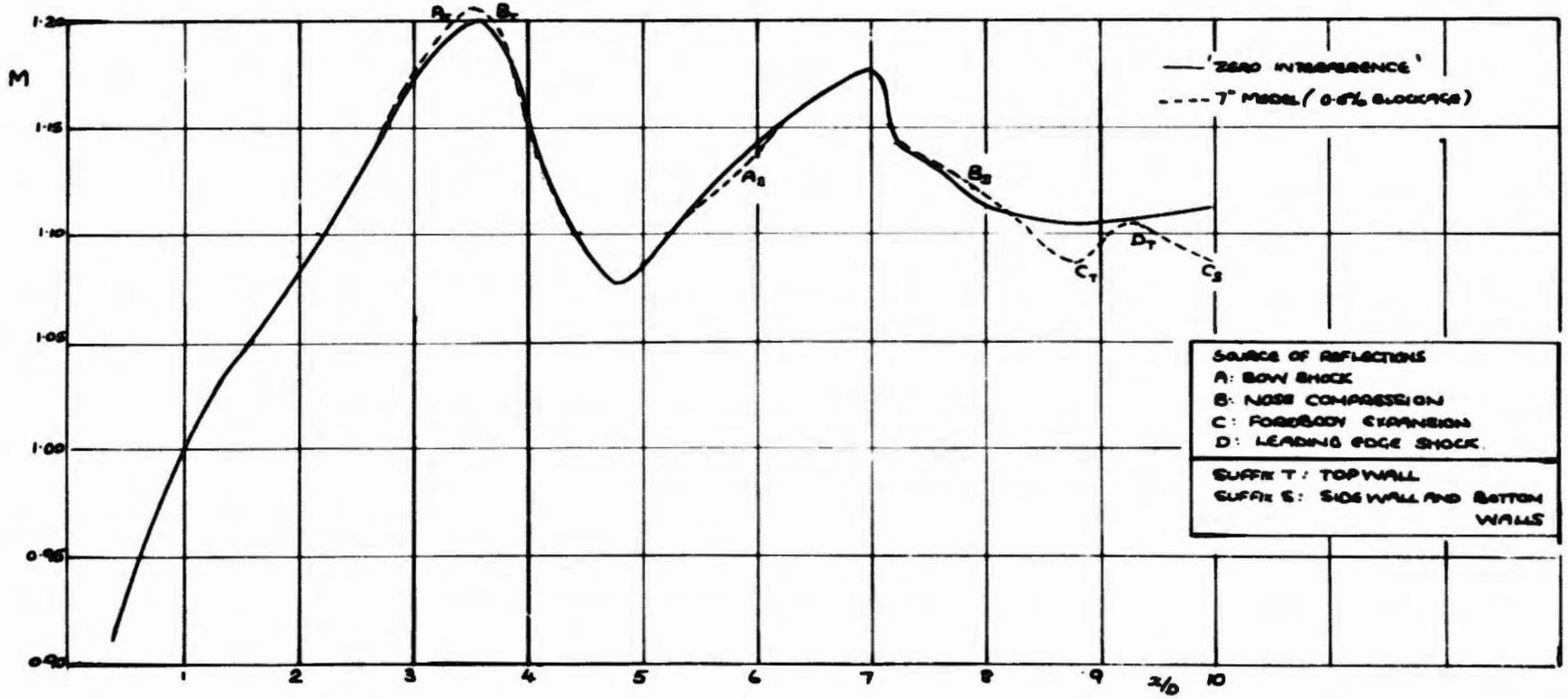

Fig.37(e) Interference effects at M = 1.10; perforated tunnel

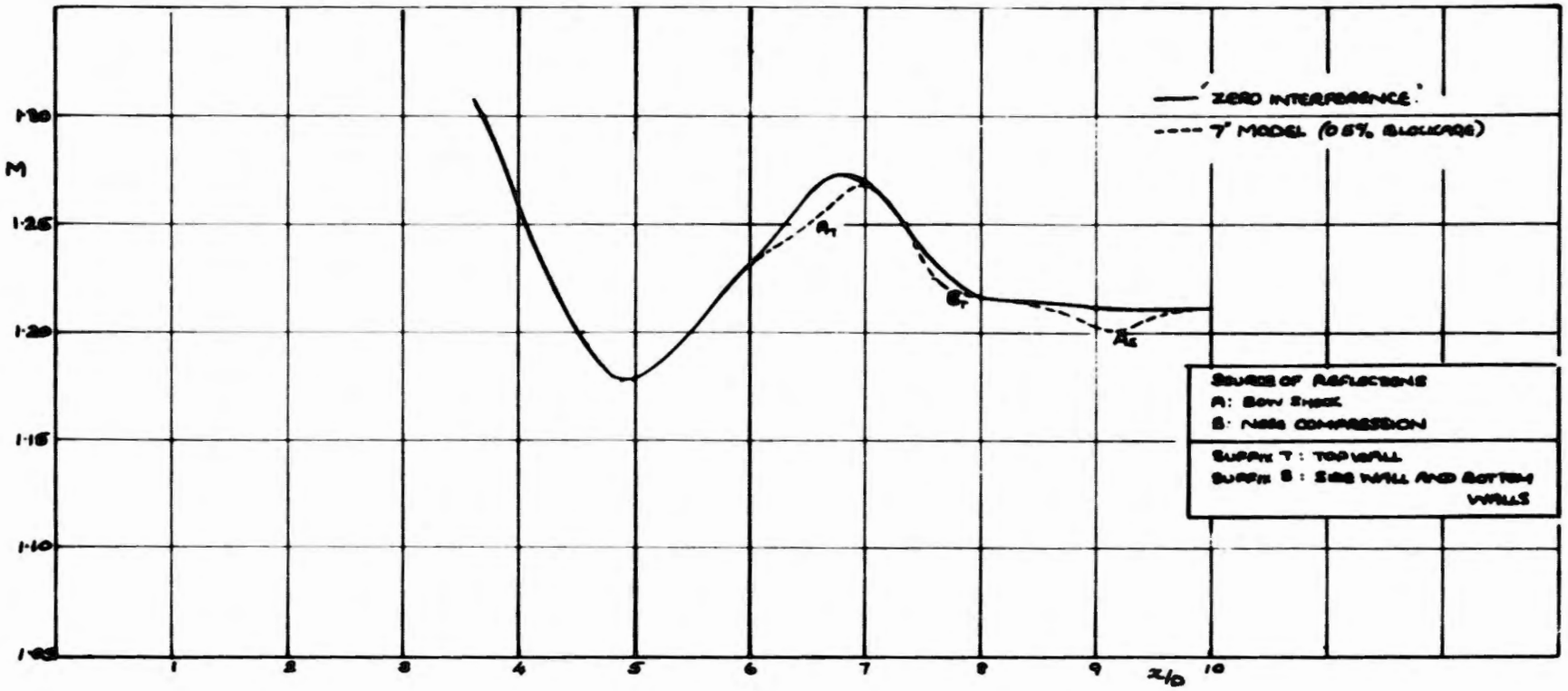

Fig.37(f) Interference effects at M = 1.20; perforated tunnel

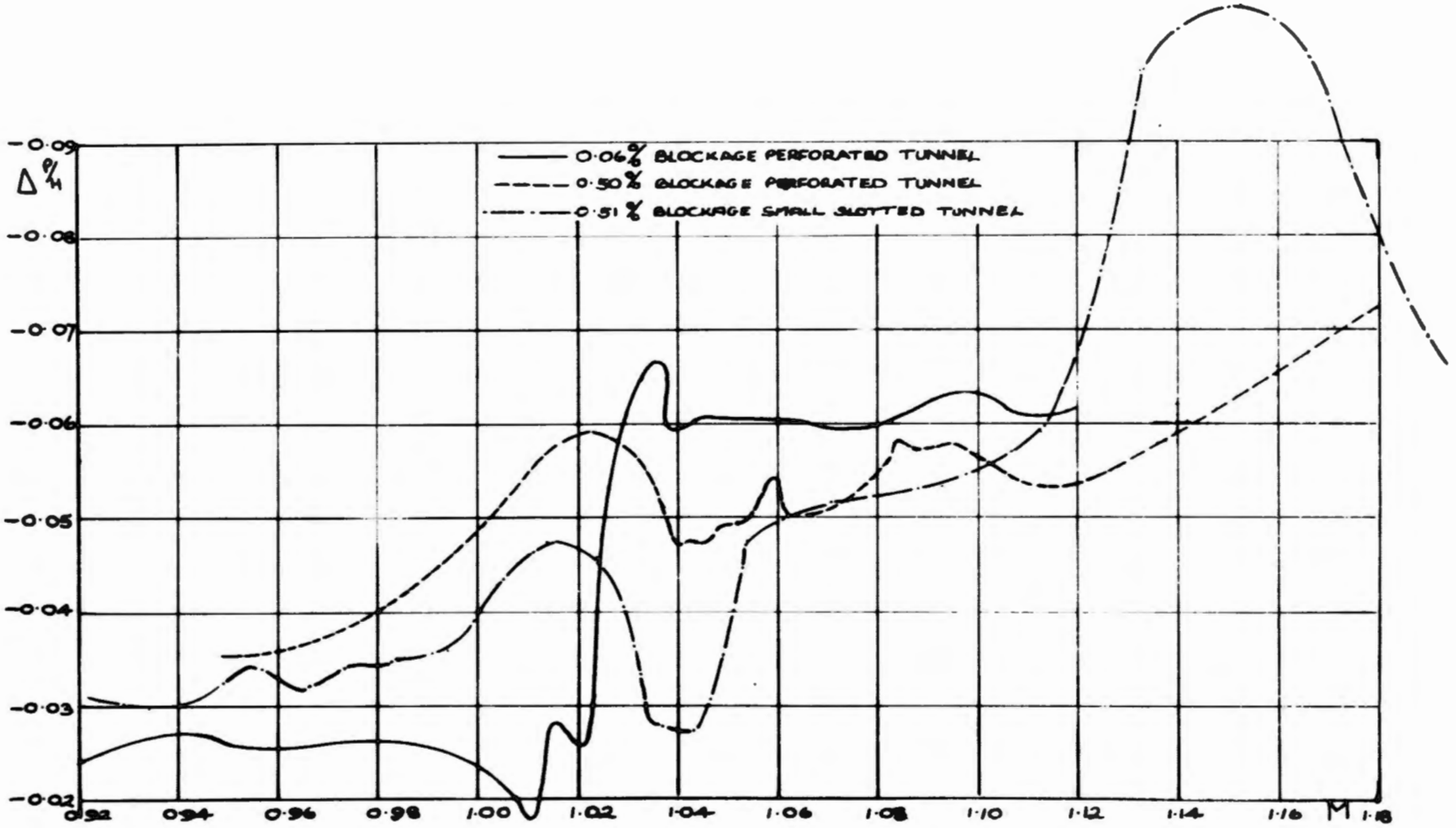

Fig.38 Interference effects for models at 0.5% blockage base pressures

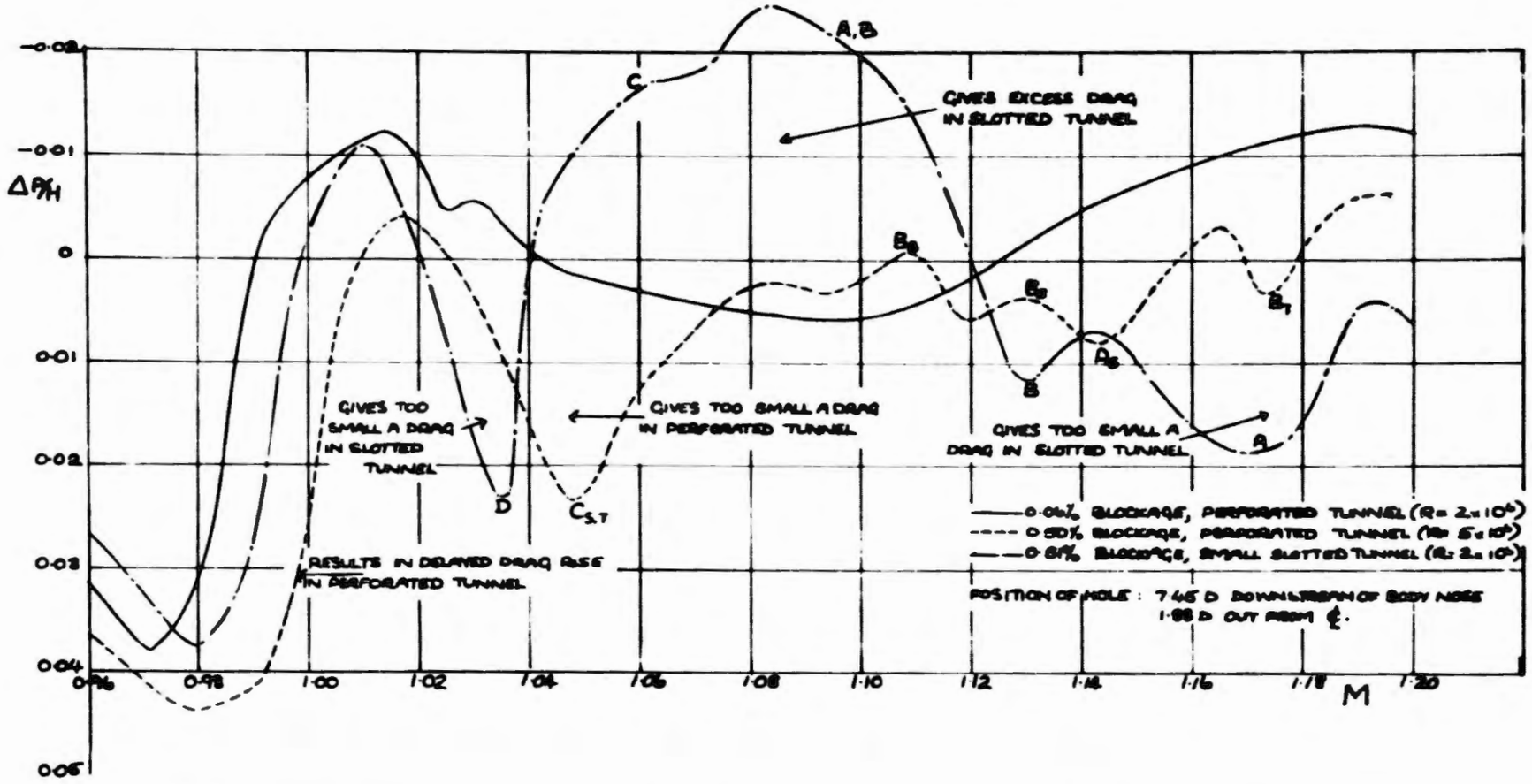

Fig.39 Interference effects for models at 0.5% blockage: pressure on wing at 0.95c, 0.7 × semispan

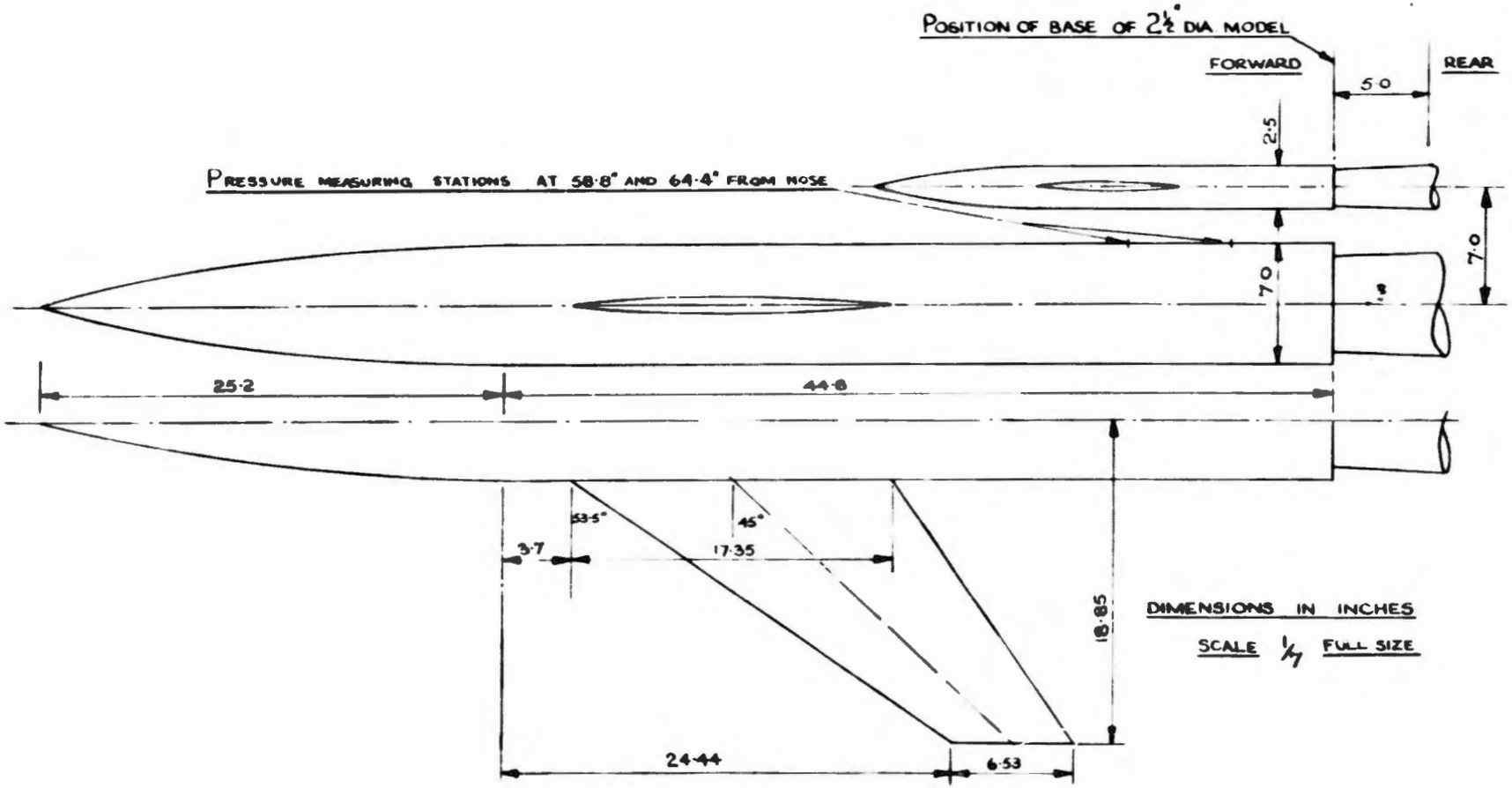

Fig.40 General arrangement of 2½in. diameter model mounted as a tailplane in presence of 7in. diameter model; 9ft x 8ft perforated wall tunnel

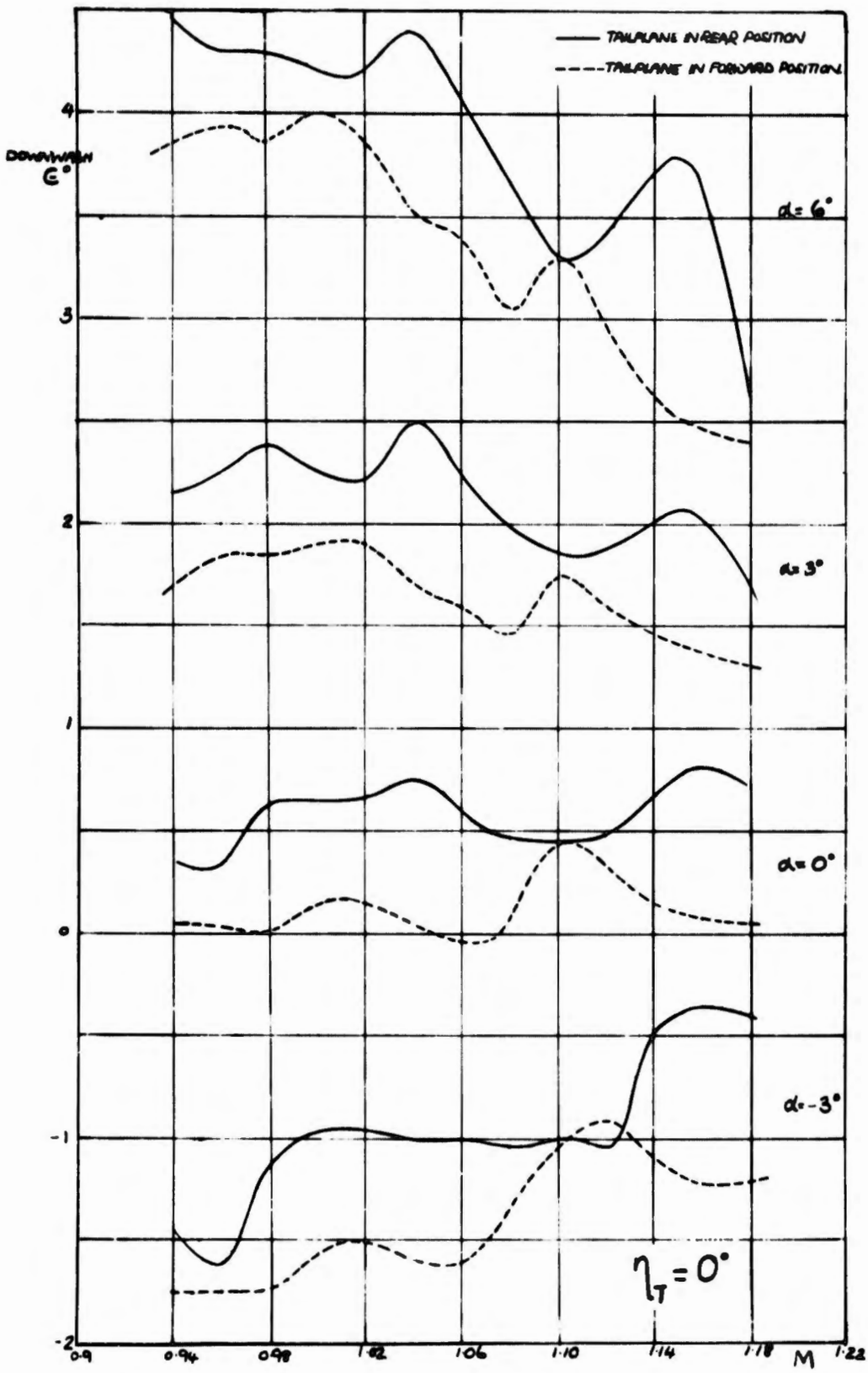

Fig.41 Variation of downwash with Mach number deduced from tests on arrangement in Figure 40; 9ft x 8ft perforated tunnel